To the University of Wyoming:

The members of the Committee approve the thesis of George Randolph presented on 12 April 2012.

Thomas Parish, Chairperson

Jonathan Naughton, External Department Member

Jefferson Snider

Robert Kelly

APPROVED

Alfred Rodi, Department, Division, or Program Chair, Department of Atmospheric Science.

Robert Ettema, College Dean/Provost

Randolph, George, Variability of the Wind Resource in Wyoming, MS Department of Atmospheric Science, May 2012.

The rapid development and expansion of wind energy in the last decade justifies its candidacy to wean the United States off traditional sources of electrical power. Wyoming, in particular southeastern Wyoming, is one of the windiest places in the country. This area's potential for electricity generation has allowed it to stay in the spotlight for most of the industry's expansion. Simply knowing that this area is windy, however, is insufficient. Model and observational data from 2008-2010 were analyzed in efforts to understand the modes of variability within the resource. North American Model (NAM) 12-kilometer (km) and 4-km output was averaged at annual, seasonal and diurnal intervals. Subsequent analysis revealed the wintertime to be the season which provides the greatest amount of wind resource. During the day, the afternoon affords the maximum amount of wind power. Compared to the observational dataset, however, the model consistently under-predicted the magnitude of the wind resource. Custom Weather Research and Forecasting (WRF) runs were simulated with varying boundary and surface layer parameterizations in hopes of improving model performance. Unfortunately the WRF simulations provided little improvement to the NAM simulations. The inherent variability within the resource, coupled with the complex terrain in the region, poses quite a challenge when trying to forecast the surface winds. Improving terrain representation within the models or even developing custom models designed specifically to predict the wind may provide the most accurate wind forecasts.

VARIABILITY OF THE WIND RESOURCE IN WYOMING

By

George Randolph

A thesis submitted to the Department of Atmospheric Science

and the University of Wyoming

in partial fulfillment of the requirements

for the degree of

MASTER OF SCIENCE

in

ATMOSPHERIC SCIENCE

Laramie, Wyoming

May 2012

ACKNOWLEDGEMENTS

I would like to thank the committee for all of their help, guidance and support. Their insightful comments and suggestions proved to be invaluable.

I would like to thank my advisor, Dr. Thomas Parish, without whose constant encouragement, counsel and patience this work would have never come to fruition. His door was always open. For this, I am nothing less than grateful.

I would like to thank my parents, Henry and Anita Randolph: always willing to listen, always providing perspective.

TABLE OF CONTENTS

LIST OF TABLES

LIST OF FIGURES

Chapter 1: Introduction

During a speech on 30 March 2011, President Obama said "We cannot keep going from shock when gas prices go up to trance when gas prices go back down. We can't rush to propose action when prices are high, then press the snooze button when they go down again." Indicative of the energy policies of the last five presidents, the time has come to implement real and permanent change. We've stayed in bed too long. It's time to get up.

Wind is a continuous meteorological phenomenon, among the most viable forms of renewable energy. The 1973 OPEC oil embargo spurred commercial scale wind turbine research and development, but those efforts dwindled when oil prices stabilized in the 1980s (Madrigal 2011). As a result, in the last thirty years, Americans have settled into a state of complacency, apathy and even denial. Establishing general awareness and requiring clear, feasible solutions will pave the way towards safer and cleaner energy independence (Krauss 2011).

Wyoming, in particular southeastern Wyoming, is one of the windiest places in the US, owing to its unique combination of elevated terrain and conveniently aligned geography. It is this region that is home to the lowest point of the Continental Divide between Montana and New Mexico. Air, moving eastward from Nevada and Utah, takes the path of least resistance and prefers to flow through this passageway, aptly labeled the "wind corridor" by Kolm (1977). Not only does the air travel through this area with remarkable consistency, but the mountain ranges to the north and south act like a funnel, further intensifying the wind, especially in the wintertime (Martner and Marwitz 1982). As such, the wind corridor presents itself as a prime location for wind turbine installations and indeed, has witnessed a staggering

outpouring of turbine development in the last decade (Brockhouse 2008). Simply knowing that this region is windy, however, is insufficient.

Möhrlen (2004), Shaw et al. (2009) and Müller (2011), among others, have attested to the poor simulation of the 10 meter (m) wind by numerical weather prediction (NWP) models-- they are designed to predict the weather, not the wind. Most wind turbines in operation today stand at a height of 50 m. Since most automated weather stations, like those used by the National Weather Service, do not measure the wind at 50 m, it must be interpolated to that height. The uncertainty in measuring or simulating the wind at 10 m propagates when calculating the wind at the turbine's height of 50 m. In estimating a region's potential for wind energy, often the quantity of wind power density (WPD) at 50 m, not wind speed, is used. WPD is proportional to the cube of the wind speed. Errors in the 10-m wind speed get amplified when interpolating to 50 m and mushroom when calculating WPD. Thus, it becomes critical to accurately measure and simulate the wind at 10 m.

Advocates for improved wind forecasts, including Cutler et al. (2009), Bessa et al. (2011), Marquis et al. (2011), and Foley et al. (2012), claim that all parties directly and indirectly affected by the wind will benefit from the ability to accurately forecast the wind. Wind farm developers' profits are directly proportional to their capacity to correctly predict how much power they will deliver to the grid (2008). Knowledge of local wind patterns could help air quality controllers efficiently site industrial plants to prevent unwanted pollutants from blowing into residential areas. These serve as just two of the many reasons to improve wind forecasts.

The geographic features responsible for the intense wind speeds observed in southeastern Wyoming, may also be the cause of inaccurate wind simulations. Because of the coupled nature of wind speed and terrain, an incorrect rendering of one directly affects the other. The limitation that wind speed can only be measured to the nearest meter per second (m s^{-1}) hampers a wind developer's ability to obtain a detailed snapshot of an area's power potential. Recalling the cubic relationship of wind speed to wind power, the difference of just a few m s^{-1} can significantly impact WPD, especially at higher wind speeds. Table 1.1 illustrates two examples: increasing the wind speed from 10 to 12 and from 20 to 22.

Table 1.1: Illustration of the sensitivity of wind speed to wind power.

Wind Speed	Wind Power $\propto$ (Wind Speed)^3	Increase
10	1000	1.73X
12	1728	
20	8000	2.5X
22	10648	

Even with this simple example, the sensitivity of wind speed to wind power becomes apparent. Just a two m s^{-1} difference can increase the potential WPD by a factor of 2.5. Accurate wind speeds, both simulated and measured, are essential for efficiently implementing this energy resource.

The wind, like most meteorological phenomena, operates within several time scales, or modes. Ascertaining the annual, seasonal and diurnal variability of the wind is the first

step in understanding how best to use the resource. The next step is investigating the atmospheric and geographic features responsible for these modes and the physical reasons why some modes may be more dominant than others. Statistical analysis of wind speeds at various locations illustrates persistence of resource and helps wind developers make informed decisions about where to build wind farms.

Model and observational data of Wyoming for the years 2008-2010 were analyzed to determine these modes of variability. To assist with this, model output of WPD was mapped at annual, seasonal and diurnal intervals. Observational WPD was plotted at several locations around Wyoming and compared with model output. Errors associated with interpolating the wind to 50 m were also analyzed. Fast Fourier Transforms were employed to study the modes of variability from a frequency standpoint and further validate the behavior observed in the WPD maps. Probability distributions were generated to investigate the variability of the resource of both the model and observational datasets. In efforts to improve model performance, custom Weather Research and Forecasting (WRF) model simulations were run with varying boundary layer and surface layer parameterizations. Initial results show that accurate wind forecasts depend heavily on improving these parameterizations. Hopefully, the knowledge gained from this study will further advance the integration of wind into the country's power supply and perhaps eventually quench the country's thirst for oil and satisfy the country's appetite for coal.

Chapter 2: Background Information

2.1: Brief History of US Wind Power

Towards the end of the Industrial Revolution, America was at a crossroads. The past eighty years had witnessed an outpouring of technological innovation, propelling the young country into the modern era with the likes of Britain and Western Europe. Standing on the cusp of yet another revolution, the United States needed to make a decision: how was it going to power itself into the twentieth century? Though many would be surprised to learn, up to that point, both renewable and "traditional" energy sources had evolved equally. The city of Pittsburgh, Pennsylvania served as an, albeit hazy, example of the promise of coal. Six hundred miles to the northwest, the city of Lowell resided at the other end of the spectrum of energy possibility. Situated on the shores of the Merrimack River in upstate Massachusetts, Lowell was the second largest city in the state and home to the largest factories in the country. And the striking thing about Lowell was its cleanliness. Waterwheels powered factories and the only coal that made its way into the city was delivered by *Santa Claus*. In Pittsburgh, however, "[i]f a sheet of white paper lie upon your desk for half an hour you may write on it with your finger's end through the thin stratum of coal dust that has settled upon it during that interval" wrote Peregrine Prolix, a traveller from the South (Madrigal 2011).

Water was not the only fluid whose power was being harnessed. Windmills began springing up all across the Midwest in the latter half of the nineteenth century. In fact, it was the advent of windmills that allowed frontiersmen to pioneer the West. Though temperamental buffalo and unfriendly natives concerned these settlers, it was lack of water that usually introduced them to their Maker. But "[i]t was the acre or two of ground irrigated

by the windmill that enabled the homesteader to hold on when others had to leave. It made the difference between starvation and livelihood" wrote Walter Prescott Webb (Webb 1931). Installation of a windmill allowed a family to live on a plot of land that received less than twenty inches of rain per year. Besides the stove, the windmill was the most popular personal mechanical power source of the nineteenth century. Windmill density was directly proportional to population density. The population of Nebraska, for example, grew from 127,000 to 450,000 during the decade of the 1870s. Contrasting the hundreds of windmills that peppered the landscape, understanding of the math and science of their operation was curiously absent from their owners' minds. During this time, function trumped scientific appreciation, which is why sometimes jerry-rigged windmills outperformed expensive production-line models. Not to say that these "MacGyvered" windmills were any more efficient than their commercial counterparts. All windmills in use at the time were atrociously inefficient. But that did not matter so long as they worked properly (Madrigal 2011).

Jump ahead one hundred years when Palmer Putnam, a MIT trained geologist and son of printing tycoon George Putnam, had the idea of building a windmill not to pump water out of the ground, but to pump electricity into the grid. Putnam envisioned a turbine with seventy-five foot blades which would produce more than a megawatt of power and, in Putnam's words, would "generate alternating current [which] might reduce the power bill" (Madrigal 2011). Dwarfing any turbine of the day, Putnam's design also called for hydropower to smooth out the inherent variability of the wind. Ironically, it was not the size of the turbine that presented the greatest challenge, but rather the lack of data available to corroborate design decisions. Though the National Weather Service was seventy years old,

the first US radiosonde launch only occurred a few years before, in 1937 (Christopher A 2009). As such, data about how strong, what direction and how consistently the wind blew did not exist. A place called "Grandpa's Knob" near Castleton, Vermont was finally selected as a test site, not because it was deemed an optimal location but because of time constraints and the fact that it "seemed like a pretty good spot" (Madrigal 2011).

Though construction was not without its setbacks, on 29 August 1941 the world's first megawatt turbine began spinning, a mere eighteen months after it had been conjured up in Putnam's head. This marvel of engineering remained in operation for the next four years until 26 March 1945 at 3:10 AM when one of the blades broke off and hurdled through the air, landing 750 feet away from the turbine.

This tragedy played right into the hands of Putnam's detractors. Within six months, the S. Morgan Smith Company, sponsors of the project, ran out of money and shut down their wind energy division. Eventually the turbine was dismantled. Even Putnam, years later, in a report written to the Atomic Energy Council in the 1950s, advocated an power repository based on atomic and solar energy.

But like the successful failure of Apollo 13, Putnam's work paved the way (and indeed was the only road) for future research and development in wind energy. During the energy crisis of the 1970s, engineers rediscovered his work, which served as the only groundwork for large scale wind turbines. The state of wind energy today is due, in large part, to the pioneering work of Palmer Putnam, a man who had the vision and courage to see what could be rather than what was. A cellphone tower now occupies Grandpa's Knob, but the "foundation of the great wind machine remains" (Madrigal 2011).

2.2: Current State of Wind Power

The revitalization of wind energy in the 1970s was the result of what Clifford Krauss of *The New York Times* has called the "foreign policy version of the movie 'Groundhog Day.'" He writes:

> [Imagine] Bill Murray playing the president of the United States. The alarm clock rings. Political Mayhem is again shaking the Middle East, crude oil and gasoline prices are climbing, and an economic recovery is under threat.
> President Nixon woke up to the same alarm during the 1973-74 Arab oil embargo and declared Project Independence to end the country's dependency on imported oil. President Carter, during the Iranian revolution called an effort to reduce dependency on foreign oil "the moral equivalent of war." President George W. Bush called oil an addiction (Krauss 2011).

President Obama followed with similar rhetoric in a speech given in March of 2011 about the necessity of smart and reliable energy policy. It seems that the enthusiasm and initiative for wind energy (and other renewables) is as variable as the wind itself. But the ebb and flow of government support for renewable energy only assures its status as a supplementary source of energy at best. To enact a more permanent policy requires guts, know-how and a little luck. Change is hard: that's probably why it doesn't occur very often. So to appreciate the hurdles that wind must overcome, it is helpful to understand what has been accomplished and what needs to be accomplished.

While running for president, Barack Obama mandated that by 2012, 10% of domestic electricity would be generated by renewable sources of energy. That goal was met in 2009 and today nearly 13% of domestic electricity is generated from renewables. Regarding wind energy, in the last decade, installed worldwide wind capacity has increased four fold from

24.3 gigawatts (GW) to 203 GW (Foley et al. 2012). Currently, wind energy alone accounts for nearly 3% of total US electricity generation (2010). Though promising, a 3% dent in the domestic electricity supply will not have much long-term impact. Several studies were conducted to investigate the feasibility of large scale wind integration within the United States before mid-century.

2.3: Past Wind Power Studies

Marquis et al. (2011) summarized the results of the Eastern Wind Integration and Transmission Study administered by EnerNex, an energy consulting firm headquartered in Knoxville, TN. This study focused on the eastern portion of the US and investigated the feasibility of generating 20% of domestic electricity by 2024. The Western Wind and Solar Integration Study, completed in May of 2010, looked at the possibility of a combination of 30% wind and 5% solar in the western portion of the US including Arizona, New Mexico, Colorado, Nevada and Wyoming (GE 2010). In the remaining western states, the report stipulated a 20% wind and 3% solar energy supply. In 2008, the US Department of Energy examined the feasibility of generating a 20% of electricity from wind by 2030 (2008). All of these reports deemed that meeting such lofty goals was possible, assuming a few changes were made.

The "20% by 2030" report estimates this project would require 305 GW of onshore wind and 54 GW of offshore wind which would cost $43 billion. This cost translates to about 0.06 cents per kilowatt hour (kW-hr) or and additional 50 cents per household per month. But the added benefits of such a sensible energy strategy surely outweigh the minimal costs

imparted to the consumer. "20 % by 2030" would reduce annual electrical sector CO_2 emissions by 825 metric tons. The electricity sector's water use would go down 8% which would save 11 trillion gallons annually. Emissions of sulfur dioxides and nitrogen oxides, the byproduct of fossil fuels, would be dramatically reduced. Wind would displace natural gas consumption by 11% and substantially reduce the use of coal fired power plants, thereby decreasing the emissions from mercury and diminishing the acidification of lakes and streams (2008).

With such a formidable increase in the number of wind turbines, the electrical grid would need to be updated to handle the additional load. As it stands now, the electrical grid is antiquated. There are three sections or "interconnections" that make up the grid: the eastern interconnect, the western interconnect and the Texas interconnect. Whenever electricity needs to cross between any of the three borders it must be converted from AC to DC, transmitted to the new interconnect and then transmitted back to AC (Boyle 2007). Put another way, if the interstate highway system worked like this, you would need to pick up your car and carry it 400 yards to cross each state border. Worse yet is the "chicken and the egg" conundrum plaguing wind developers and transmission operators: wind developers will commit to building a new wind farm if they know transmission lines will be built and transmission operators will install new lines if they know that a wind farm will be installed (2008).

In conjunction with an updated grid, these reports also dictate the need for additional balancing authorities (BA). A BA is an entity that balances supply and demand of electricity throughout the grid. Supplementary BAs would lower the overall cost and increase reliability of large scale wind farms (GE 2010). The best thing about enhancing transmission lines,

however, is that the wind energy industry would not be the sole benefactor: all entities connected to the grid, both industrial and domestic, would benefit.

A common theme throughout all three reports and perhaps the most critical hurdle to overcome is improving wind forecasts. Any significant integration of wind energy into the US electricity supply demands accurate knowledge of both the current and future states of the wind. An excerpt from "20% by 2030" summarizes:

> Improved short-term wind production forecasts let operators make better day-ahead market operation and market commitment decisions, help real-time operations in the hour ahead and warn operators about severe weather events. Advanced forecasting systems can also help warn the system operator if extreme wind events are likely, so that the operator can implement a defensive system posture if needed (2008).

In addition to the challenges of upgrading the grid and improving wind forecasts, the American Wind Energy Association (AWEA), an industry trade group which represents all major players within the wind industry, highlighted areas they considered in need of advancement (Marquis et al. 2011):

- expanded observational datasets
- deployment of rapid refresh, high-resolution weather models
- further boundary layer research
- creation of a data repository

AWEA argued that, like upgrading the grid, developing rapid update, high-resolution weather models would not just benefit the wind industry but also the surface/ air transportation sectors, fire safety and air quality industries, other weather organizations and even homeland security. Bouts of good weather, like a person's health, are taken for granted; only when the weather

turns bad do people take notice.

2.4: Importance of Wind Forecasts

The need for accurate wind forecasts is rooted in the basic functionality of the grid. The wind is variable, meaning that the power generated from it is variable (Foley et al. 2012). The grid is designed to accommodate invariable supplies: find coal, dig it up and store it. When demand increases, burn more coal. In this sense, the grid is demand oriented and demand is relatively easy to predict (Ernst et al. 2007). For example, the television show *M*A*S*H* was exceedingly popular and the day the series finale aired, grid operators knew they would need to supply electricity to meet the demand of thousands of televisions. But with wind, this theory of operation is no longer valid. It is not possible to store the wind and so supply becomes the limiting factor. In fact, wind is the first non-storable primary energy resource to be widely deployed within large scale power systems (Cutler et al. 2009).

Both grid operators and wind forecasts are associated with timescales. The various timescales system administrators operate on are as follows (Möhrlen 2004):

- ultra short range (0-9 hours): also referred to as "nowcasting" this timeframe is important for electricity trading within energy markets and for the prevention of mechanical damage of the turbine.
- short range (0-48 hours): this timeframe is required for power system planning and unit commitment.
- medium range (3-5 days): within this timeframe, operators plan for plant, system and grid maintenance as well as storage management.

Accurate forecasts on all of the timescales is needed, no one being more important than the next. A nightmare scenario would be a grid operator shuts down a wind farm for maintenance only to be delayed because of an unanticipated wind storm. Accurate wind forecasts will help system operators avoid such economically costly mistakes.

Since wind is variable, traditional methods of generating electricity must be employed to ensure that supply equals demand. In an electric grid, this fundamental economic principle must hold true at all times (Ernst et al. 2007). The idea is that, if demand increases and there is not enough wind, fossil fuel plants must supply the difference. When it is windy, the plants shut down. But within this basic framework, grid operators have several factors to consider. When running at optimal capacity, fossil fuel plants produce the maximum amount of energy and the minimum amount of CO_2. Reducing this capacity results in lower thermal efficiency (Marquis et al. 2011). However, it can take up to twelve hours to reboot a plant from a so called "cold start." It is much faster to increase production of a plant that is already running at a low capacity (Cutler et al. 2009). The challenge, then, is to maximize plant efficiency and minimize cost. Improved wind forecasts will help operators strike this balance. Knowledge of the current and future state of the wind will allow the grid operator to optimize the ratio between wind and fossil fuels, thereby ameliorating the dispatch, scheduling and unit commitment of BAs (Foley et al. 2012). This removes the need for unnecessary reserve power, further reducing cost (Marquis et al. 2011).

Arguably the most vexing characteristic of the wind with which system operators must contend are ramp events: large and fast changes in grid supply over a short period of time which impose significant challenges to other system resources (Cutler et al. 2009). As was

stated, the grid is just as unhappy with a surplus of electricity as it is with a deficit. These ramp events may be caused by large thunderstorms/ weather systems, boundary layer processes such as vertical mixing, diurnal heating, terrain effects, thermally forced flows like sea breezes and drainage flows and the diurnal development of low level jets. Because these ramp events operate on short time scales, they mostly impact the day-to-day market trading of electricity. Improved short-term wind forecasts would allow a more competitive energy market trading strategy to unfold, more attuned to the variable nature of the wind (Marquis et al. 2011). Ramp events may also damage wind turbines. For safety reasons, wind turbines are designed to shut down when the wind speeds surpass a certain value. If the wind speeds of forthcoming ramp events are known, operators will be better equipped to prevent damage to the turbine (Manwell 2009).

Up to this point, grid operators have gotten all the attention, but wind companies actually have the largest financial stake in wind energy. As such, it is imperative that the two groups be separated. Wind farm owners participate in electricity trading within the energy market and load operators are responsible for balancing supply and demand throughout the grid. There is an underlying economic incentive to make money. Here is how it works:

- The wind company bids a certain amount of electricity each day (typical until noon) for every hour of the next twenty-four hour period. So until noon each day, the wind company is bidding on energy it will produce for the next day.
- If the actual energy generation is above the market bid, the excess is paid at a discounted price. This price can actually be negative, representing a cost to the wind company.

- If the actual energy generation is below the market bid, a penalty is assessed according to the cost of the amount of energy the system operator needs to purchase to compensate for the deficiency.

Each market specifies its own rules for calculating penalty costs (and in some markets, no penalty is assessed for overbidding) (Bessa et al. 2011). This is obviously a simplified explanation of electricity trading, but even this elementary viewpoint highlights the value of accurate forecasts to wind companies. If wind farm developers are able to accurately forecast the wind, their profits increase.

Between the penalties assessed for incorrect bidding and the costs related to keeping BAs online, accurate wind forecasts have the potential of saving upwards of $2.5 billion annually (Marquis et al. 2011). But given the fundamentally different motivations between grid operators and wind companies, the criteria for "accurate" forecasts may be in direct conflict with each other (Bessa et al. 2011). This begs the question of how to improve forecasts and satisfy everyone who is involved.

2.5: Methods of Predicting the Wind

The "forecast horizon" is the period between the time that the forecast is available and the forecast point in time (Marquis et al. 2011). Three terms are used in assessing an area's potential for wind power (Landberg et al. 2003):

- atlas: a collection of regional wind climates for a large area
- regional climate: a collection of wind statistics, temporal and spatial, of variations of wind speed reduced to standard conditions

- resource: the actual long-term kinetic energy content of the wind at a specific location and height

There are three basic methods for predicting the wind resource (Ernst et al. 2007):

1. Physical Approach: describes the physical process of converting wind to usable power by modeling all the steps involved.
2. Statistical Approach: describes the direct correlation between the predicted wind and the corresponding power by statistical analysis of past time series of wind speeds (has certain elements of a "black box" method).
3. Learning Approach: artificial intelligence is used to learn the relationship between predicted wind power and actual power output from past time series in efforts to more accurately predict future scenarios.

The first method utilizes numerical weather prediction (NWP) models to forecast the wind. This has been the most common method of predicting the weather (and the wind) since the advent of the computer in the mid-twentieth century. The last two methods require significant amounts of past data to establish verifiable relationships between the past and the future; datasets this large are not always available. The third method is a newcomer to the field of wind (and for that matter, general weather) prediction (Foley et al. 2012).

Cutler et al. (2011) describe six desirable traits of a forecast:

1. output at least one plausible wind outcome
2. provide information on the time varying forecast uncertainty
3. provide multiple representative scenarios formulated from a series of NWP model runs which produce different future and plausible evolutions of the atmosphere

4. provide multiple representative scenarios formulated from plausible displacement errors in a single NWP model run
5. provide representative scenarios containing sub-hourly information
6. provide clear and concise representative scenarios for aggregated wind power generation from multiple wind farms

At the very least, the authors assert, a forecast should provide information about its uncertainty, provide multiple outcomes based both of several different model runs and based on the error propagation of those model runs. Sub-hourly information is needed for energy day trading purposes and grid maintenance.

Unfortunately, the quality or "goodness" of the output of a forecast with these traits is not as easy to critique. A common belief is that forecast quality is related to the error: the higher the error, the worse the forecast and vice versa. Bessa et al. (2011) argue that "the "goodness" of a forecast should be strongly related to the use given to it." Meteorologists are not the only people who use wind forecasts: system operators and wind farm developers also analyze wind forecast output. All three groups may have contrasting underlying objectives in mind when assessing wind forecasts. The errors in these forecasts may also impact these three groups differently. The three types of "goodness" of a forecast, outlined by Bessa et al. (2011) are:

1. consistency: the correspondence between forecasts and forecasters' judgements
2. quality: the correspondence between forecasts and observations
3. value: the incremental benefits (economical or otherwise) when employed by users as input to their decision making process

The third criterion speaks to the central point of the argument. These forecasts affect the decisions of different groups and so their value cannot simply correspond to a single quantitative scoring metric. This is what Bessa et al. (2011) describes as the "forecaster's paradigm." That is, fit the prediction to the observation in a signal processing sense to minimize the error. This mindset places no importance or consequence of the nature of the errors and whom those errors affect. They argue that output from a forecast should be described by two paradigms:

- forecaster's paradigm: concerned with the time series, signal processing aspect of the forecast and therefore with the quality of the forecast itself
- forecast consumer's paradigm: focuses on the use given to the forecast and therefore is related to the value of the forecast

Though the difference between these two paradigms, quality and value, is subtle, it is important. For a grid operator, environmental costs may be a nonissue, unlike with wind companies. Conversely, the costs associated with keeping BAs online is inconsequential to wind companies. Bessa et al. (2011) continues, contending that

> [F]orecasts must be appreciated in the framework that decision making is carried out by multiple agents and that agreement may not be possible among agents [companies and operators] regarding what constitutes a "good" forecast. [For example], the relationship between forecast error and market profit occurs in situations involving more complex forecasting systems and electricity market rules (Bessa et al. 2011).

Decisions made based on the forecast are arguably just as important as the quality of the forecast itself. Care should be taken during development of wind forecasts to ensure these aspects are not omitted or, at the very least, considered.

Information relating to the various trends in the wind is needed to determine a site's wind power potential (Marquis et al. 2011):

- diurnal
- seasonal
- annual
- decadal/ climatological

These trends span all the timeframes in which grid supervisors operate. The longer trends (annual and decadal) are needed to verify the validity of the data (*i.e.* confirm the data are representative of the area).

Several methods exist for obtaining this data, as outlined by Landberg et al. (2003).

- Folklore: the cheapest, fastest and (usually) method of last resort is to talk to people who live in windy areas. People tend to overestimate wind speeds, however (wind chills tend to make people think that the wind is blowing harder than it really is). Onomatology is a method whereby windy locations are determined by their name (*e.g.* "Windy River Range"). Observing the vegetation of an area may also help determine if an area is windy: if the trees are perpetually bent, chances are there is a goodly amount of wind. This is the method Putnam used to determine the location for his turbine.
- Measurements: this method is often used to estimate the wind resource in a particular area. Once a few measurements are taken, they can be compared to a climatologically representative time series (data for five to ten years) via a simple linear correlation. Though not much data is required for this method, the possibility remains that the correlation between the data and climatology is inaccurate.

- Global datasets: these datasets contain wind, temperature and pressure at several heights in a grid covering the entire globe. These databases are about a decade old (climatologically stable) and can be applied to any location. But because these are global data, the grid resolution is low (on the order of hundreds of kilometers (km)).
- Wind atlases: in countries with an established network of observation stations, this is the preferred method of resource assessment. Different atlases can be compared and understood by a large community. The scales on which this method works are reversible: output can either be a generalized regional wind climatology or the wind climatology at a specific location (see Figure 2.1).

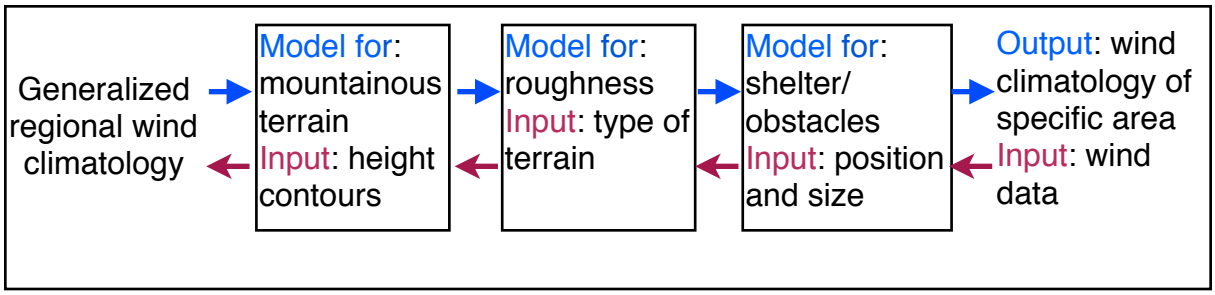

Figure 2.1: Various scales for wind atlas data acquisition method (adapted from Landberg et al. 2003).

- Computational Fluid Dynamic (CFD) models: these are models primarily used by the engineering community, but within the last decade have been applied to wind farms and prediction. Wind flow over rough, complex terrain is difficult to simulate in conventional NWP models, owing to the interaction of the surface winds with the topography. A finer scale CFD model perhaps may reduce simulation errors and improve accuracy.
- NWP modeling: this is one of the most popular methods of obtaining data for assessing wind potential, especially since computational power has made significant strides in the

last decade. Areas of a few hundred kilometers are typically modeled.

All of these methods are used in combination with one another in hopes of producing the most accurate and detailed wind assessment of the site of interest. Though it can be argued that one method may be superior to another, fundamentally the goal is to determine a site's wind power potential. Consequently, these methods are merely just tools to help achieve this objective.

Once the necessary data has been acquired, forecasting of the wind can begin. Recall, there are three basic categories of wind forecasts: statistical, learning and physical. Since statistical analysis forms the basis of two of these approaches, it suffices to briefly explain their operation under the same umbrella (Ernst et al. 2007).

Statistical methods employ a general class of models such as auto regressive moving averages and auto regressive integrated moving averages to identify patterns in past behavior used to predict future states. The simplest method is called the persistence method: "The average wind speed for the next hour is equal to the average wind speed over the current hour" (Kavasseri and Seetharaman 2009). Converting from wind speed to wind power only requires a single step and so this process is sometimes referred to as a "black box" (Foley et al. 2012). Recent statistical analysis revealed that temporal variations of averaged hourly wind speeds were stochastic (random). As such newer, more sophisticated statistical models are being developed, hence the interest in adaptation of artificial intelligence (Kavasseri and Seetharaman 2009).

Physical methods generally make use of global databases of meteorological data or employ NWP models. At its core, a weather model is a computer program that rapidly solves the so-called primitive equations governing the dynamics of the atmosphere to predict its state

at a future time (the forecast horizon). Equations from the realm of fluid mechanics describing the conservation of momentum, energy and mass as well as the ideal gas law comprise the set of primitive equations. These equations are discretized in time and space and describe how air is affected by pressure gradient forces (forces due to pressure imbalances) and the Coriolis force (the apparent force felt due to the rotation of the Earth) (Möhrlen 2004).

The scale of these models generally falls within two categories: synoptic and mesoscale. In atmospheric science, the synoptic scale (hundreds of kilometers) encompasses larger weather systems while the mesoscale (kilometers to tens of kilometers) describes smaller phenomena like thunderstorms and orographic flows. Although strong winds can be caused by events at both these scales, wind turbines (and wind farms for that matter) span distances significantly less than synoptic scales. Thus the popularity of using mesoscale models for forecasting wind. This comes with a cost: the higher the resolution of the model, the more computational power it requires (Foley et al. 2012).

Regarding resolution, there are two techniques to aid in the compromise forecasters make between accuracy and computational power. For reference, increasing the spatial resolution from 2 km to 1 km over the same geographic area increases the required computational power by a factor of ten. Upscaling involves applying high-resolution data in a small geographic area over a larger domain in efforts of reducing the time and effort of forecasting. Wind power output from a sample number of wind farms forms the basis of a reference dataset. Model output can then be averaged over an entire region using only the reference dataset. Downscaling is essentially the opposite: taking coarsely spaced data over a large area and applying it to a smaller, higher resolution domain. Global climate models, for

example, have rather coarse resolution. The output from these models is typically downscaled so it can be analyzed in the context of a specific geographic region, say near a wind farm. Wind speeds from low-resolution models can be downscaled via statistical means using wind observations at actual wind farms in combination with NWP output (Foley et al. 2012).

The modeling region is divided into boxes or grids, the size of which is sometimes at the forecaster's discretion. The state variables (pressure, temperature, humidity and wind) in the primitive equations to describe the state of the atmosphere are calculated at each grid point and then mathematically interpolated to "fill in the gaps" between grid points. Simulations for the entire globe have coarser grid spacing than mesoscale simulations run in an area of only a few square kilometers. The terrain in these models is typically "hard coded" into the model: the topography is a vast matrix, proportional to the resolution of the model, of elevations at certain latitude and longitude coordinates. A higher resolution model will have more topographic information bounded within the model.

Parameterization is a mathematical method of representing processes that are too small in scale to be accurately represented within a model-- *i.e.* processes that occur between grid points which are essentially invisible to the model (Foley et al. 2012). With regards to the boundary layer, vertical diffusion of turbulent fluxes is generally too small to be captured by NWP models. To compensate for this, the time evolution of turbulent fluxes is determined by solving vertical diffusion equations. These equations relate the sub-grid time dependence of turbulent fluxes with the state variables (Shin and Hong 2011).

NWP models, particularly of the mesoscale variety, can either be run hydrostatically or non-hydrostatically, depending on, among other things, model resolution. The hydrostatic

assumption is valid so long as the horizontal length scale is greater than the density scaled height of the atmosphere (Möhrlen 2004). In other words, the hydrostatic assumption neglects vertical accelerations. Assuming the troposphere is ~8 km high and knowing that the smallest feature a NWP can resolve is four times the horizontal grid spacing, the hydrostatic assumption is reasonable for model resolutions no smaller than 2 km. At finer scales with nontrivial vertical motions, the hydrostatic assumption is no longer valid. Depending on the model, the forecaster can choose to run the simulation hydrostatically or non-hydrostatically (Möhrlen 2004).

The selection of a NWP model is a critical step and can impact the quality and value of the output depending on how the forecast will be used. Model characteristics to consider include geographic area, temporal and spatial resolution, forecast horizon and the number of simulations and the corresponding computational time required (Foley et al. 2012). Once these model attributes have been chosen, the simulation can begin. The current state of the atmosphere obtained from observations is input to the model. Upon completion of the simulation, the wind forecast can either be upscaled or downscaled across various forecast horizons depending on the situation (Ernst et al. 2007).

2.6: Information About Mesoscale Models

Current mesoscale NWP models are a useful tool for wind forecasters and model accuracy continues to improve. Shaw et al. (2009) describes the valuable traits of mesoscale models to the wind industry:

- help identify optimal sites for wind farms

- evaluate impact of turbines on local meteorology
- capture qualitative aspects of diurnal phenomenon like low level jets, thermally driven circulations near complex terrain or coastal areas and the overall structure of the boundary layer
- aid in mapping the wind resource and the subsequent assessment of the wind resource in a particular region

But these models are not without their limitations:

- timing and magnitude of mesoscale phenomena are frequently incorrect
- strength and structure of turbulent mixing, especially under stratified (stable) conditions remains poorly represented

Shaw et al. (2009) continues, stating that "these weaknesses arise from fundamental gaps in our knowledge of the boundary layer."

- inadequate representation of the boundary and surface layers, especially under unsteady conditions over complex topography
- in complex terrain, the flow may become separated, creating areas of zero flow dominated by eddies. This can lead to a loss of kinetic energy not accounted for in classical fluid mechanics equations. Flow separated at steep slopes creates less terrain induced acceleration
- parameterization of turbulence in boundary layer pose computational challenges stemming from inadequate measurements of the boundary layer

The challenge, again, is to strike a balance between resolution and capturing these details in the boundary layer pertinent to wind energy, but doing so with a reasonable amount of

computational time. A sub-kilometer resolution model is worthless if simulations take years to finish (Shaw et al. 2009).

Since NWP models are sensitive to initial conditions, a method called ensemble forecasting may be implemented to address some of the primary sources of error within a single NWP model (Cutler et al. 2009):

- vary initial conditions
- vary underlying physical assumptions used to make forecasts

It has been shown that, when several NWP forecasts are used, the overall error decreases, especially when combined for day ahead forecasting. The computational requirements for ensemble forecasting, however, increase because of the additional amount of simulation. But, one added benefit of ensemble forecasting is that it provides an estimation of the reliability of the forecast. Extreme variance between different model runs implies uncertainty in the forecasts. When the variance between forecasts is low, the uncertainty is correspondingly low (Foley et al. 2012).

Several studies have been conducted to investigate the correlation between accuracy and model resolution. It has been assumed that the relationship between forecast error and model resolution is inversely proportional: increase the model resolution and the error decreases because the model is now able to capture additional small scale motion which was otherwise omitted. However, Rife and Davis (2005) contend that, after objectively analyzing several high-resolution models, the added benefit is not supported by the results. The biggest benefit to high-resolution models is to "resolve the statistics of different scales of motion... translating to improved forecasts of temporal variance, with the implication that the growth of

errors is more realistic in the finer resolution." Cutler et al. (2011) describes the effect of misplacement errors on high-resolution models. Misplacement errors are associated with a phase (timing) discrepancy associated with the passing of some meteorological feature over particular grid points (*e.g.* a synoptic system predicted to pass through an area at 6:00 but did not pass through until 7:00). When going to a finer resolution, these misplacement errors get amplified because the density of grid points increases. Rife and Davis (2005) conclude by urging that the "understanding of errors and systematic progress toward model improvement must have a phenomenological basis. To argue otherwise is to segregate weather prediction from weather itself."

In general, error increases with the length of the forecast horizon (Foley et al. 2012). The sources of these errors, however, is incredibly difficult to pinpoint. Nonetheless, it is useful to separate forecast errors into two groups: local and nonlocal.

- Local errors, according to Möhrlen (2004), "are constant over the prediction horizon and are mostly a result of the inaccurate surface representation in the model system." These errors can be classified as model bias, since the accuracy of the surface parameterizations depend on the horizontal resolution.
- Nonlocal errors are meteorologically motivated, signifying the limits to which the atmosphere can be predicted. These errors can be the result from a lack of observational data to provide accurate initial condition scenarios or simply deficiencies within the NWP model leading to unrealistic error growth.

Most NWP model errors are of the nonlocal flavor and as a consequence, cannot be attenuated with statistical or physical corrections (Möhrlen 2004). Other sources of errors within NWP

models include (Müller 2011):

- uncertainty in initial conditions
- uncertainty in parameterizations of the model
- uncertainty due to the model's discrete representation of the physical world
- temperature and wind computed at various intra-grid locations have no real world comparator: the location in the model is not where the observation took place

These error sources differ on a daily basis, depending on the general flow or "mood" of the atmosphere. But of the many sources of errors, perhaps the most serious for wind farm operators are phase/ timing errors of frontal passages. These synoptic events generally supply considerable wind resource. Thus, the time at which they pass by wind farms becomes critical for accurately delivering power to the grid (Möhrlen 2004). Fortunately, larger wind farms tend to have lower overall errors because of cancelation effects. In a large wind farm, one sub-region may over-predict the wind and a different sub-region may under-predict the wind. In effect, these two errors negate each other (Ernst et al. 2007).

2.7: Past Wind Resource Assessments

Given all this information about how the electrical grid operates with variable sources of electricity, how to obtain wind data and how NWP models and other mathematical tools are used to generate wind forecasts, actual wind power assessments can be made. Too numerous to detail, five wind resource assessments are summarized: Arizona, Appalachian Mountains, South Africa, Denmark and Wyoming.

In 2006, Arizona specified a new Renewable Portfolio Standard (RPS) that by 2025,

15% of the state's electricity would come from renewables. A RPS is a state regulation specifying a percentage of electricity that must come from renewable sources of electricity such as wind, solar, biomass or geothermal. The Arizona wind resource assessment (WRA) conducted in 2003 has proved invaluable as the state overhauls its energy strategy to meet this goal. Surface and upper air data were collected at several locations statewide which served as the basis for the WRA. Geographic Information System (GIS) software analyzed this data and generated a 4-km resolution map of the state. (A GIS provides a succinct way of presenting and interpreting a variety of geographic data). Each 4-km region, accompanied by the Wind Energy Resource Atlas of the United States, was evaluated for wind energy development based on the following criteria:

- wind power resource potential
- distance to transmission lines and substations
- distance to roads
- land use and ownership
- tribal reservation information

This study revealed that mountainous regions in the north and south provided the best wind resource in the wintertime. These areas contain 26,695 megawatts (MW) of developable wind. This translates to a consumer price of 5.2 to 7.5 cents per kW-hr (in 2005 dollars), depending on the wind speed (Acker, Williams et al. 2007).

Between 2002 and 2005, data from nine ridge top stations along the Appalachian Mountains near the Tennessee-North Carolina border was collected 50 m above the ground. Figure 2.2 outlines these locations. These areas exhibit annual average wind speeds of 5.5 to

7.4 m s^{-1} translating to 50 to 74 million kW-hr of annual energy output. Winds in this region blow from the west, orthogonal to the Appalachians, accounting for the northeast-southwest linearity of the stations. Strong diurnal and seasonal cycles distinguish this area, the nighttime and winter both exhibiting a 20% increase from the baseline wind speeds. Though the area harbors considerable wind potential, the development of this resource is not without its barriers:

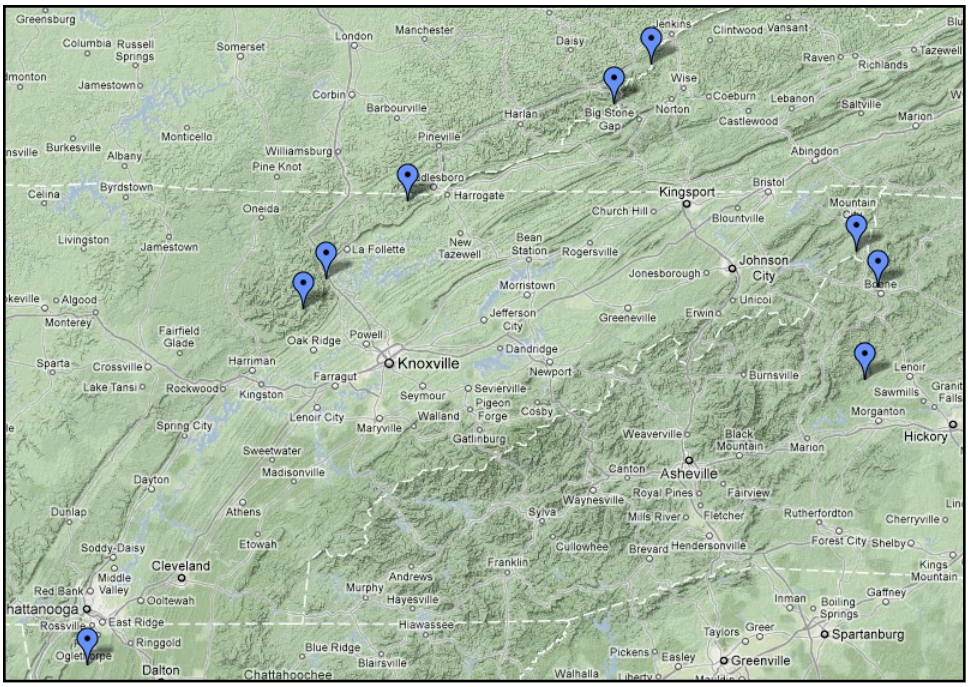

Figure 2.2: Data collection sites for the Appalachian Mountain WRA conducted from 2002-2005.

- already low electricity prices
- installation costs associated with complex terrain
- potential land value for residential development

The low price of electricity makes it difficult to justify new wind projects in this area. However, the cost of electricity could rise and the information gained from this WRA may

prove valuable in the future (Raichle and Carson 2009).

A two dimensional numerical weather model assisted with the 1984 WPA of the coastline of South Africa. Two contrasting locations were selected as case studies, one on the eastern coastline and one on the western coastline, to investigate possible locations for wind turbines. Local wind patterns were evaluated via decadal synoptic weather maps and served as input to the model. After running several simulations, no one configuration suited both locations. This highlights the individuality inherent with WRAs: model output is not "universal" in the sense that the same configuration will work for all areas. Local topographic, synoptic and mesoscale effects must be considered when performing a WRA. In this South African case, the optimal locations for the east coast and west coast was 55 km inland, and 10 km offshore, respectively. The fact that one WRA was conducted at a maritime location and the other near a forested continental region further emphasizes the importance meteorologically oriented, site specific WRAs (Diab and Garstang 1984).

As of 2004, Denmark generates 22% of its domestic electricity from wind, double the target set by the European Union for 2010. This lofty claim, however, is not without its caveats. Current Danish wind forecasts, like their American counterparts, are not without errors. But because of the infrastructure in place, this high integration of wind is able to continue without major hiccups. In the event of power surpluses, the extra electricity is sent to Norway to refill hydroelectric reservoirs. Used in conjunction with wind, hydroelectricity serves as an ideal BA: it is reliable, efficient and renewable. When unexpected short-term electricity deficits occur in Denmark, Norwegian hydropower replenishes the Danish supply. Denmark is also connected to the German and Norwegian grids for assistance during times of

prolonged electrical drought. It must be noted that, without these BAs, the high integration of wind in Denmark would not be economically viable at this time. The intermittent supply of electricity from German and Norway negates the need for a high volume of continuously available reserve power (Möhrlen 2004).

No doubt the growing popularity of wind power in the last decade has benefitted from the early WRAs of Wyoming conducted in the 1980s. The Wyoming Climate Atlas, published in 1986 (Martner 1986), summarized the synoptic and orographic features responsible for the tremendous wind resource in the state. Wind measurements amassed from airports, National Weather Service stations and research project sites functioned as the basis of the dataset. Annual, seasonal, monthly and hourly trends of wind speed and direction were determined at various locations across the state. A strong diurnal cycle dominated most locations throughout the year, and in the southeast corner of the state, the wintertime exhibited the highest yearly wind speeds (Martner 1986). Field campaigns utilizing research aircraft were flown to study the interaction between wind flow and topography in southeastern Wyoming. The first 1 km was profiled via soundings launched near the research site (Marwitz and Dawson 1984). Several wind turbine related experiments were also conducted in the southeastern corner of Wyoming. The wind speeds in the wintertime are about a factor of 1/2 greater than those observed in the summertime. During the day, the minimum wind speeds occur during the morning and reach their maximum in the afternoon. During the night, wind speeds increase significantly with height. This behavior gradually tapers off beginning at sunrise. The winds blow primarily from west to east owing to the local topography (Martner and Marwitz 1982).

Chapter 3: Model and Observational Data Sources

3.1: How Wind Turbines Work

Modern wind turbines are complex systems. For this discussion, though, it suffices to only consider the primary turbine components: the tower, nacelle, rotor (consisting of the blades and the hub) and generator. Figure 3.1, adapted from Manwell (2009), illustrates the locations of these parts.

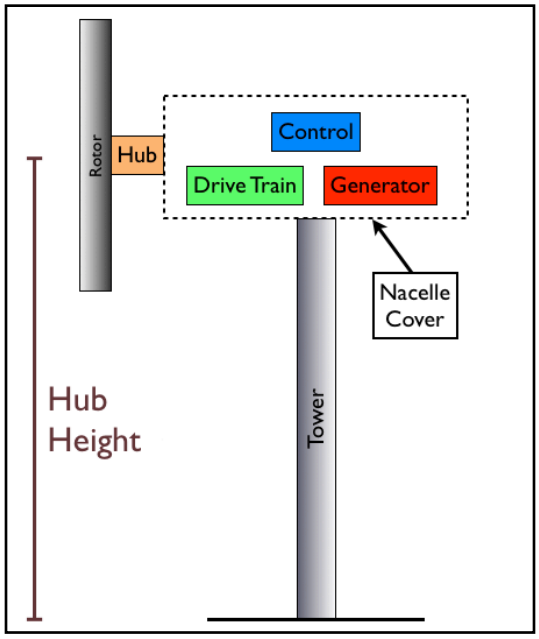

Figure 3.1: Locations of the primary components on a typical wind turbine and illustration of the hub height.

Regarding nomenclature, the hub height is the distance from the ground to the center of the hub. A common hub height is 50 m, corresponding to blade lengths of 24 m and a nacelle weight of 30 tons (about the weight of a Sherman tank). Needless to say, these are big machines.

Turbine blade design parallels airfoil design. As air flows across the convex blades, differences in velocity occur on either side of the blade. Elementary fluid mechanics dictates that this induces a pressure difference, resulting in lift. In the context of the turbine, the lift translates to rotational motion. This rotation, sourced to a generator, produces electricity. Recall, a generator is a device that converts mechanical energy into electrical energy-- the exact opposite of an electrical motor (Manwell 2009).

On modern wind turbines, the gearbox is arguably the least reliable component. To circumvent this problem, the industry has been adopting direct drive systems, short circuiting the need for gearboxes. Figure 3.2 depicts an operational flow chart involving these generators:

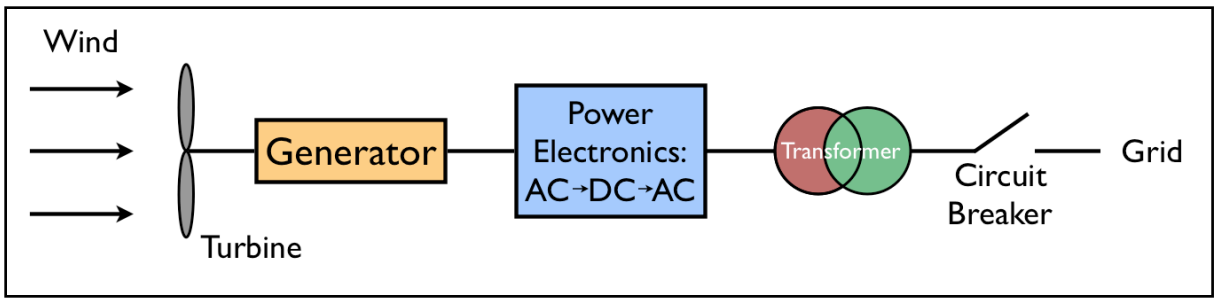

Figure 3.2: Operational flow chart of a wind turbine with a direct drive generator.

These devices have the advantage of producing electricity from the moment the wind turbine starts to rotate. The absence of a gearbox dramatically lowers mechanical power losses. The caveat, though, is that these systems incur higher electrical power losses due to the AC to DC to AC conversion. This is necessary to ensure the electricity fed into the grid has the proper phase and amplitude. The improved reliability of direct drive systems, though, trumps the additional electrical power losses. Machines this imposing demand that ease of maintenance

be a top design priority (Manwell 2009).

3.2: How to Calculate Wind Power Density

Meteorological wind conditions are typically recorded 10 m above the ground. Consequently, the wind at hub height (50 m) must be interpolated. A common method employs the power law, expressed as

$$u_{50} = u_{10}\left(\frac{50\ m}{10\ m}\right)^{n} \qquad (3.1)$$

where n is an empirically derived constant, known as the contour number. The wind speeds, u_{50} and u_{10} refer to the wind speeds at 50 m and 10 m, respectively. The wind industry assumes a contour number of 1/7 and refers to Equation 3.1 as the "1/7 Power Law" (Manwell 2009).

Another method of interpolating the wind is known as the log law described in Equation 3.2. This assumes an adiabatic profile, meaning that it should only be applied when the boundary layer is well mixed, under conditions of neutral static stability (Manwell 2009).

$$u = \frac{u^{*}}{k}\ln\left(\frac{z}{z_{o}}\right) \qquad (3.2)$$

Here, u^{*} is the friction velocity which acts as a proxy for wall shear stress. It is related to the stress and density. The Von-Karmen constant, k, is typically around 0.4. The roughness length, denoted by z_o is the height at which the velocity goes to zero. Given these parameters, it is possible to calculate the wind speed u at some height above the ground z.

A site's electrical output potential is estimated from wind power density. This quantity is derived from kinetic energy (KE). Beginning with the equation for KE

$$KE = \frac{1}{2} mv^2 , \qquad (3.3)$$

power (P) is the time derivative of KE

$$P = \frac{d(KE)}{dt} = \frac{1}{2} \overline{v}^2 \frac{dm}{dt} . \qquad (3.4)$$

Here $\overline{v}$ is some average velocity and *dm/dt* is a mass flow rate. If the 50-m wind is used, then the resulting power calculated is referred to as the 50-m wind power. The ideal gas law for dry air can be used to calculate ρ. Changes of pressure (p) and temperature (T) in the representative atmospheric layer of 50 m can be neglected and the values recorded at 10 m can be used in the density calculations.

After computing ρ, the mass flow rate can be expressed as

$$\frac{dm}{dt} = \rho \frac{d\forall}{dt} \qquad (3.5)$$

where ∀ represents volume and *d*∀*/dt* is a volume flow rate.

An upwind length, L, can be defined as some distance upwind of the turbine. The swept area (A) of a wind turbine is the area occupied by the blades. These concepts are illustrated in Figure 3.3.

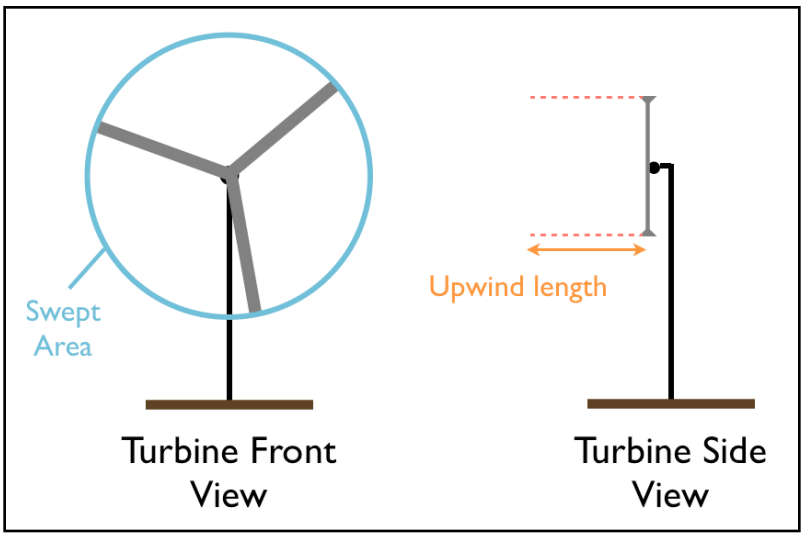

Figure 3.3: Upwind length and swept area of a wind turbine.

Substituting L and A in for ∀ in Equation 3.5, the volume flow rate can be expressed as

$$\frac{dm}{dt} = \rho \frac{d\forall}{dt} = \rho A \frac{dL}{dt}. \qquad (3.6)$$

A unit analysis reveals *dL/dt* is a velocity. Substituting 3.6 into 3.4, the equation for wind power becomes

$$P = \frac{1}{2}\rho \bar{v}^3 A. \qquad (3.7)$$

To remove the dependence on A (and therefore on turbine type and size), 3.7 is divided by A yielding wind power density (2009).

$$WPD = \frac{1}{2}\rho \bar{v}^3. \qquad (3.8)$$

The wind industry separates the wind into classes, determined by wind speed and corresponding wind power density. Table 3.1 summarizes the seven standard wind classes.

Table 3.1: Standard wind classes at 10 m and 50 m.

Wind Class	10-m Wind Speed ($m\ s^{-1}$)	10-m Wind Power Density ($W\ m^{-2}$)	50-m Wind Speed ($m\ s^{-1}$)	50-m Wind Power Density ($W\ m^{-2}$)
1	0-4.4	0-160	0-5.6	0-200
2	4.4-51	160-240	5.6-6.4	200-300
3	5.1-5.6	240-320	6.4-7.0	300-400
4	5.6-6.0	320-400	7.0-7.5	400-500
5	6.0-6.4	400-480	7.5-8.0	500-600
6	6.4-7.0	480-640	8.0-8.8	600-800
7	7.0-9.4	640-1600	8.8-11.9	800-2000

These wind classes are calculated under the assumption that the wind follows a Weibull probability distribution function (PDF). Recall, that a probability distribution is just a mathematical expression describing the probability of a random variable, u, taking on a particular value. In the context of this work, the random variable is the wind speed. A PDF is derived from a histogram, a graphical representation of the frequency of data. On a histogram, the data is divided into bins and the number of instances the data takes on values of each bin is recorded. The PDF of the data is obtained by Equation 3.8

$$PDF(u) = \frac{hist(u)}{N \cdot \Delta u} \qquad (3.8)$$

Here, $hist(u)$ is the histogram of the data, u. N are the number of data and Δu is the bin increment. By this definition, the integral of the PDF is equal to one (Everitt; Skrondal 2010).

In the wind energy industry, the wind is represented as a distribution and not as discrete, independent measurements. Several types of probability distributions exist, but the one typically employed by the wind energy industry is the Weibull distribution described by Equation 3.9 (Sedefian 1980).

$$PDF(u) = \left(\frac{k}{c}\right)\left(\frac{u}{c}\right)^{k-1} \exp\left[-\left(\frac{u}{c}\right)^{k}\right] \qquad (3.9)$$

Here, k is the shape parameter and c is the scale parameter, the values of these parameters can be calculated using empirical formulas, as given by Equations 3.10 and 3.11 (Manwell 2009). For a given value of c, increasing k narrows the PDF.

$$k = \left(\frac{\phi}{\overline{u}}\right)^{-1.086} \qquad (3.10)$$

$$c = \overline{u} \cdot \left(0.568 + \frac{0.433}{k}\right)^{-1/k} \qquad (3.11)$$

Here ϕ is the standard deviation of the wind speed and $\overline{u}$ is the mean wind speed.

A final consideration involves cut in, rated and cut out velocities. Wind turbines only operate within a designated range of velocities. The cut in velocity is the minimum wind speed at which the wind turbine can generate power, typically on the order of 3 to 5 m s^{-1} at 50 m. The rated velocity is the wind speed at which the wind turbine produces maximum power, typically between 15 and 20 m s^{-1} at 50 m. The cut out velocity is the maximum wind speed at which the wind turbine can generate power, typically around 25 or 30 m s^{-1} at 50 m. As a safety feature, wind speeds beyond the cut out velocity force the turbine to shut down by

feathering the blades. The blades are rotated such that no lift can be generated as air flows over them (Manwell 2009).

Truncating wind speeds to the rated velocity in the power density calculations produce much more accurate energy estimations. Consider the effect of a strong synoptic event passing through a normally calm area. Cubing those abnormally high wind speeds distorts the area's potential for wind energy development. Hence, incorporating rated velocities filters out those fleetingly intense wind speed episodes and provides a more accurate representation of energy potential. Various rated velocities are accounted for in the analysis in Chapters 4 and 5.

3.3 The Betz Limit

The Betz limit, developed almost 100 years ago by the German physicist Albert Betz, describes the power from an ideal wind turbine. Betz discovered this when performing analysis on ship propellers. Adapting the derivation in Manwell (2009), the Betz limit can be shown with a momentum analysis using a simple model for a wind turbine, seen in Figure 3.4. The dark grey line in the middle of the stream tube boundary represents a wind turbine "blade."

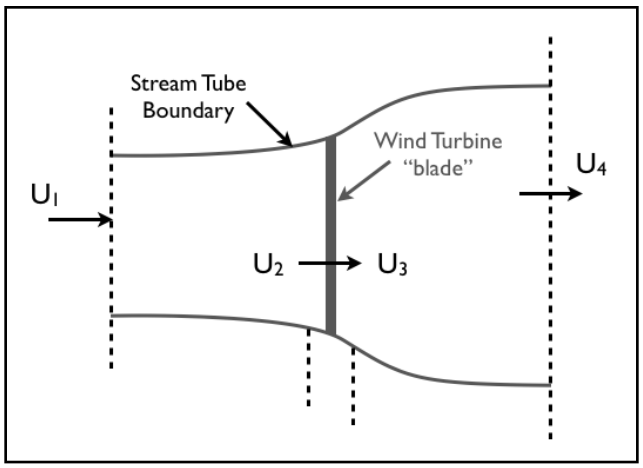

Figure 3.4: Model of wind turbine, adapted from Manwell (2009).

The following analysis assumes the following:

- homogenous, incompressible, steady state fluid flow
- no frictional drag
- non rotating wake
- uniform thrust over the blades
- static pressure far upstream and downstream is equal to the ambient static air pressure

Conservation of momentum and the Bernoulli equation can be applied to a control volume surrounding the blade characterized by inflow velocity U_2 and outflow velocity U_3. As the wind blows past the blades, some of it is converted to mechanical power (and then electricity) and some flows past the blades. The power coefficient, C_P describes this behavior:

$$C_P = \frac{\text{Power in Rotor}}{\text{Power in Wind}}$$

As the wind encounters the blades, it slows down. Equation 3.12 defines the induction factor, *a*, the percentage of velocity slowdown once it enters the stream tube boundary:

$$a = \frac{U_1 - U_2}{U_1} \qquad (3.12)$$

$$U_4 = U_1(1-2a) \qquad (3.13)$$

Equation 3.13 describes the relationship between the free stream inflow velocity, U_1 and the free stream outflow velocity, U_4 based on the Bernoulli equation.

The Betz limit explains the balance between these two quantities: turbine designers aim to maximize the power coefficient and minimize the induction factor. Figure 3.5 is a graph illustrating the Betz limit. The peak of the curve corresponds to the maximum power coefficient: 0.59. This value of C_P coincides with an induction factor of 1/3 or 0.33. Thus, a wind turbine can, at most, convert 59% of the wind to mechanical power. Real world limitations peg this efficiency to somewhere around 50%. Induction factors past 0.5 are physically impossible. When a=0.5, Equation 3.13 says the outflow velocity is zero, which does not make any physical sense (Manwell 2009).

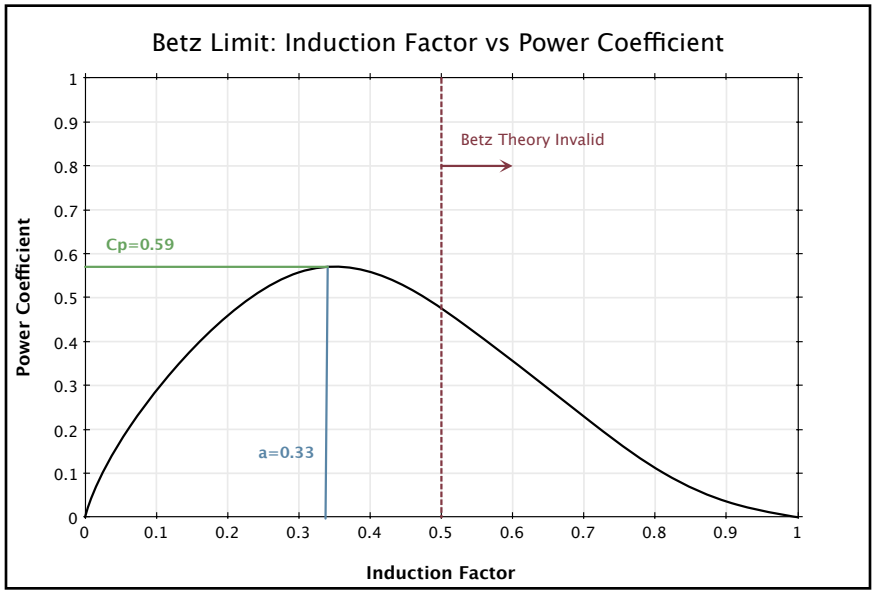

Figure 3.5: Graphical representation of the Betz limit. The horizontal axis corresponds to the induction factor and the vertical axis corresponds to the power coefficient.

Because the wind power density is proportional to the cube of the velocity, minor perturbations in wind speed can have drastic effects on the power density. This sensitivity also places undue criticality on the 1/7 Power Law: incorrect 50 m wind speed interpolations create a ripple effect throughout the remaining equations.

3.4: Weather Model Description

In June 2006, the Weather Research and Forecasting (WRF) model replaced the Eta prediction scheme. WRF was designed to unify the academic and operational circles within the atmospheric science community, thereby reducing the lead time of operation implementation and development of NWP models. The model was designed to be easily modified and expanded by users-- not purely open source, but resonant of that mindset. It was also designed to be compatible with a variety of computer resources: parallel processing, multi-core architectures, *etc*.

For the past twenty years, the Eta model has served as the *de facto* standard for all NWP models. The name of the model stems from the eta coordinate system, developed to minimize errors when calculating pressures near mountain surfaces. Eta (η) levels range in value from 0-1 and are calculated via Equation 3.13:

$$\eta = \frac{p_r(z_s) - p_t}{p_r(z=0) - p_t} \qquad (3.13)$$

Here, p_t is the pressure at the top of the model (dictated by the forecaster), $p_r(z{=}0)$ is the standard mean sea level pressure (MSL) of 1013 millibars (mb). The pressure at terrain height, $p_r(z_r)$, varies and determines the different η levels. Figure 3.6, adapted from a MedEd

COMET program, illustrates this concept (2009):

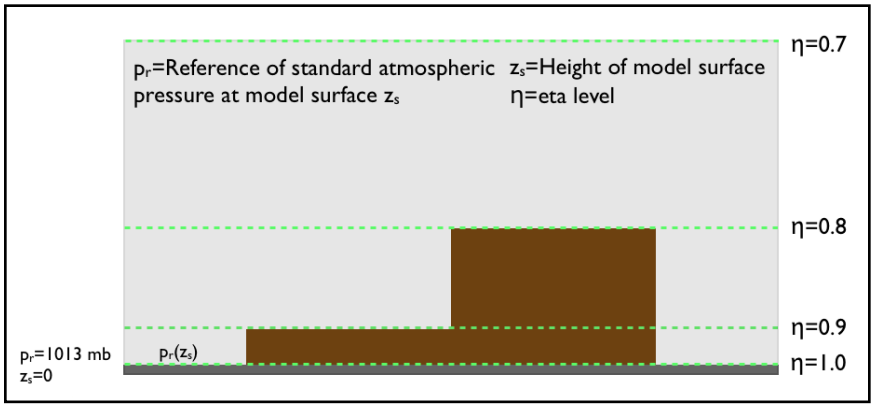

Figure 3.6: Theory of eta levels in the eta coordinate system.

The top of the "mountain" in Figure 3.6 is represented by η=0.8 while at the ground level η=1.0. All η levels are horizontal. But like with any parameterization scheme, there are advantages and disadvantages. The advantages of the η coordinate system are:

- The terrain shadowing nature of the η system improves forecasts of wind, temperature and moisture near the surface, especially near areas of steep sloping topography.
- Though the calculations near the surface are more complex, the results are far more representative of actual atmospheric conditions.

The disadvantages are:

- Detailed information about the boundary layer may be lost due to the discretized vertical representation inherent in the η scheme.
- Since the reference pressure level within the η coordinate system is the mean sea level pressure, several η levels may be underground in areas of high terrain.
- The η scheme had difficulty capturing gradually sloping terrain.

WRF utilizes a hybrid eta-sigma vertical coordinate system to help alleviate some of the errors prone to the eta system. Sigma (σ) levels are strikingly similarly to η levels:

$$\sigma = \frac{p}{p_s}. \qquad (3.14)$$

In Equation 3.14, p is the pressure of a level within the model and p_s is the pressure at the ground, *not* mean sea level pressure. Equation 3.14 is essentially the same as Equation 3.13 except that on σ levels, p_r is the pressure at the ground. This is a terrain-following coordinate system as illustrated by Figure 3.7, again adapted from a MetEd COMET program (2009).

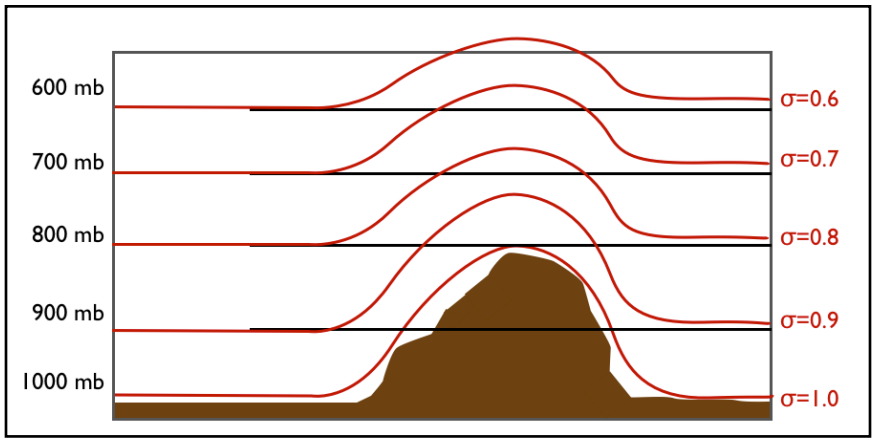

Figure 3.7: Theory of sigma levels in the sigma coordinate system. The horizontal lines signify various isobaric levels.

They hybrid sigma-pressure vertical coordinate system implemented in WRF aims to minimize errors both near the surface and aloft. Near the surface, σ levels characterize the vertical structure of the model, while isobaric levels characterize the model aloft. The advantages of this system are:

- The fundamental pressure relationship within σ is easy to program

- Because σ references the pressure at ground level, no sigma levels will ever reside underground
- More realistic behavior associated with incoming solar radiation results from isobaric vertical profiles at upper levels
- The surface heating and mixing in the boundary layer is well represented
- The σ is easily applied to higher resolution models

The disadvantages of the σ scheme are:

- The smoothing of σ levels can misrepresent the actual elevation of the topography leading to errors associated with pressure and moisture
- Blending coordinate systems can be difficult to program

Though both schemes have their assets, in regions of high elevation, such as Wyoming, the σ coordinate system is preferred because no σ levels are underground. Choosing the optimal coordinate system, then, depends on geographic location and the specific meteorological phenomena modeled.

WRF is a non-hydrostatic model (with options to run hydrostatically) with nesting capabilities. Running WRF in a nested environment improves accuracy and reduces computational time. Typically, as the size of each nest or "domain" decreases, the resolution of the domain increases. For example, if one wanted to simulate flow through wind corridor of southeastern Wyoming, a wise approach would be to specify three domains: an outer, rather coarse domain of the western portion of the United States, a finer resolution domain of the state of Wyoming and a high resolution domain of the wind corridor. This framework simulates the area of interest at a high resolution and the surrounding coarser domains capture

the large scale atmospherics. Computational time is minimized because the high resolution domain only surrounds the small area of the wind corridor. The nested structure of the model improves accuracy, resulting in the most realistic model output.

The basic functionality of WRF follows four basic steps and is outlined in Figure 3.8.

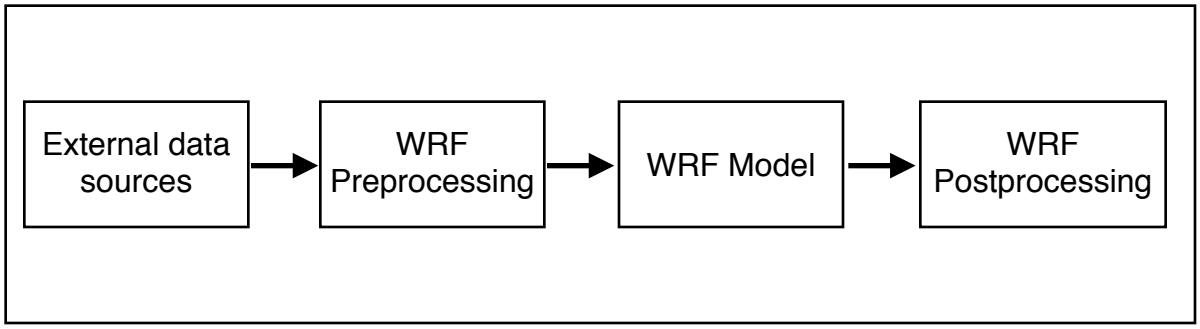

Figure 3.8: Basic flowchart of the Weather Research and Forecasting model.

External data sources are fed into the WRF preprocessor which prepares the data to be run inside the WRF model. After the simulation, the output can be read into a variety of meteorological software packages. From the user's perspective, the WRF preprocessor is the module where all the forecast specifications are defined. Figure 3.9, adapted from the WRF user's guide, highlights the main components of the WRF preprocessor (2011).

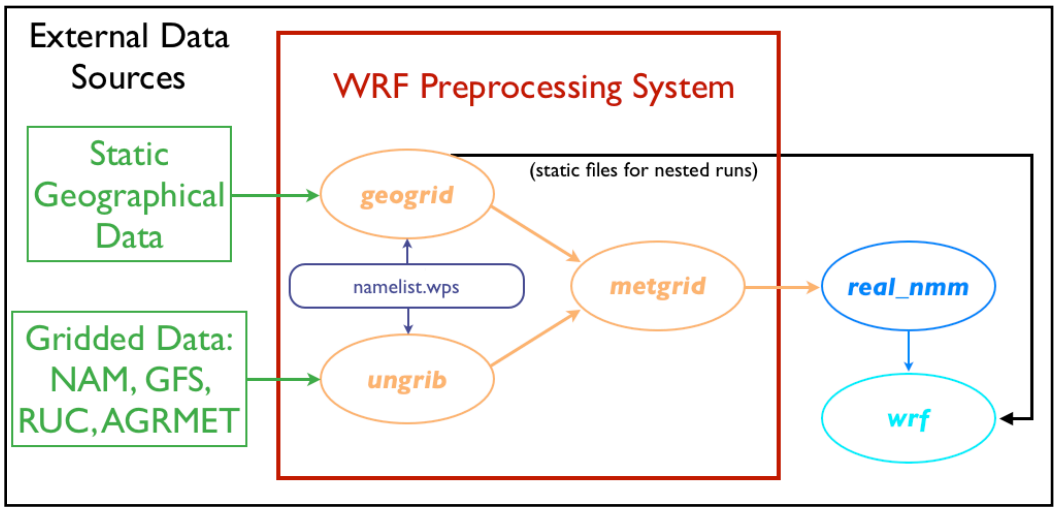

Figure 3.9: Various components of the WRF Preprocessor.

The namelist.wps file, common to all three preprocessing programs (ungrib, geogrid and metgrid) contains information about the number and resolution of domains of the simulation. If the input data is in Gridded Binary (GRIB) format, then the ungrib program must be run before running geogrid and metgrid.

GRIB files, common to atmospheric science, concisely store historical weather data. When operational weather models are run, the output is typically in GRIB format. There are two parts to every GRIB file: the header which describes the data contained in the file and the actual binary data. GRIB files can conveniently be appended or separated with no risk of data loss or corruption. The GRIB header contains two parts, only one of which is mandatory. The first part, the Product Description Section or PDS contains information about who created the data, the NWP model involved, a description of the actual data including units, a specification of the vertical structure of the data and a timestamp. The second (optional) part, the Grid Description Section or GDS, provides a more detailed description of the data.

The ungrib program extracts or "degribs" the relevant data from the GRIB files using variable tables or vtables. These vtables tell ungrib which parts of the binary data to extract. The ungrib program creates intermediate files to initialize WRF. Geogrid defines the surface domains specified in the namelist.wps file. In addition, geogrid interpolates terrestrial information throughout the domains (terrain height, soil and vegetation information, albedo, *etc*). The metgrid program merges the meteorological output of geogrid and the domain information from ungrib into a file for use in the WRF model.

The actual WRF model is comprised of three layers as illustrated in Figure 3.10, adapted from Michalakes et al. (2004): the driver, mediation and model.

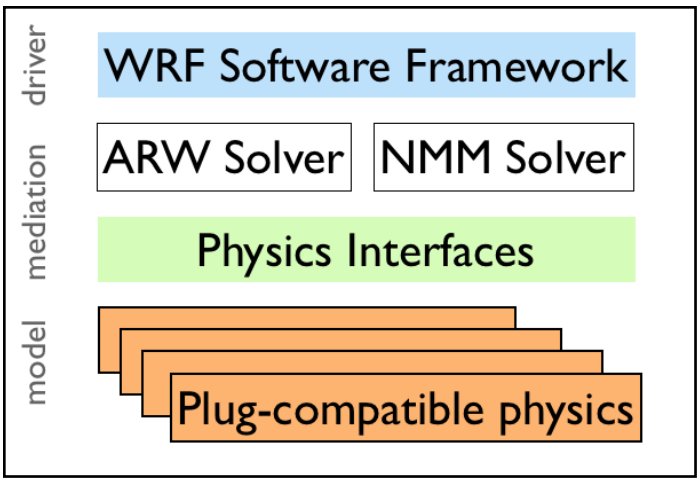

Figure 3.10: The three layers of the WRF model.

The first layer, the driver, allocates memory, controls nesting and relays the model timestep. The mediation layer includes the various solver cores of WRF which communicates information regarding the terrain, vertical coordinate system, nesting, grid spacing and equations/ variables. The model layer contains all the computer code detailing the physical computational routines executed by the model: advection, diffusion, physical parameterizations, *etc.* Once WRF is finished, the output can be viewed in a variety of meteorological software packages.

Like the Hatfields and the McCoys, the research and operational sectors were never meant to stay together. The National Center for Atmospheric Research (NCAR) began developing Advanced Research WRF (WRF-ARW) and the National Centers for Environmental Prediction (NCEP) began developing the Non Hydrostatic Model (WRF-NMM). Though both models appear similar on the surface, it is "what's under the hood" that separates them.

WRF-ARW is an update from the Fifth Generation NCAR/ Penn State Mesoscale Model (MM5). WRF-ARW is much more flexible than its predecessor, offering a plethora of additional dynamical and physical parameterizations. Currently on version 3, this model is available to the general public for download at no charge. The non-hydrostatic, terrain following model utilizes a third order Runge-Kutta time split difference technique. The model code that estimates the primitive equations are of fifth and sixth order to improve accuracy.

WRF-NMM is an update from the Eta prediction scheme used by NCEP. WRF-NMM is designed primarily as a forecasting tool and is much faster than its research oriented counterpart. WRF-NMM uses an Adams-Bashforth time differencing scheme. The representation of terrain has been vastly improved compared to the Eta scheme. Like the Eta scheme, WRF-NMM uses the same domains and same number of vertical levels. WRF-NMM also includes a separate set of equations for hydrostatic simulations if such a configuration is desired by the forecaster.

NCEP oversees the operational weather forecast models and subsequent numerical analyses used by the meteorological community. Included in its suite of models is the North American Model (NAM). Since 2006, WRF-NMM has formed the core of the NAM's anatomy. Chosen for its widespread applicability, the NAM has been tested and refined for forecast simulations. Of the assorted flavors of the NAM, the 12-km and 4-km horizontal resolution variants for 2008, 2009 and 2010 comprise the basis of the model dataset for this work. The NAM 12-km output stems from the 0000 universal time (UTC) 84 hour forecast, extracted in 3 hour increments. Owing to spin up, the first three hours of simulation are

disregarded, resulting in daily model sets from 0300 to 2400 UTC. The NAM 4-km output, still in experimental stages, is available in one hour increments beginning at the 0600 UTC 72 hour simulation. However, the NAM 4-km runs are frequently preempted for hurricane modeling and as such, continuous daily records are only available from November to May.

Daily NAM 4-km forecasts, in GRIB format, were downloaded from NCEP in real time. The NAM 12-km forecasts were downloaded from NOAA's Operational Model Archive Distribution System (NOMADS), also in GRIB format. Because the General Meteorological Package (GEMPAK) was employed as the primary cartographer for the model data, the GRIB files were converted to a GEMPAK-friendly format.

3.5: Averaging Schemes of the Data

GEMPAK is a meteorological display software package developed and maintained by NCEP. Originally developed by the Severe Storms Laboratory at the Goddard Space Flight Center at NASA in the 1980s, GEMPAK continues to be a popular method of displaying meteorological data. GEMPAK consists of a suite of graphical programs that are capable of generating a variety of visual aids. When a user initializes one of these graphical programs, background processes are initiated to parse the user's input and evaluate variables at specific grid points, stipulated by the user. A graphics driver is also loaded to display the completed calculations either on the screen or in postscript format. Each of these modules (the application, the background processes and the graphics device) communicate with each other via mailboxes. When a command is sent to one module, it is passed to another module and perhaps sends a different command back to the first module or sends a command to a different

module. GEMPAK is completely scriptable, meaning that UNIX scripts can be written and interpreted by GEMPAK instead of manually sending commands to the various graphical programs (2005).

Included in the GRIB files and the subsequent GEMPAK versions, are standard 10-m weather variables: temperature, pressure and wind (broken into urel and vrel, the u and v components of the wind). As per the equations previously discussed, these standard variables were used to calculate the 50-m wind and the 50-m wind power density. Additional 10-m wind variables incorporating various rated speeds were also calculated. Tables 3.2 and 3.3 describe the variables added to the GEMPAK files.

Table 3.2: Added Wind Variables. These variables were computed and added to each GEMPAK file under the stated criteria and using the specified equations.

Wind Variable	Description
wnd10	magnitude of the 10-m wind
wnd50	magnitude of the 50-m wind calculated from the 1/7 Power Law using wnd10
wndr50	magnitude of the 50-m wind calculated from the 1/7 Power Law using wnd10 and a 10-m rated speed of 12-m s^{-1}
wndr1550	magnitude of the 50-m wind calculated from the 1/7 Power Law using wnd10 and a 10-m rated speed of 15-m s^{-1}
wndr2050	magnitude of the 50-m wind calculated from the 1/7 Power Law using wnd10 and a 10-m rated speed of 20-m s^{-1}
wndr2550	magnitude of the 50-m wind calculated from the 1/7 Power Law using wnd10 and a 10-m rated speed of 25-m s^{-1}

Table 3.3: Added Power Variables. These power variables were calculated using the specified wind variables

Power Variable	Description
pow5017	50-m wind power density calculated using wnd50
powr5017	50-m wind power density calculated using wndr50
powr155017	50-m wind power density calculated using wndr1550
powr205017	50-m wind power density calculated using wndr2050
powr255017	50-m wind power density calculated using wndr2550

Upon completion of calculating and adding the relevant wind and power variables, the GEMPAK files were averaged in a variety of ways to better understand basic trends in the data. None of these schemes involved cross model computations: the NAM 12-km and 4-km datasets were averaged independently, albeit identically. Appendix A describes the various GEMPAK programs invoked to manipulate the model output and Appendix B outlines the UNIX scripts used to average the GEMPAK files.

Initially, all the GEMPAK files were averaged by month. All forecasts for each day of each month were averaged, resulting in a single GEMPAK file for each month with only one timestamp. Next, the GEMPAK files were averaged by forecast hour by month, resulting in a single GEMPAK file for each month with eight timestamps: 0300, 0600, 0900, 1200, 1500, 1800, 2100 and 2400 UTC. Since the NAM 4-km dataset included hourly forecast files, consistency mandated that only the 0300, 0600...2400 UTC daily forecasts be averaged. Also, because the NAM 4-km preempted during the summer and fall, data for only the moths of January, February, March, April, May and December for each year were available. Combined, these two averaging schemes output 36 GEMPAK files for each yearly dataset: 24

for the NAM 12-km consisting of 12 monthly averages with grids existing at only one timestamp and 12 monthly hourly averages with grids existing at eight timestamps: 12 for the NAM 4-km consisting of 6 monthly averages with grids existing at only one timestamp and 6 monthly hourly averages with grids existing at eight timestamps.

The averaging interval was then extended from a monthly basis to a seasonal basis. Table 3.4 describes how the months were divided into seasons. The seasonal averaging schemes paralleled the monthly averaging schemes. Four seasonal and four seasonal hourly average files were generated. These average files were computed for both the 12-km and 4-km datasets. As an example, the 2009 12-km winter average file is the mean of the 12-km December (2009), 12-km January (2009) and 12-km February (2009) monthly averages.

Table 3.4: Seasonal divisions by month

Season	Months
Winter	December, January, February
Spring	March, April, May
Summer	June, July, August
Autumn	September, October, November

The 2009 12-km winter hourly average file is the mean of the hourly 12-km December, January and February averages.

Finally, the averaging interval was extended to the entire year, but only for the NAM 12-km dataset, as a complete yearly dataset of 4-km data does not exist. The mean for all four seasonal average files was calculated. No yearly hourly average files were generated.

For trending and tendency identification purposes, all mean 12-km datasets were averaged over the three year period. Thus, three year monthly, monthly hourly, seasonal, seasonal hourly, and yearly averages were calculated for the NAM 12-km dataset. That is, all three January monthly means were averaged, yielding a three year January mean; all three January monthly hourly means were averaged, yielding a three year January hourly mean, *etc*. All told, 180 mean GEMPAK files were generated: 132 for the NAM 12-km dataset and 48 for the NAM 12-km dataset. Tables 3.5, 3.6 and 3.7 summarize the averaged GEMPAK variables. The variables are written with UNIX variable syntax to avoid a table with 180 entries. The term ${year} means 2008, 2009 and 2010 and ${month} means jan, feb, mar, *etc* while ${season} means summer, spring, autumn and winter for the NAM 12-km; for the NAM 4-km the only seasons averaged were winter and spring.

Table 3.5: NAM 12-km average files. Following this naming procedure, there are 99 files for all three years.

Monthly	Seasonal	Yearly
${month}${year}hour.gem	${year}_${season}.gem	${year}ave.gem
${month}${year}mean.gem	${year}_${season}_hr.gem	

Table 3.6: NAM 12-km three year average files. There are an additional 33 files.

3 Year Monthly	3 Year Seasonal	3 Year Trend
${month}_3yr_ave.gem	${season}_3yr_ave.gem	3yr_ave.gem
3yr_${month}avehr.gem	${season}_hr_3yrav.gem	

Table 3.7: NAM 4-km average files. Since the 4-km dataset does not contain a complete yearly record, the only seasons averaged were spring and winter. Refer to Table 3.4 for the months corresponding to those seasons. No yearly average was computed for the same reason. There are a total of 48 files for the three year period.

Monthly	Seasonal
${month}${year}_wind.gem	${year}_${season}.gem
${month}${year}_time.gem	${year}_${season}_time.gem

3.6: Information About Observational Data

The Automated Surface Observing System (ASOS), operated and controlled by the National Weather Service (NWS), provides firsthand weather data across the entire US observational network. Included among the commonly recorded variables are the 2-m temperature and pressure and 10-m wind speed. The Wyoming ASOS subnet, comprised of roughly two dozen of these stations statewide, affords near complete weather records for 2008, 2009 and 2010. These yearly ASOS reports were downloaded from the University of Wyoming Atmospheric Science Department weather website and served as the basis for the observational dataset.

Since ASOS stations recorded weather conditions at hourly intervals, the first step was to remove extraneous data to coincide with the models' three hourly intervals. MATLAB scripts were written to eliminate unwanted data and sort the records by station. Invoking the 1/7 Power Law, the 50-m wind was calculated from the 10-m wind. No rated speeds were incorporated into the wind computations. After computing the density using pressure, temperature and the ideal gas law, wind power density was calculated at 50 m. These

quantities were all calculated for every station at the customary three hour intervals for all three years.

Similar averaging schemes were applied to the observational dataset, once it had been sorted and formatted. Station averages of wind and wind power density were calculated via MATLAB scripts at monthly, monthly hourly, seasonal, seasonal hourly, yearly and yearly hourly periods for all three years. These yearly means were then averaged, as with the model dataset, to obtain a sense of the variability of the wind and power over the three year period. In addition, all the station means were averaged together to get a sense of the statewide wind and power output. All mean values were saved to text files so the data could be easily imported into MATLAB for analysis and comparison with the model data.

Chapter 4: Model and Observational Comparison

4.1: Topographic Information About Southeastern Wyoming

Remarkably, the route that today's truck drivers take to transport goods across the Rocky Mountains is almost identical to the passageway taken by the frontiersmen who tamed the West and the Chinese-Americans who later built the transcontinental railroad. The lowest region of the Continental Divide between Montana and New Mexico resides in the southeastern portion of Wyoming (Martner and Marwitz 1982). This area, located west of Rawlins amidst the Red Desert, is known as the Great Divide Basin and claims an elevation of roughly 2000 m. The surrounding terrain, in comparison, pierces the sky at heights above 3000 m with several peaks boasting elevations over 4000 m (Marwitz and Dawson 1984). Just as truck drivers and train engineers prefer the path of least resistance, so too, does the wind.

In the wintertime, pools of cold air collect in the Great Divide Basin as the jet stream moves southward from Canada (Martner 1986). A ridge in the jet stream, centered over the eastern valleys of Utah, Nevada and Idaho as well as the Great Divide Basin, stimulates an anticyclonic rotation. As a result, an area of high pressure develops in the center of these cold air reservoirs (Marwitz and Dawson 1984). The trough of the jet stream, characterized by a core of low pressure, generally positions itself over the Dakotas and eastern Colorado. These two synoptic entities trigger an intense pressure gradient across Wyoming, forcing the pools of cold air in the Great Divide Basin eastward towards the Great Plains (Martner and Marwitz 1982). These synoptic pressure systems routinely occur in the wintertime when the jet stream has drifted southward from Canada. In the summertime, when the jet stream has retreated

back to Canada these synoptic events occur at a markedly lower frequency and intensity (Martner 1986). Figure 4.1, depicting a particularly wind day in January 2008, illustrates the required alignment of high and low pressure systems. What makes this flow noteworthy, however, are the orographic barriers encountered along the way.

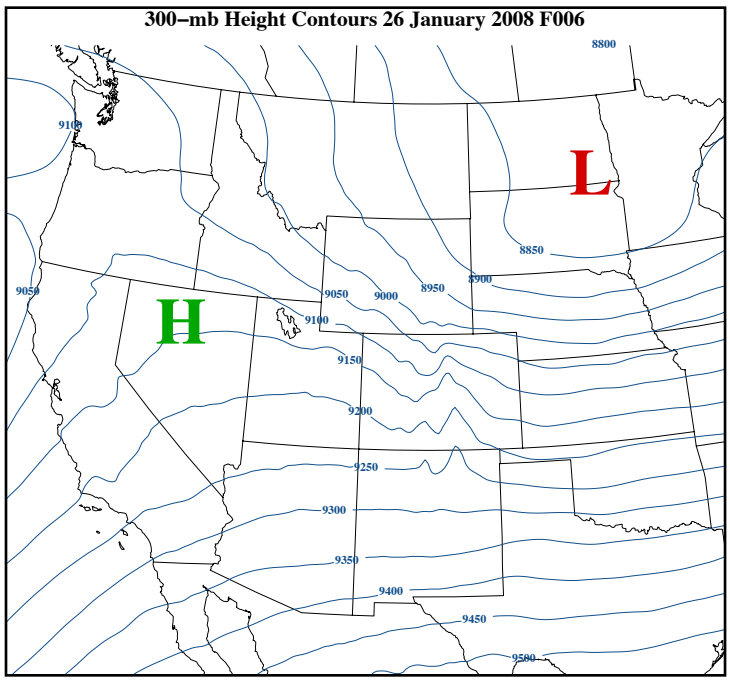

Figure 4.1: Synoptic features inducting a pressure gradient across Wyoming on 26 January 2008. The high pressure system (H) west of Wyoming and the low pressure system (L) above the Dakotas.

The mountain ranges in southeastern Wyoming form a natural topographic funnel through which these winds blow, as evidenced by Figure 4.2. Aptly named the "wind corridor" by Kolm (1977), this region harbors some of the strongest winds in the country and indeed the world. To the north, the wind corridor is bounded by the Wind River Mountains and Sweetwater Graben and to the south, the Sierra Madre and Medicine Bow Mountains.

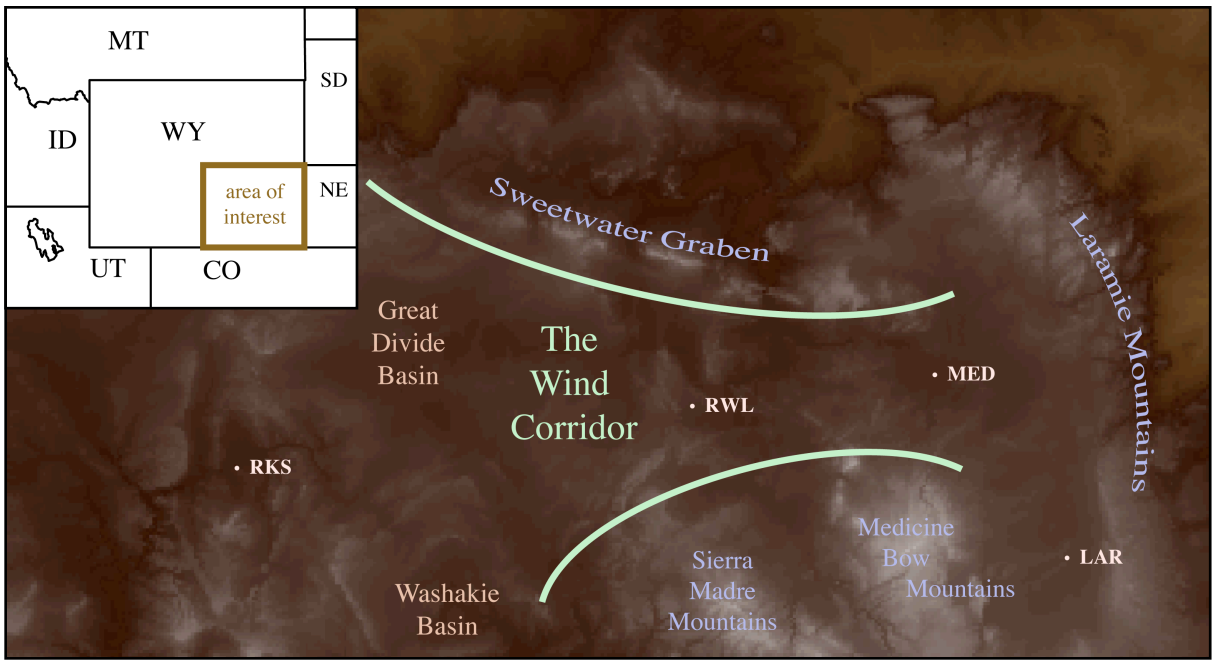

Figure 4.2: The wind corridor (outlined in light green) of southeastern Wyoming. Lighter white areas correspond to higher terrain.

The widest part of the wind corridor, west of Rawlins (RWL), is about 110 km and narrows to 45 km near the town of Medicine Bow (MED) (Martner and Marwitz 1982). The orographic channeling accelerates the flow as it approaches Medicine Bow. In fact, Medicine Bow has hosted several wind energy research projects and now serves as a poster child for the viability of wind power. Additional winds from the Washakie Basin converge into the wind corridor, joining the primary winds from the Great Divide Basin (Kolm 1977). Subsidence inversions, derived from the high pressure systems west of Rawlins, tend to cap the flow at mountaintop, forcing the air through the wind corridor rather than over it. The absence of trees, in combination with the relatively flat terrain, help to minimize surface friction effects (Martner and Marwitz 1982).

In addition to accelerated flow, thermal gradients can potentially develop within the

wind corridor. Constrained by the topography, an indirect circulation cell may emerge in the lowest 1 km of the atmosphere. The cold air escapes to the north while the warm air flows to the south, creating a thermal gradient in the center of the wind corridor (Marwitz and Dawson 1984).

The dominant annual wind direction is westerly. The summertime variance of wind direction, compared to the wintertime, is understandably higher. During the winter, when the winds are stronger, the channeling of the flow by the wind corridor results in a more uniform westerly wind direction. The weaker summertime winds, still maintaining a westerly component, meander about the left side of the compass rose (Martner and Marwitz 1982). During the summer, when the large scale flow is weak, the wind direction exhibits a diurnal cycle: at night, cool air drains down mountain slopes, only to rise again at sunrise (Martner 1986).

4.2: National Renewable Energy Laboratory Maps

The National Renewable Energy Laboratories (NREL) located in Golden, CO have been at the forefront of wind energy research for much of the previous decade. As discussed, wind is a standard atmospheric variable and is included in numerical weather model output. Calculating wind power density is accomplished by applying Equations 3.1 and 3.4. Once wind power density is known, it can be plotted on a map.

In addition to the wind industry, a wind resource map can be useful to the slew of other industries indirectly impacted by the wind. Knowledge of local wind patterns assists in siting mines, refineries and and power stations in preventing unwanted pollution from drifting

into residential areas. Other aspects of air quality control also benefit from informed policymakers. Farmers and ranchers living in windy areas use wind breaks to curb soil erosion. A better informed transportation sector can institute policies and regulations that increase safety and streamline conveyance. Ground blizzards occur because of high surface winds, adversely affecting livestock and travelers alike. Large scale construction projects are, at times, at the mercy of the wind: storms, even gusts, can jeopardize workers' lives and even bring all activity on the job site to a standstill. The information wind resource maps provide can help all of these groups efficiently and effectively perform their duties (Kolm 1977). But, a wind resource map's primary constituent remains the wind developer.

Figure 4.3 is an example of a typical wind resource map generated by NREL valid at 50 m. It divides the resource into the seven wind classes discussed in Chapter 3 and was generated using a combination of high and low resolution numerical weather prediction models. Ignoring the coastlines, the colors of rich wind resource, reds and dark blues, are disappointingly absent from the map. The midwest appears to offer the most wind resource potential, ranging from "Good" to "Excellent." The detail of this map, however, masks the wind potential in smaller parts of the country. A wind resource map of just Wyoming, shown in Figure 4.4, reveals where these blue and red areas have been hiding.

Valid at 50 m, this map outlines the incredible wind resource in Wyoming. The dark black lines represent electrical transmission lines. The area of interest resides in the lower triangular region bounded from the southwestern corner to the northeastern corner of the state. This area has been the focus for the majority of Wyoming related wind energy research.

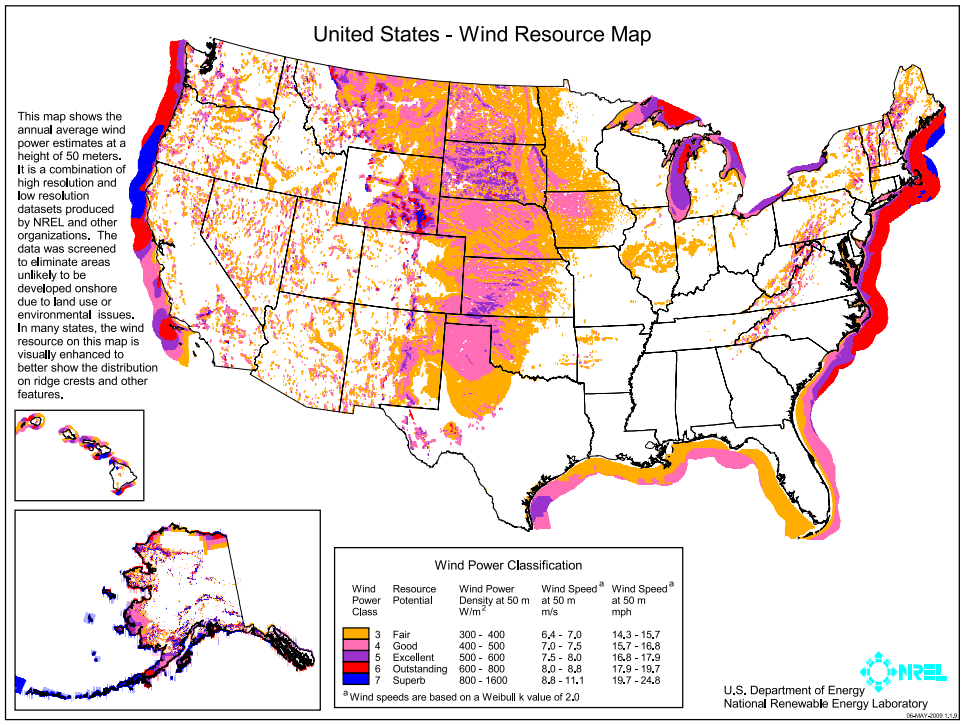

Figure 4.3: US WPD at 50 m generated by NREL. Dark blues and reds correspond to areas of high wind resource.

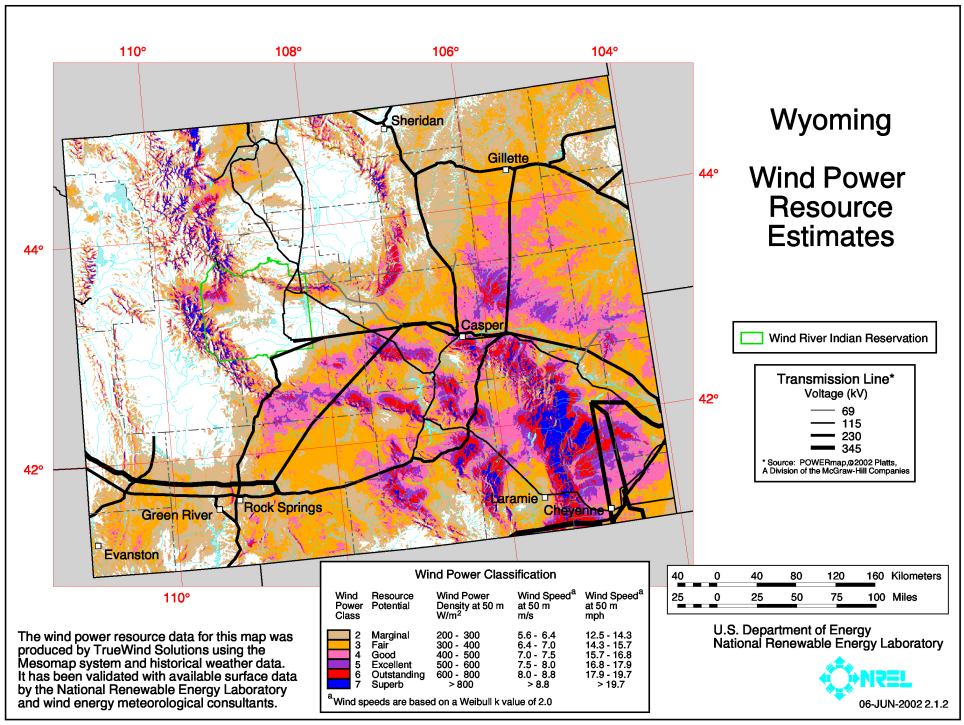

Figure 4.4: NREL 50-m WPD map for Wyoming.

These maps, however, only tell a small part of the story. They provide no information about the variability of the resource.

4.3: Maps Generated From Model Simulations

Figure 4.5 is a map of average US 50-m WPD for 2008-2010 using output from the NAM 12-km. All WPDs were calculated at 50 m, so if not specified, assume a height of 50 m. The same color scheme will be invoked in all subsequent maps: brown corresponds to Class 1 sites, green to Class 2 sites, yellow to Class 3 sites, light orange to Class 4 sites, darker orange to Class 5 sites, red to Class 6 sites and white to Class 7 sites. The color bar labels are in W m^{-2}. These maps illustrate the available power in the wind, and, since WPD is proportional to the cube of the wind speed, WPD is plotted rather than just the wind speeds. This cubic relationship also means that minor changes in wind speed get amplified when calculating WPD. Plotting WPD also makes it easier to recognize minor changes in wind speed. The forecast times, prefixed with an "F," are in UTC. Laramie is seven hours behind UTC, so F000 means 5 P.M. Mountain Standard Time.

As with the NREL maps, Wyoming stands out as a source of fantastic wind resource, especially the southeastern corner of the state. Averaged over a three year period, the data plotted in Figure 4.5 are fairly climatologically stable. Obviously, a larger dataset further validates this. This map was generated using no rated speed. Returning to the discussion in Chapter 3, high wind events can conceivably skew a region's wind power potential. The same map can be generated, as seen in Figure 4.6, utilizing a reasonable rated speed of 15 m s^{-1} at 50 m. That is, 50-m wind speeds beyond 15 m s^{-1} were truncated to 15 m s^{-1}.

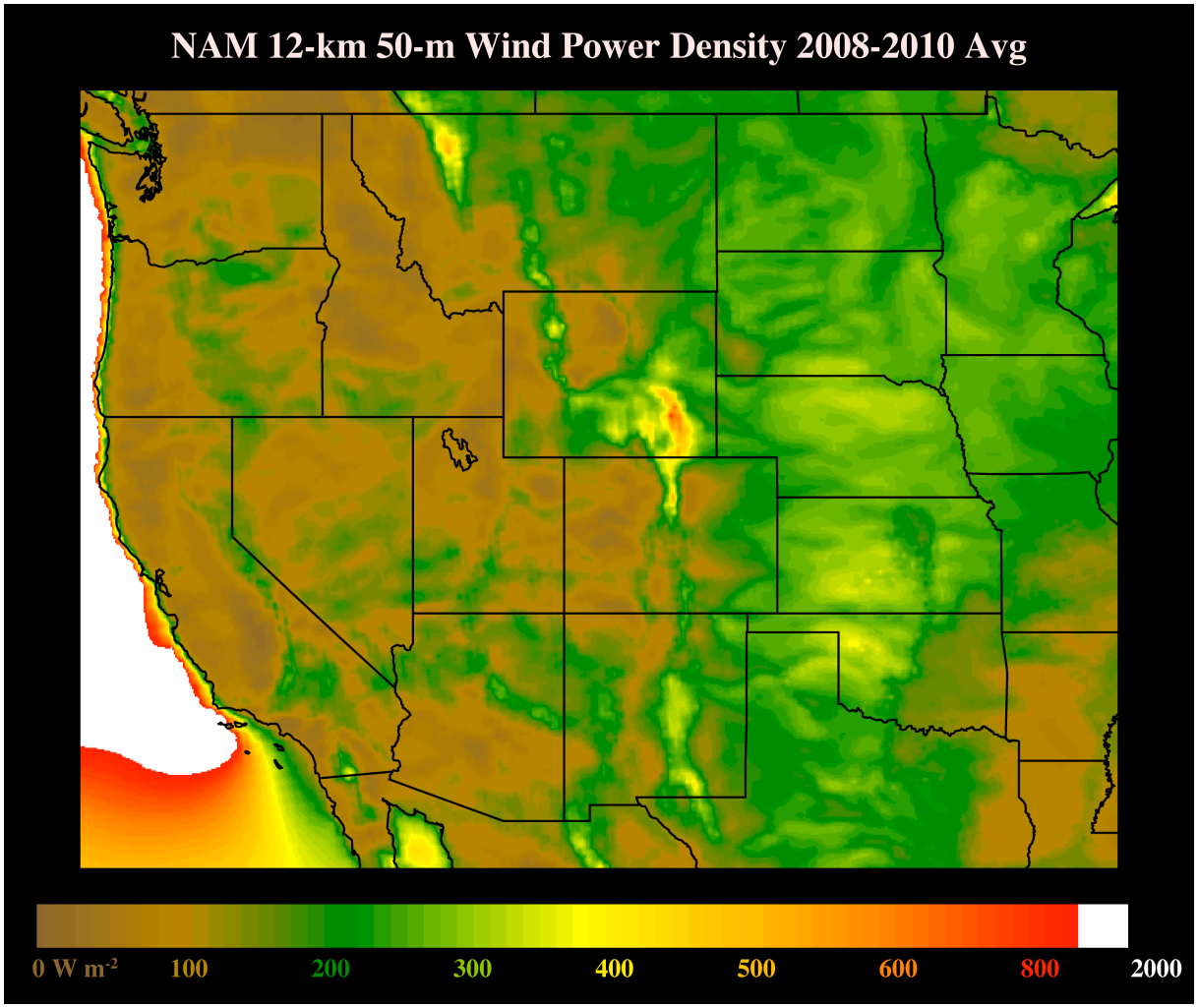

Figure 4.5: US 2008-2010 average of WPD at 50 m via NAM 12-km output.

Armed with only a quick glance at these maps, it is perfectly reasonable to expect a declaration of indiscernibility. Indeed, the minute differences center on the lack of dark oranges in the map employing a rated speed; otherwise, the two maps are nearly identical. From an energy standpoint, this is encouraging. The difficulty in distinguishing these two maps speaks to the persistence of the resource. Even when utilizing a rather conservative rated speed of 15 m s^{-1}, the southeast corner of Wyoming still averages to about 500 W m^{-2}. As with the NREL national wind resource map, plotting WPD across the western part of the US masks the details in places of copious wind power.

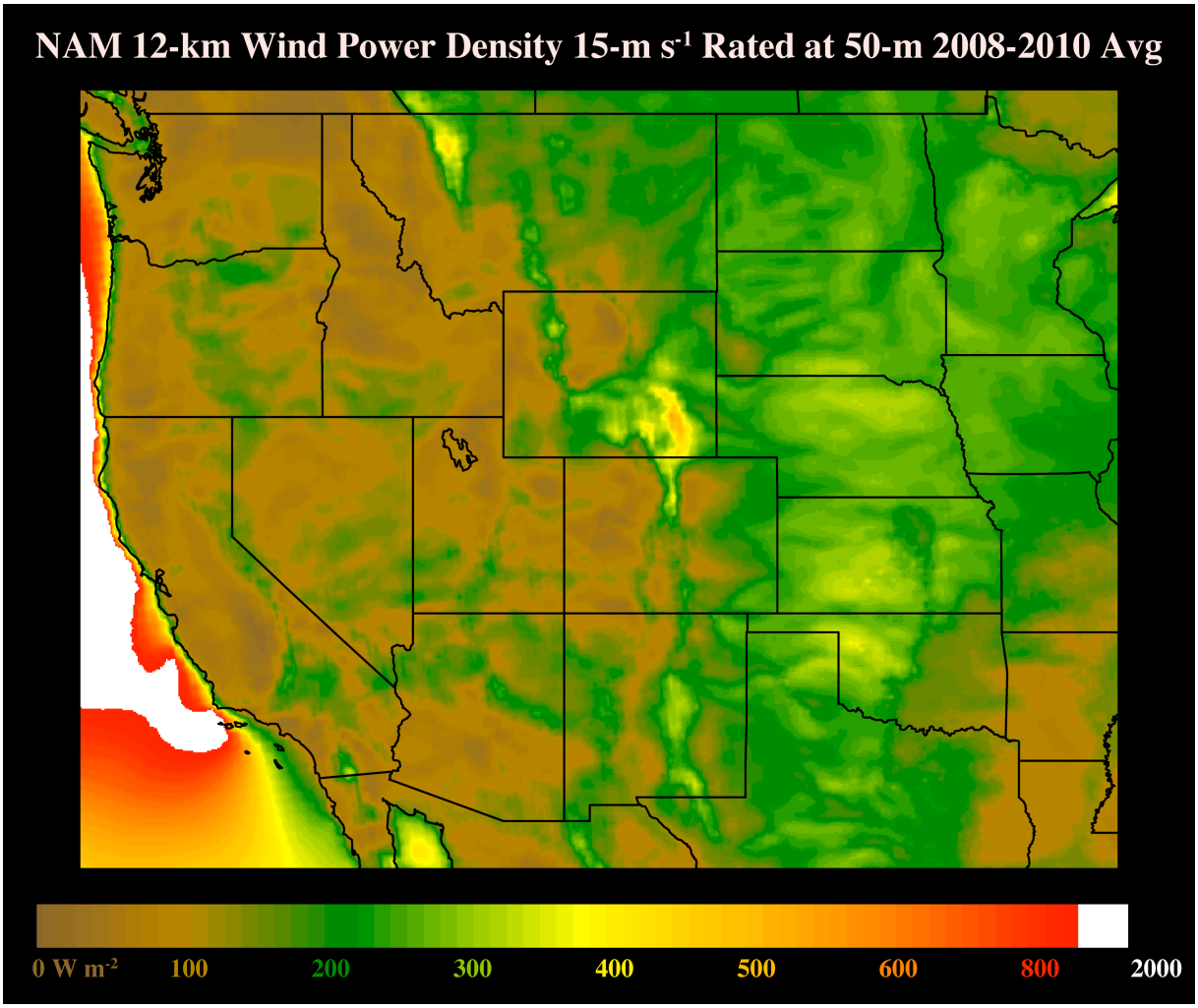

Figure 4.6: Average US WPD map at 50 m 2008-2010 using NAM 12-km data and a 15 m s^{-1} rated speed.

Wind power density in Wyoming for the same time period is illustrated in Figure 4.7. Cities and counties are outlined (thin black lines) as well as interstates 80, 90 and 25 (squiggly dark purple lines) for geographic reference. The color scheme is the same as in the maps of US wind power.

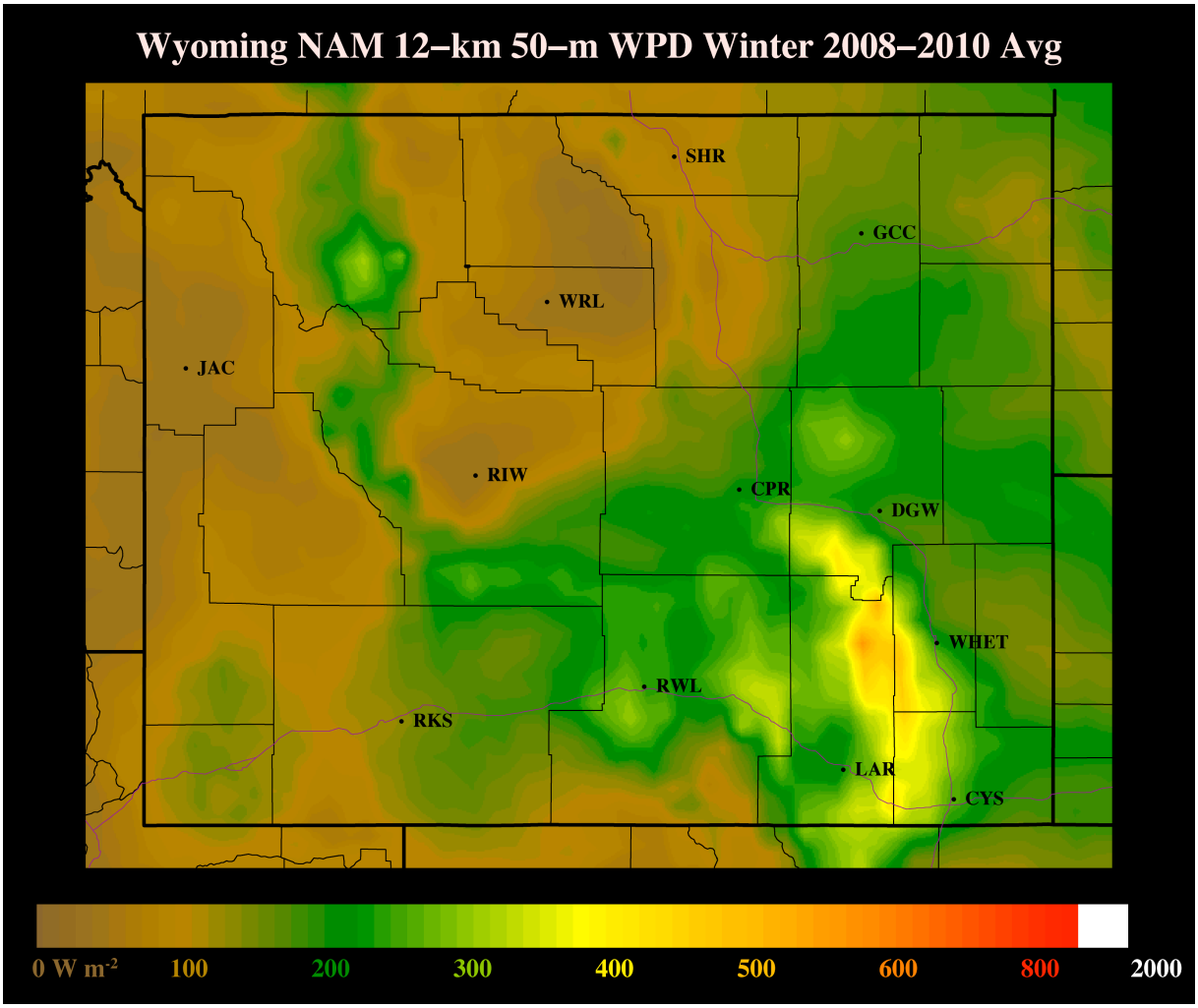

Figure 4.7: Average NAM 12-km 50-m Wyoming WPD 2008-2010.

This map utilizes no rated speed. The bottlenecking of the wind through the wind corridor near LAR becomes quite apparent, even when averaged over the three year period. The Wyoming equivalent of Figure 4.6 is shown in Figure 4.8. The same 50-m 15 m s^{-1} rated velocity was employed. Like the US maps, the two Wyoming maps are almost indistinguishable. When a rated velocity is applied, the small bit of orange north of Laramie (LAR) becomes muted.

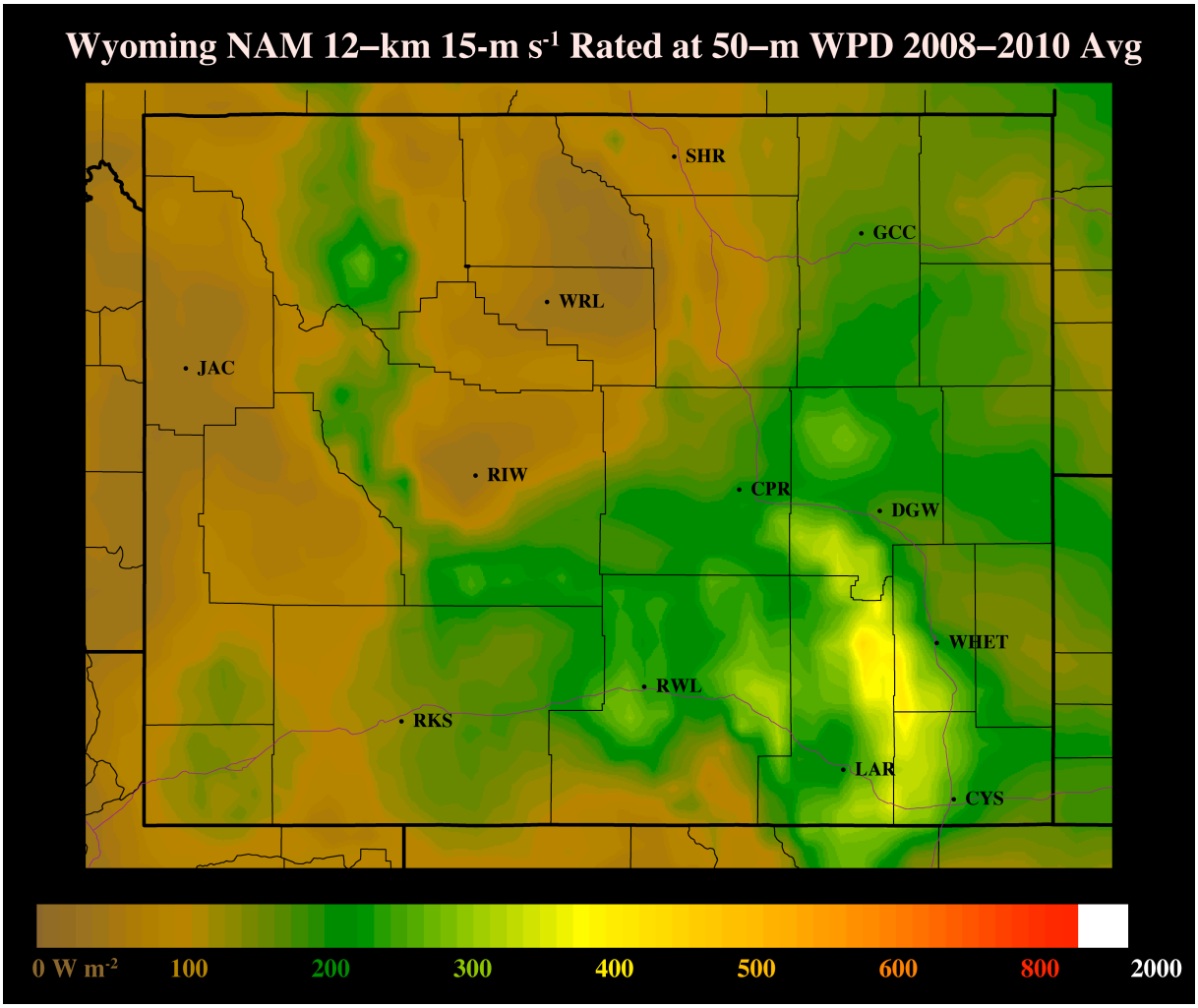

Figure 4.8: Average NAM 12-km 50-m Wyoming WPD 2008-2010 utilizing a 15 m s^{-1} rated speed.

Recognizing that the persistence of the resource is not due to some numerical artifact, the individual years can be analyzed in efforts of further understanding the nuances associated with this finicky atmospheric phenomenon. Figure 4.9 shows WPD for each year in Wyoming.

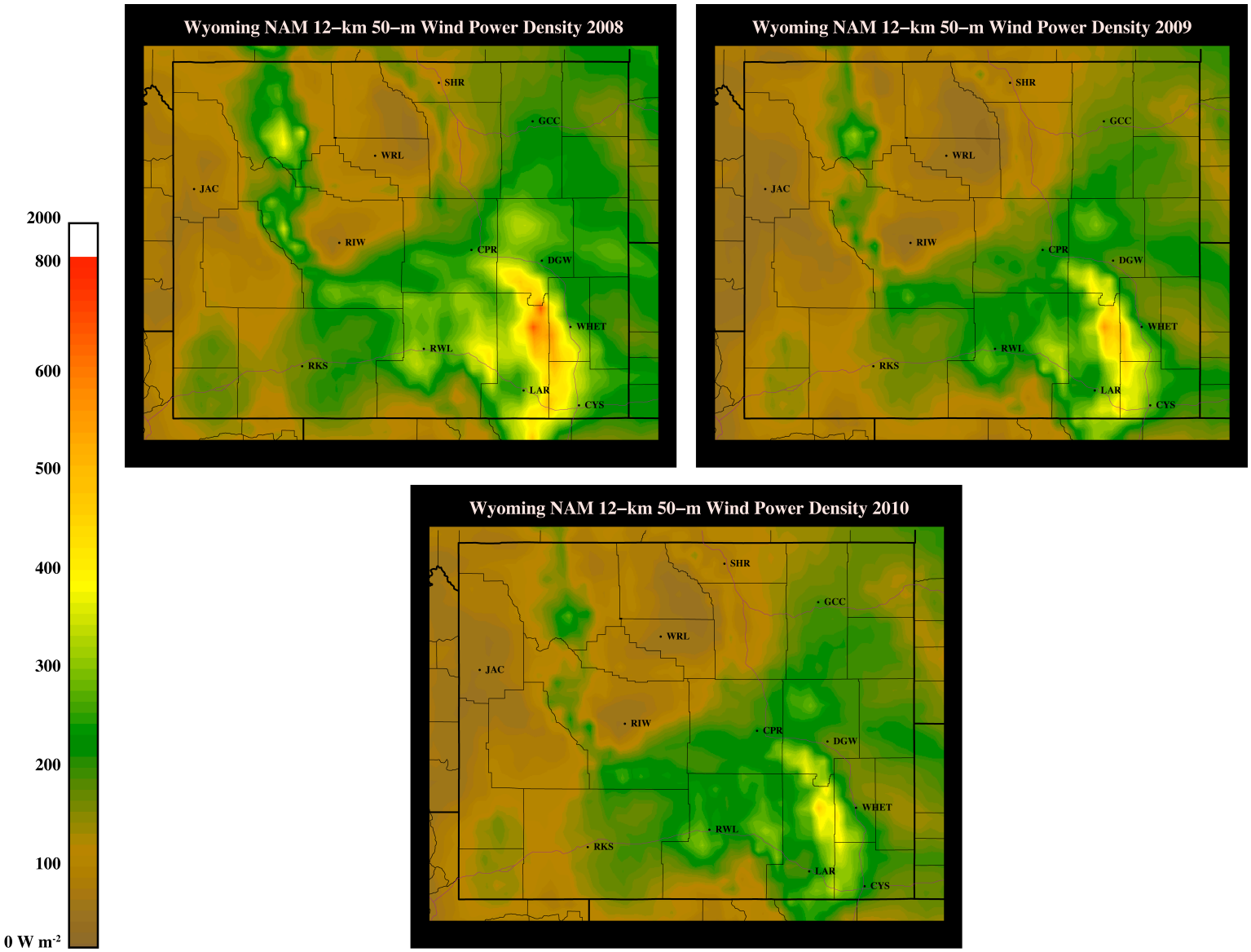

Figure 4.9: Wyoming wind power density for 2008, 2009 and 2010 utilizing the 12-km NAM and no rated speed.

Between years there appears to be some variability in the overall strength of the wind power: 2010 was a bit weaker and 2008 was a bit stronger. Inter-year variability becomes important, especially to wind farm operators. Knowing that the southeastern corner of Wyoming is windy does not provide enough information. Even the small variability between each year complicates the integration of wind into the energy supply if the resource cannot be predicted. Recall the discussion in Chapter 2: the wind farm owners are penalized for incorrect power bids. Nonetheless, the southeastern corner of Wyoming maintains its status as a region of high wind resource. Though these maps compare to the NREL Wyoming map, the area of Class 7 wind resource (blue on NREL's map, white in the NAM maps) is nonexistent in Figure 4.7. The highest WPD values in the NAM maps barely qualifies as Class 6. Is Figure 4.7 wrong? Not exactly. Averaging WPD over the entire year smooths out the overall picture: days, or even months, of low WPD negate periods of high WPD.

To appreciate some of the modes of variability inherent in the resource, Figures 4.10, 4.11, 4.12 and 4.13 illustrate the seasonal trends of WPD for the 2008-2010 average and 2008, 2009 and 2010 individually. These four panel plots divide the year into the seasons as outlined in Table 3.4.

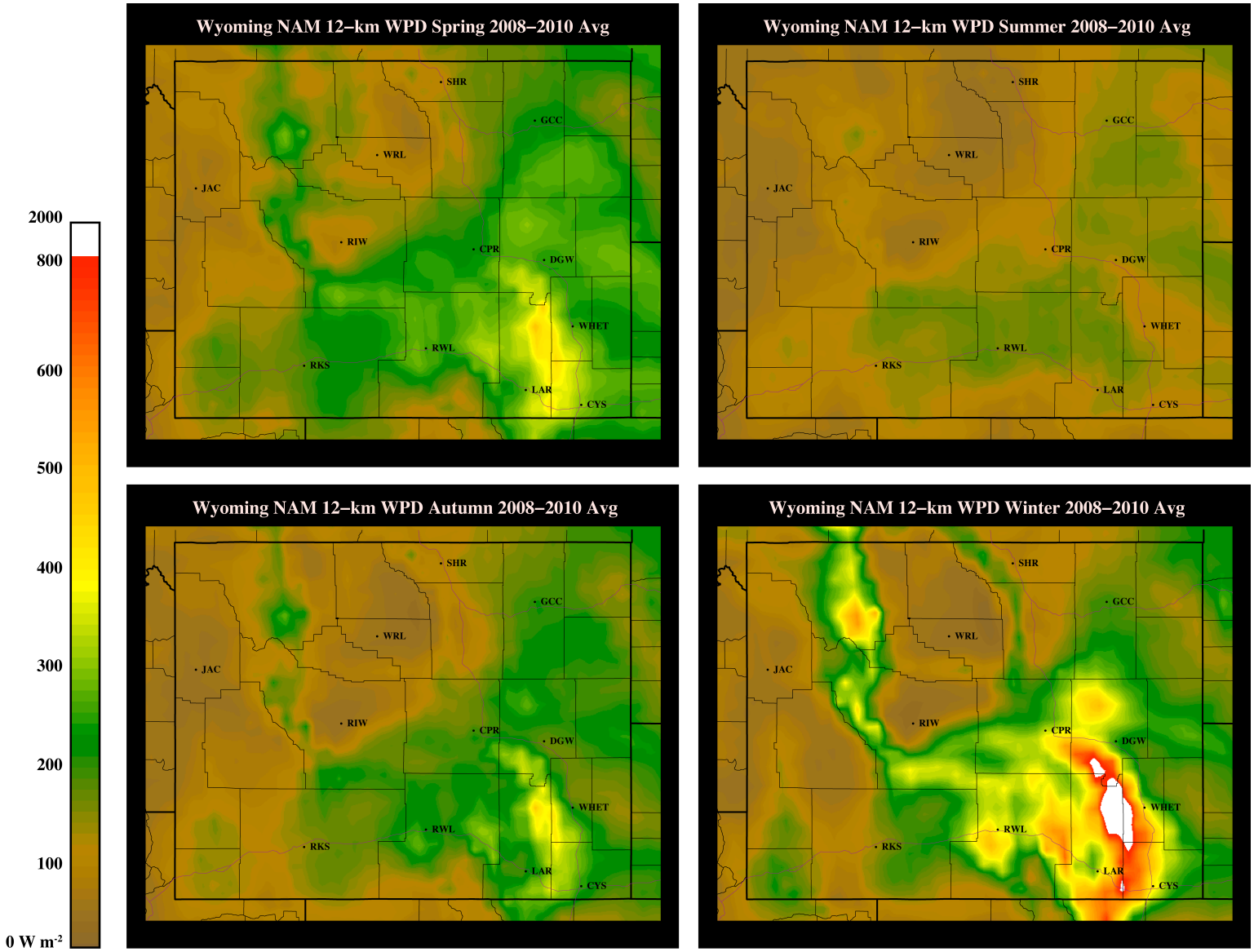

Figure 4.10: Seasonal variability of 2008-2010 average WPD using no rated speed.

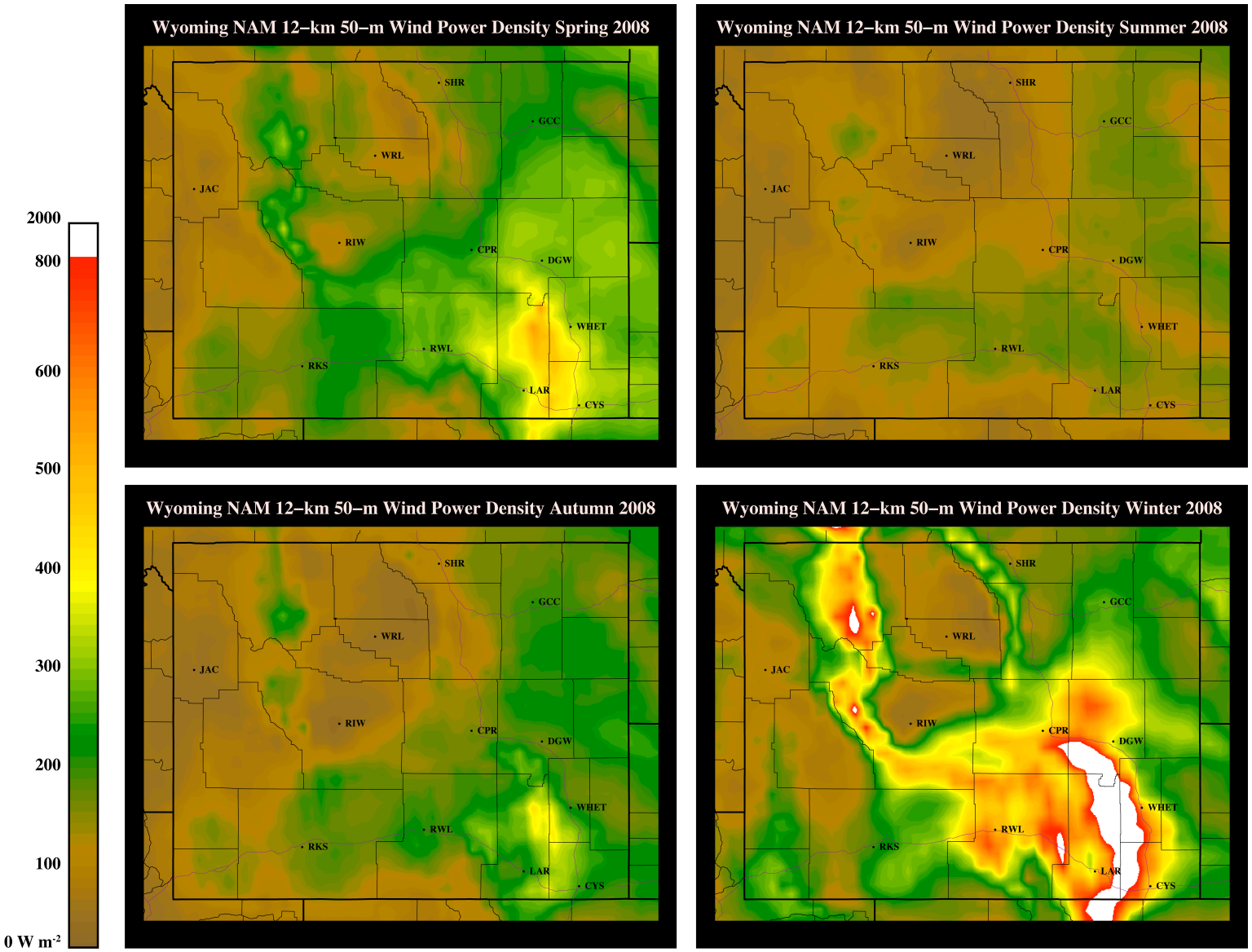

Figure 4.11: Seasonal variability of WPD for 2008 using no rated speed.

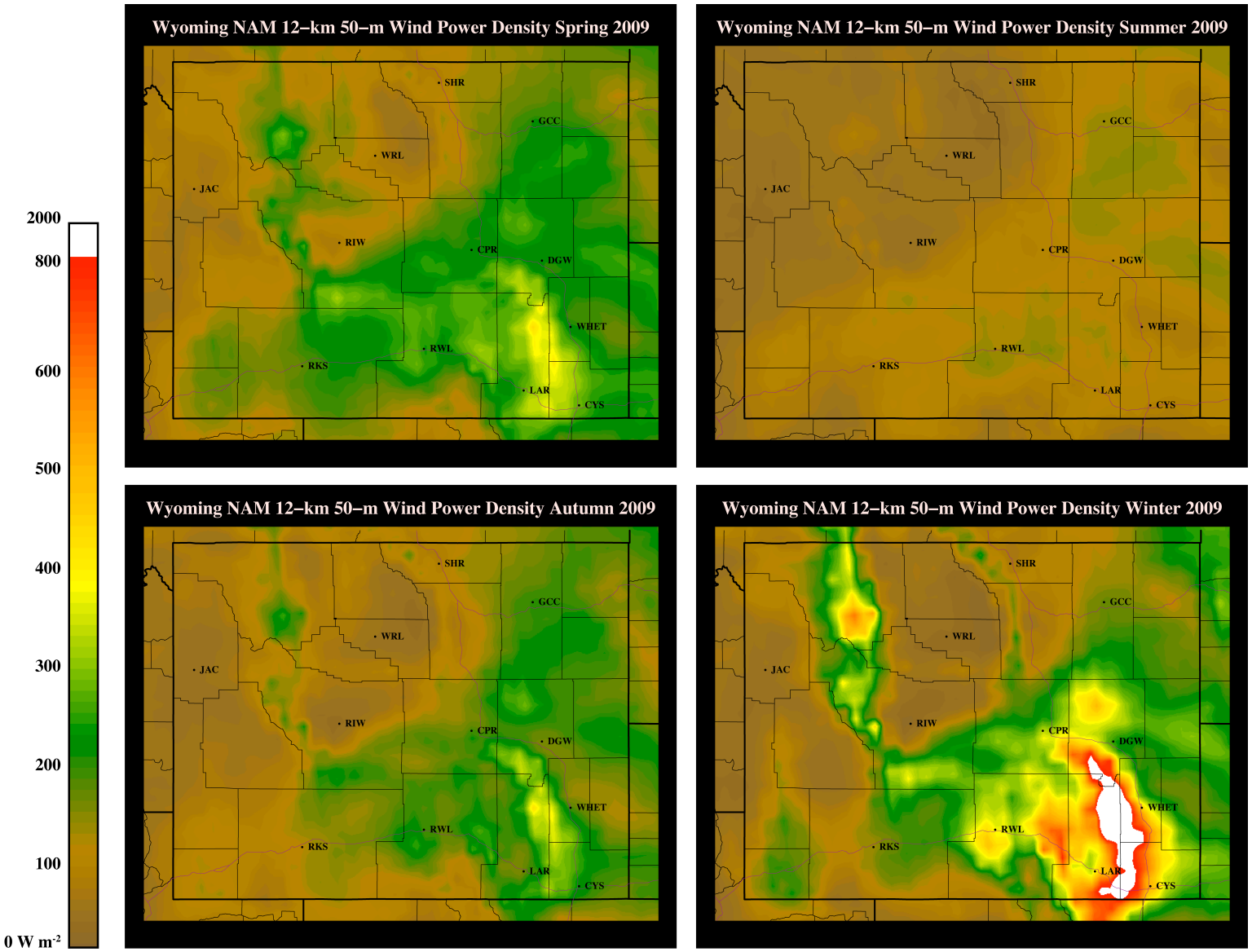

Figure 4.12: Seasonal variability of WPD for 2009 using no rated speed.

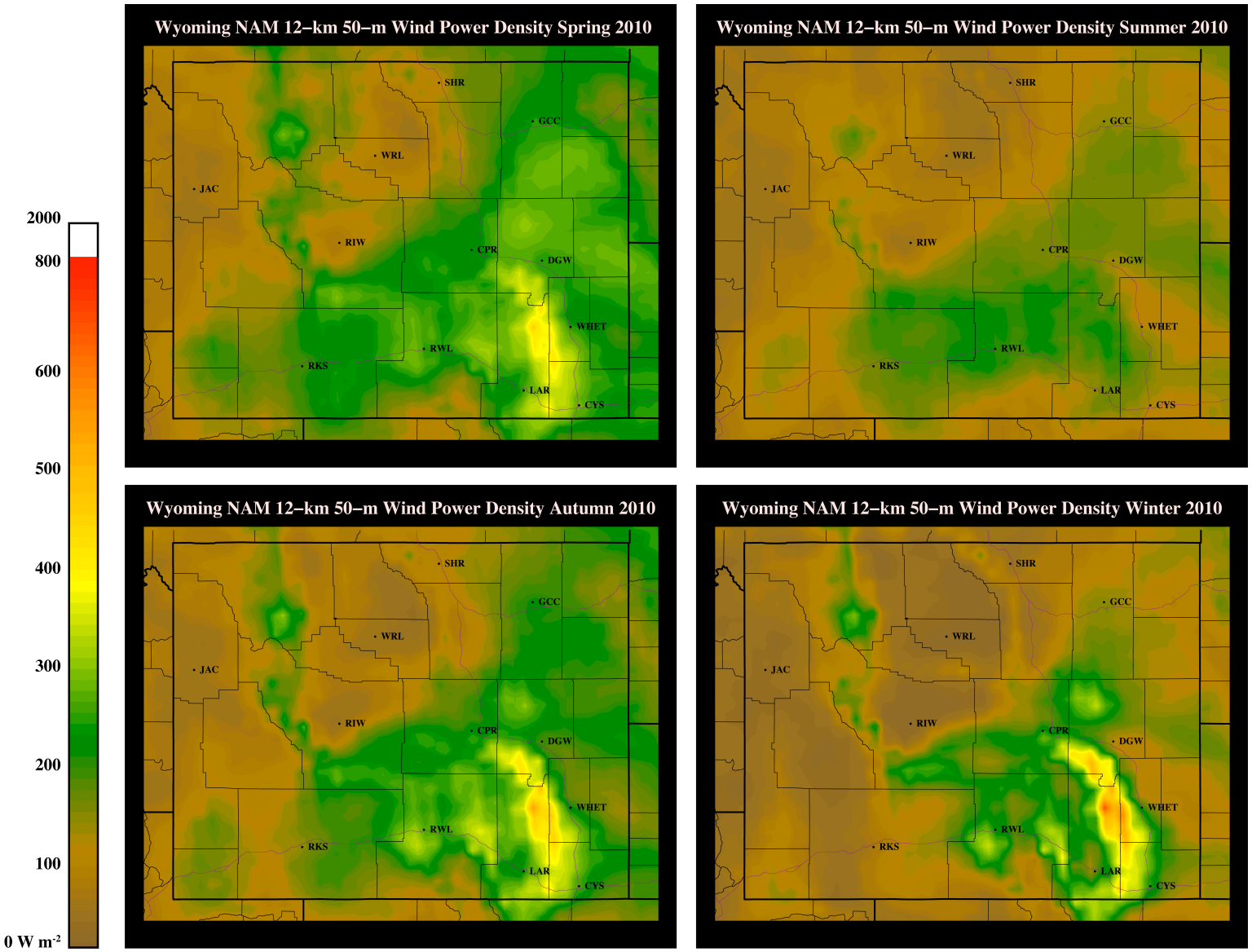

Figure 4.13: Seasonal variability of WPD for 2010 using no rated speed.

Immediately, the stark seasonal contrasts become apparent. The Class 7 resource seen in NREL's map reflects the WPD available in the wintertime in the NAM maps. The spring and autumn afford decent WPD and almost all of Wyoming is brown in the summertime, reflecting Class 1 quality wind resource. Of the four seasons, spring and autumn exhibit essentially the same behavior while summer and winter exemplify a classic dichotomy. When averaged over the entire year, the summer and winter "cancel out" and the spring and autumn serve as the template for annual WPD.

The year-to-year variability manifests itself even further when comparing these four panel plots from each year. 2009 seems fairly representative: maximum WPD in the winter, spring and autumn comparable and mostly Class 1 WPD in the summer. 2008 essentially follows this same pattern, albeit every season in 2008 was stronger compared to 2009; 2010, however, seems to be the odd-ball of the bunch. Spring, summer and autumn of 2010 all exhibit the same trends as 2008 and 2009. But it is the wintertime 2010 that is the source of the abnormality. No Class 7 wind is generated during the winter of 2010 (or, for that matter, the entire year of 2010). This anomaly is the reason for the weak annual average seen in Figure 4.13. Also odd is that, while winter of 2010 was the weakest of the three years, summer of 2010 was the strongest of the three years. The entire wind corridor is stained with dark green, whereas the summers of 2008 and 2009 are hardly green at all. These differences speak to the seasonal variability of the resource, in regards to both the inter-seasonal variations of the wind and the year-to-year intra-seasonal variance. Though Figure 4.10 provides a sturdy foundation for assessing the wind resource, the discrepancies in Figures 4.11, 4.12 and 4.13 illustrate the importance for accurate and continuous wind measurements.

Just because Figure 4.10 depicts winter as providing lots of WPD, it does not mean that WPD is guaranteed. 2010 serves as a perfect example of this, demonstrating that these seasonal trends are just that: trends.

Up to now, the WPD maps have all utilized the NAM 12-km data. And for good reason: the NAM 4-km, as discussed in Chapter 3, is preempted during hurricane season and thus no complete yearly data record exists. Fortunately, data for the time of interest, winter, exists. A three panel plot of the winter WPD generated from the NAM 4-km can be seen in Figure 4.14. Intuition presumes that the higher resolution model should more accurately simulate the wind. Upon inspection, the 4-km output does provide more spatial detail. The maps in Figure 4.14 are indicative of more terrain-dependent locations of WPD. The areas of high WPD are much more concentrated near the mountain ranges in the wind corridor. But oddly, the NAM 4-km tends to under-predict the wind compared to its lower resolution counterpart. Overall, the 4-km map contains much less red and white corresponding to Class 7 wind sites. The year-to-year wintertime variability matches between the two models: as the years progressed, WPD decreased, though the difference between 2008 and 2009 is tougher to perceive with the 4-km maps. Despite that, the weakness of 2010 is glaringly conspicuous from both intra- and inter-model comparisons.

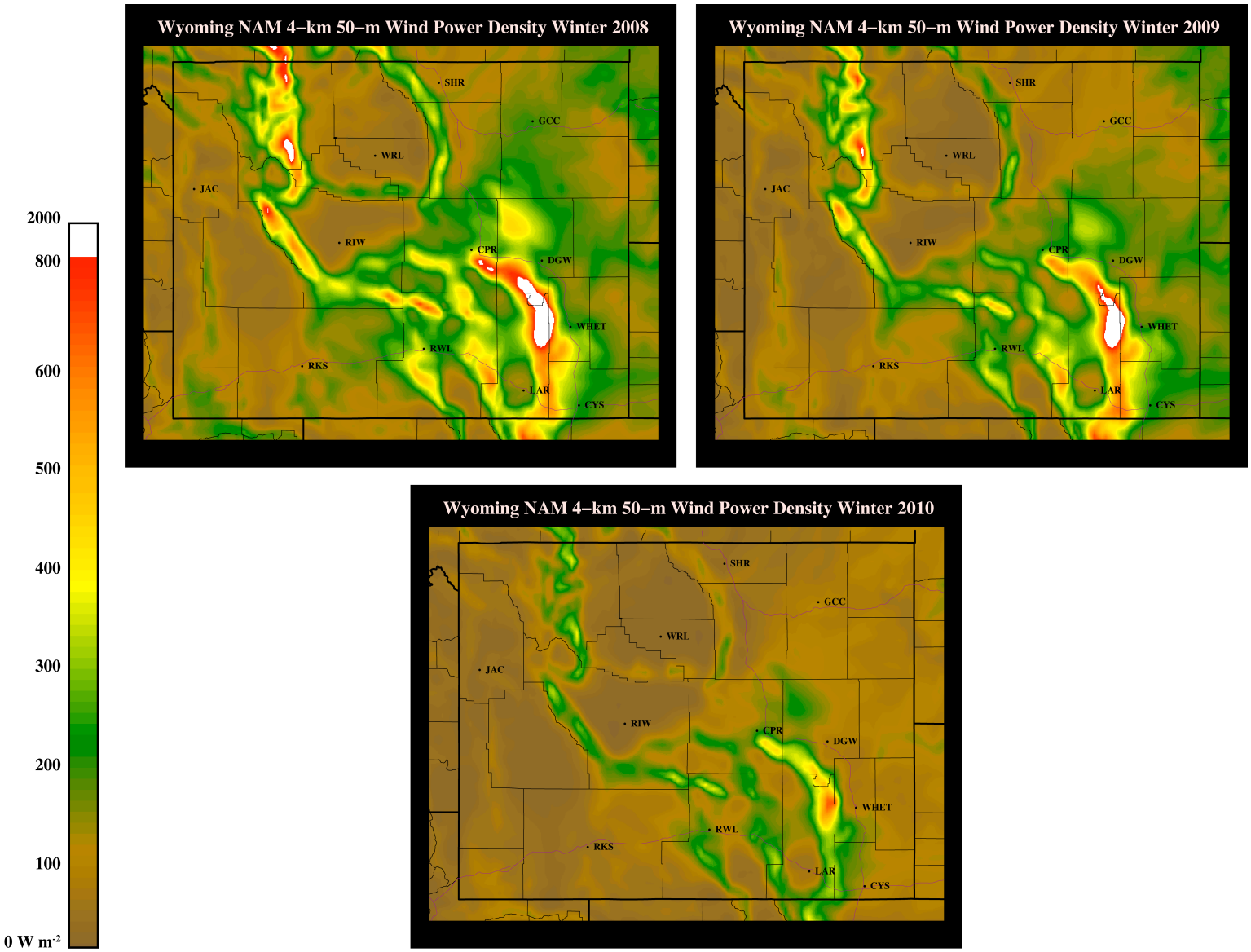

Figure 4.14: Winter WPD for 2008, 2009 and 2010 from the NAM 4-km.

Of special interest is the Laramie valley, one of the windiest inhabited areas in Wyoming. The NAM 12-km estimates wind power density on the order of 500 W m^{-2}, whereas the NAM 4-km estimates wind power density on the order of 200 W m^{-2}: a difference of three wind classes! Situated between two mountain ranges, this particular area presents a challenge in representing the surrounding terrain. Higher resolution models may not always be better, especially if they cannot render the terrain accurately. This reflects the discussion in Chapter 2. Simulations with unrealistic topography result in incorrect atmospheric flow dynamics, handicapping the prediction of the wind. Minor differences in wind speed will quickly propagate when plotting wind power density. The 4-km output clearly demonstrates misplacement errors that occur when transitioning from a low resolution model to a high resolution model. Encouragingly, the simulated NAM 4-km WPDs for all three years appears to be the same in Figure 4.14. The zone of brown encircling the Laramie valley is in each wintertime simulation. Even though the NAM 4-km under-estimates the wind in this region, it does so with remarkable consistency.

The final mode of variability, the diurnal cycle, is shown in the following Figures. This is arguably the most important mode to understand and be able to predict. Energy is traded on a twenty-four hour cycle and the more accurate wind farm operators can predict their power output, the more money they make. Potentially damaging (or alternatively, profitable) ramp events also occur within this mode further highlighting its significance. Since winter is the time of interest and both 12-km and 4-km data exist, the next two Figures illustrate the diurnal cycle for 2009 for each model.

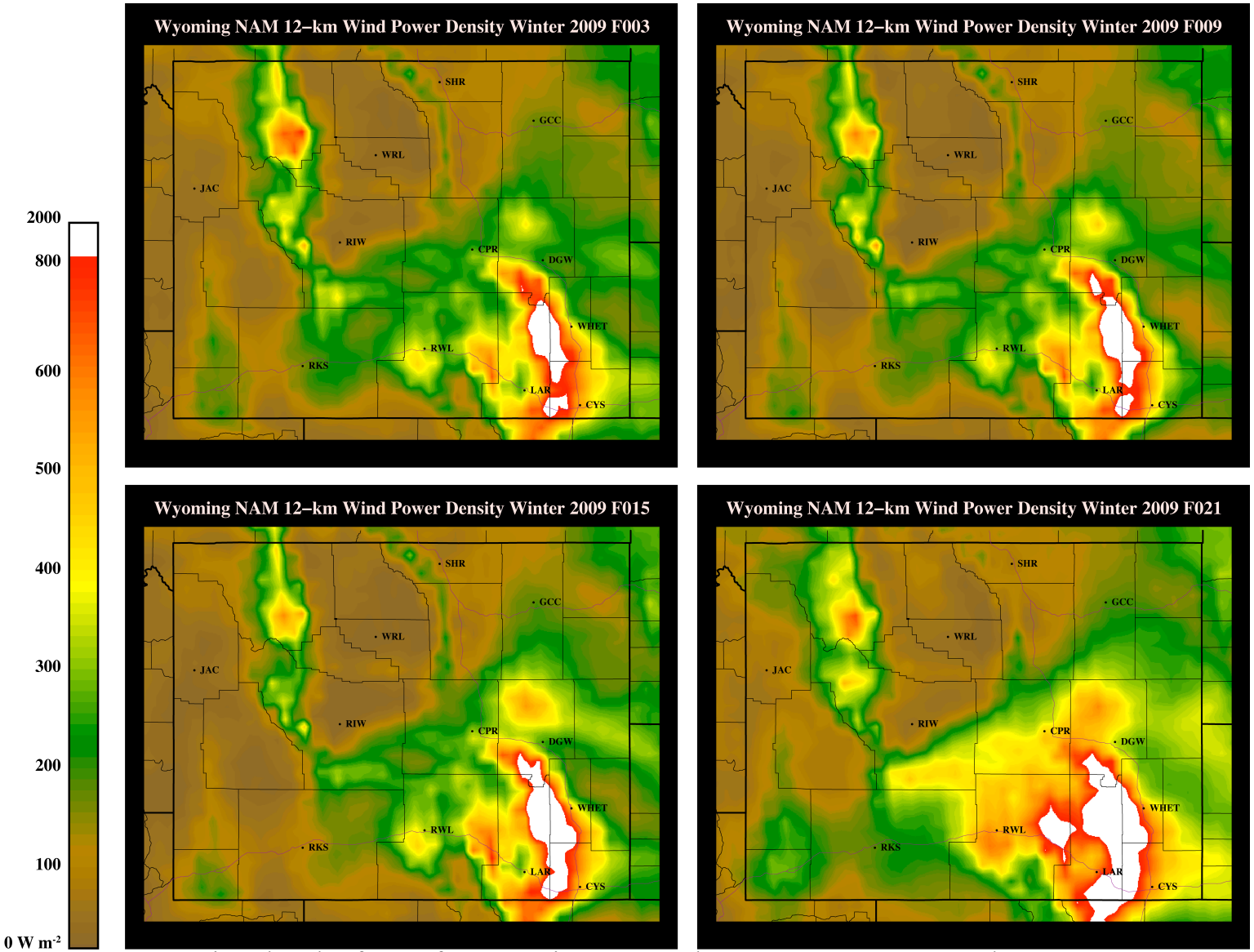

Figure 4.15: Diurnal cycle of WPD for 2009 using NAM 12-km output. F003 corresponds to 8 P.M. MST, F009 to 2 A.M. MST, F015 to 8 A.M. MST and F021 to 8 P.M. MST.

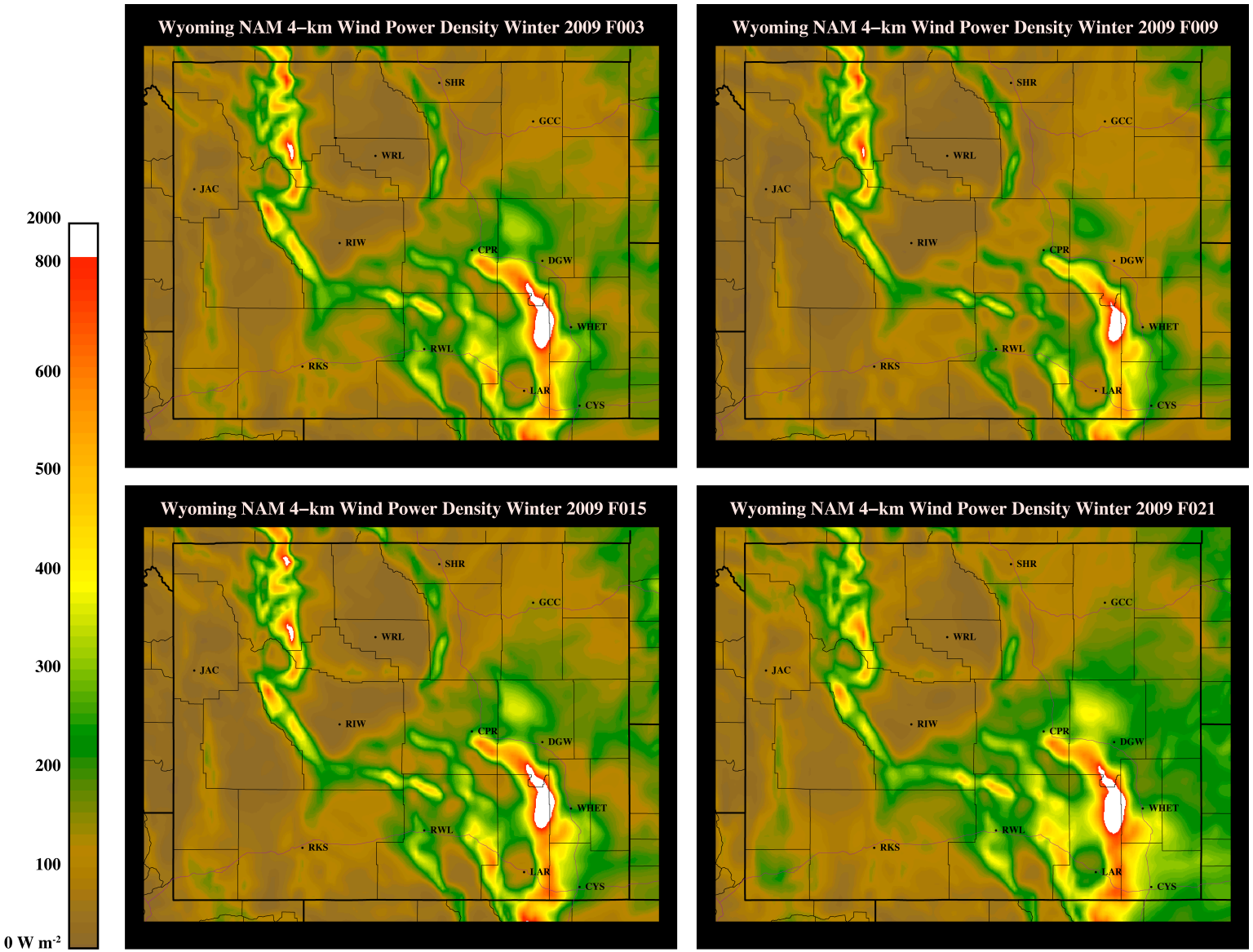

Figure 4.16: Diurnal cycle of WPD for 2009 using NAM 4-km output. F003 corresponds to 8 P.M. MST, F009 to 2 A.M. MST, F015 to 8 A.M. MST and F021 to 8 P.M. MST.

The times in each map are the valid forecast time for the NAM. Wyoming is seven hours behind UTC so Figures 4.15 and 4.16 depict the diurnal variation from late evening to early afternoon. The daily change in WPD is much clearer with the 12-km maps. Peak WPD occurs at F021 which is 2 P.M. Mountain Standard Time (MST). From a meteorological standpoint, this makes sense. Wind is the result of pressure gradients. Pressure gradients are caused by the uneven heating of the Earth's surface. In the afternoon the solar insolation is at a maximum corresponding to the time of maximum WPD. The NAM 4-km does not appear to be as cut-and-dry. In Figure 4.16, it is much more difficult to identify the diurnal cycle. If the timestamps were removed and the maps placed out of order, one would be hard pressed to correctly reorder them. Rather than using the areas of Class 7 wind resource as a proxy, as was done with the NAM 12-km maps, the Laramie valley can instead be used to gauge WPD intensity with the NAM 4-km maps. The brown circular area surrounding the valley is mostly green at F021, which arguably corresponds to the time of maximum wind resource. Basing the time of peak WPD on the amount of Class 7 wind resource would yield a false-positive: the maps at F003 and F015 both have roughly the same amount of white in them. The Laramie valley exhibits a more tangible diurnal cycle. The green areas to the east of the Class 7 zone at F021 also help single out that time as the peak.

Zooming into the southeastern corner of the state, the behavior of the Laramie valley and the entire Class 7 wind resource zone can be more closely examined. Figure 4.17 outlines the area of interest.

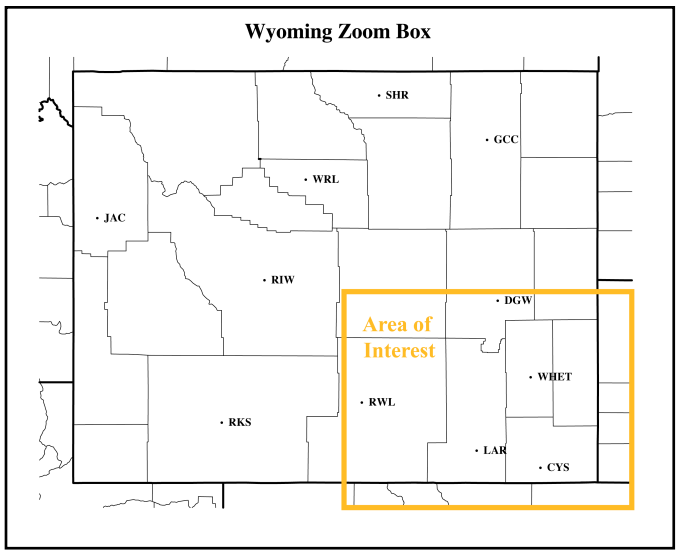

Figure 4.17: Zoom box for the subsequent Figures.

Figure 4.18 illustrates the NAM 12-km winter diurnal cycle for 2009 and Figure 4.19 illustrates the NAM 4-km winter diurnal cycle. The increased level of detail in these Figures further illustrates the tremendous resource in the portion of the state. Unfortunately, when compared, Figure 4.19 makes the underrepresentation of WPD by the NAM 4-km even more apparent. The time of peak WPD is the same for both models, but the overall trends are oddly different. The WPD in the NAM 12-km gradually increases throughout the day, as one would expect. The WPD in the NAM 4-km, though, does not seem to follow the same tendency. WPD seems to decrease from F003 to F009 and from F009 gradually increase. These discrepancies between the models further speak to the importance that wind farm operators use NWP model output as a tool and not as a crutch.

Returning to the concept of rated velocities, Figure 4.20 depicts the same 2009 winter diurnal cycle for Wyoming, only this time incorporating a 15 m s^{-1} rated speed. Understandably, the diurnal cycle is muted when incorporating a rated velocity. But the

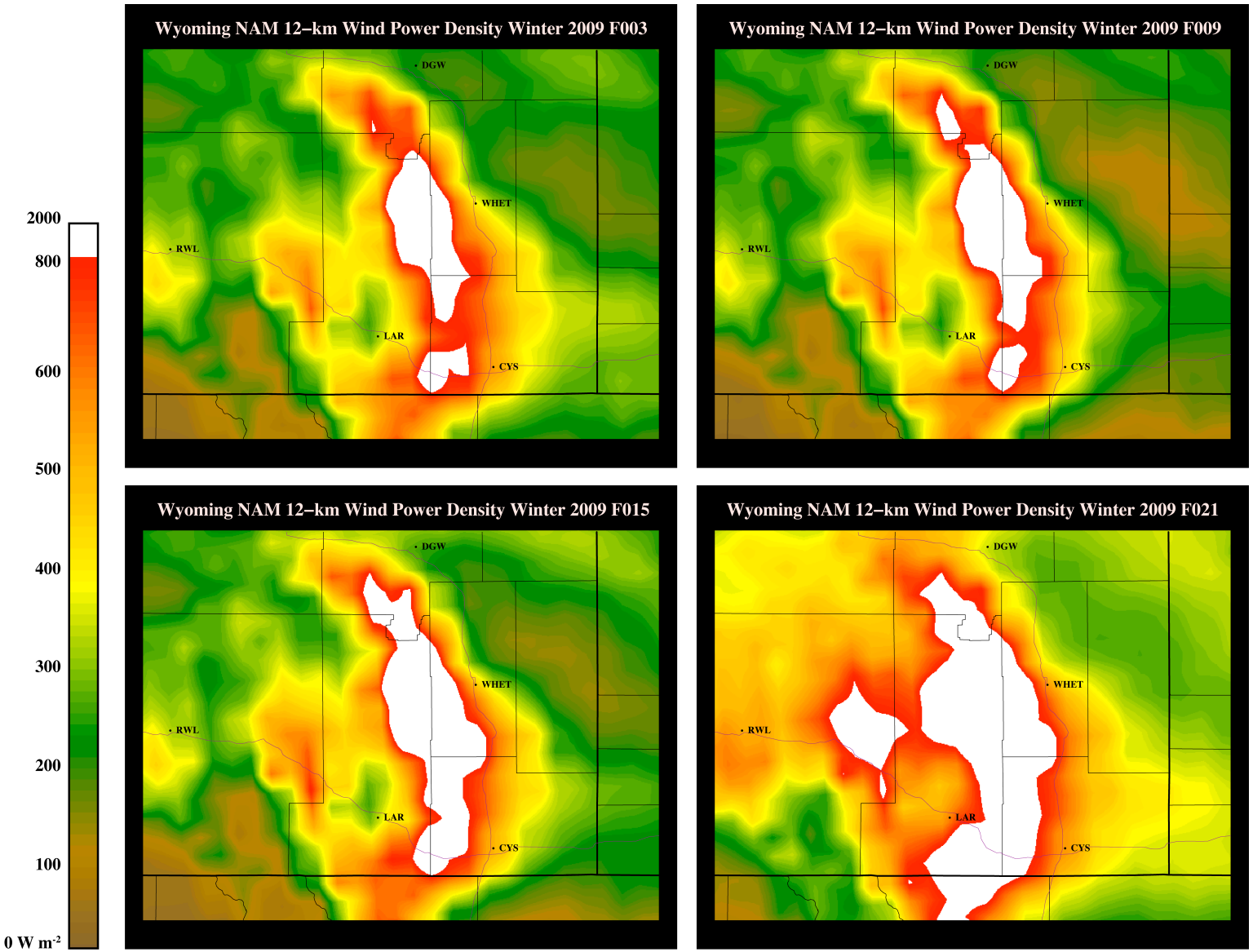

Figure 4.18: Southeast Wyoming NAM 12-km winter 2009 diurnal cycle. F003 corresponds to 8 P.M. MST, F009 to 2 A.M. MST, F015 to 8 A.M. MST and F021 to 8 P.M. MST.

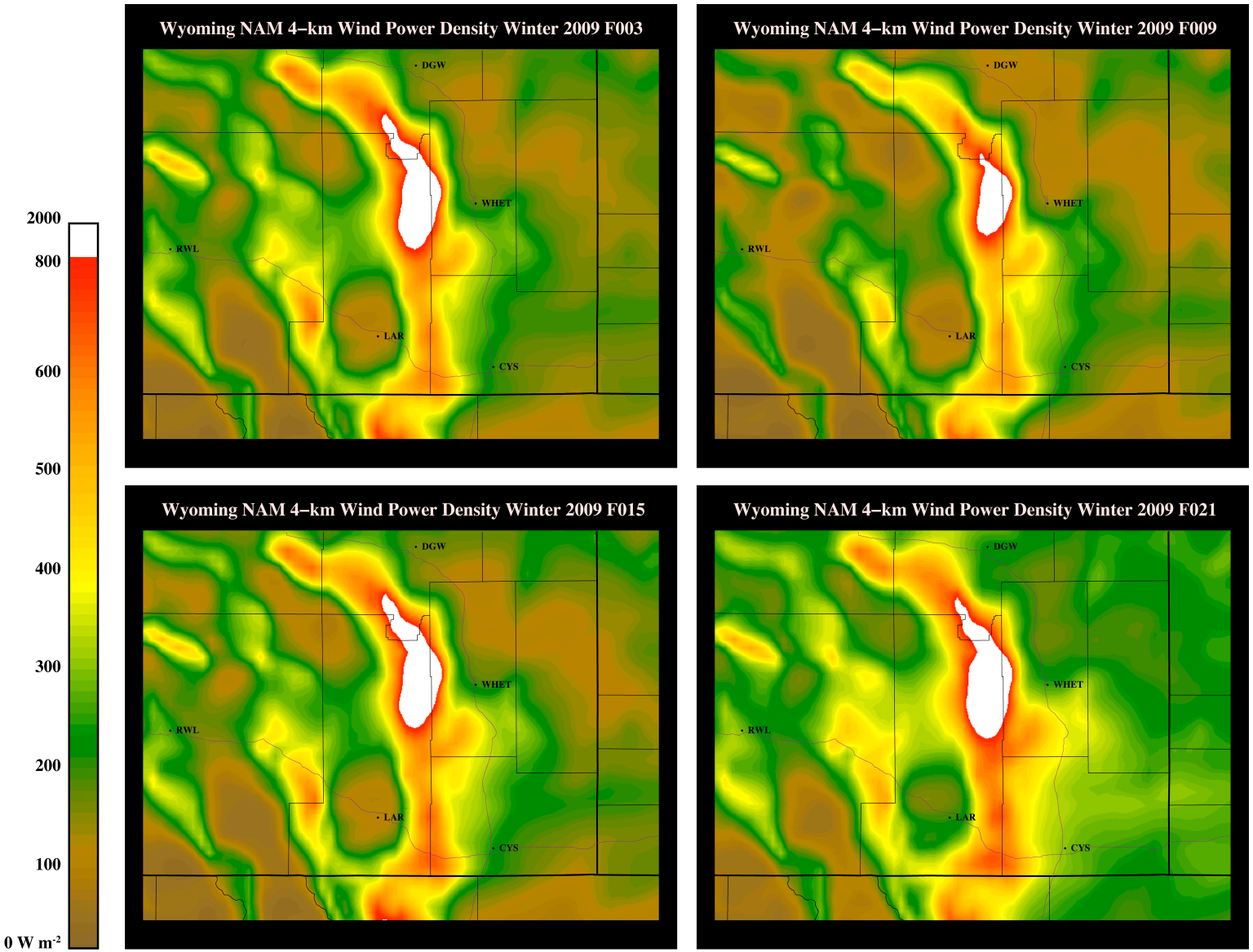

Figure 4.19: Southeast Wyoming NAM 4-km winter 2009 diurnal cycle. F003 corresponds to 8 P.M. MST, F009 to 2 A.M. MST, F015 to 8 A.M. MST and F021 to 8 P.M. MST.

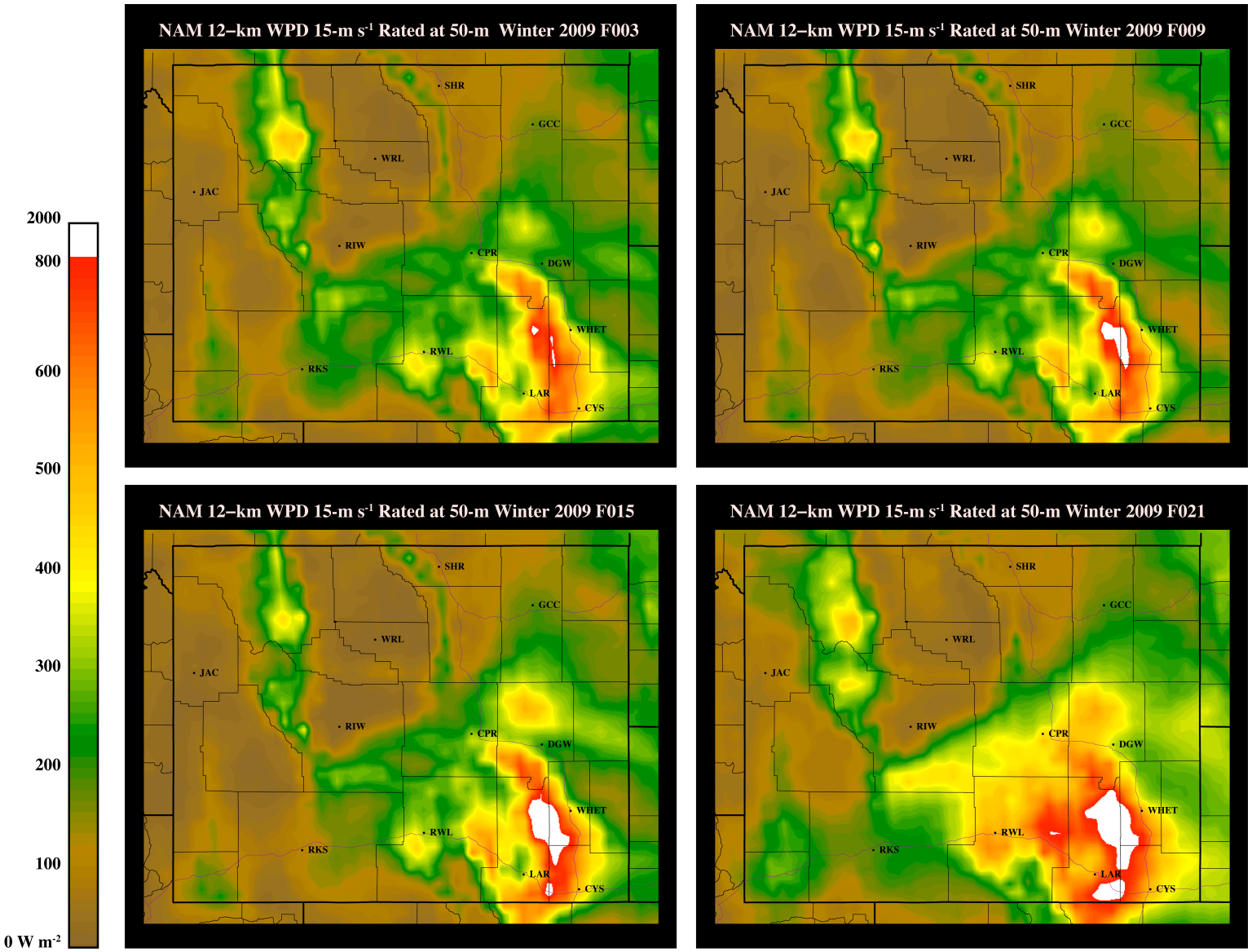

Figure 4.20: Wyoming NAM 12-km winter 2009 diurnal cycle utilizing a 15-m s^{-1} rated speed at 50-m.

overall patterns remain and the respectable amount of Class 7 wind at F021 highlights the absolute gold mine of wind resource available in the wintertime.

4.4: Observational Surface Plots

From a meteorological standpoint, these trends all make sense: windy in the wintertime, windiest in the afternoon. However, this is just model output. To validate model output, comparisons to observations must be made. As outlined in Chapter 3, observational data exists for the eighteen ASOS stations around the state of Wyoming. Picking three representative stations: Laramie, Cheyenne (CYS) and Rock Springs (RKS), comparisons can be made between the model output at those locations and the actual wind speeds recorded. Gillette (GCC), in northern Wyoming is also included to highlight the sharp contrast between the three windy sites of Laramie, Cheyenne and Rock Springs with the not-so-windy site of Gillette. Since these surface plots correspond to the entire year, the NAM 12-km output served as the source of the model data.

The following surface plots help summarize the observed wind power density at the three windy sites for the years 2008-2010 and Gillette for 2009. The horizontal axes correspond to time of day (in UTC) and month of the year. The vertical axis corresponds to wind power. The color scheme is somewhat different than what was used in the wind power maps. Dark blues and purples correlate to low wind power densities and dark oranges, reds and maroons correlate to high wind power densities. The colorbar stops at 800 W m^{-2} and values greater than or equal to 800 W m^{-2} remain a dark maroon. The vertical axis, however, adjusts to the highest value of wind power density.

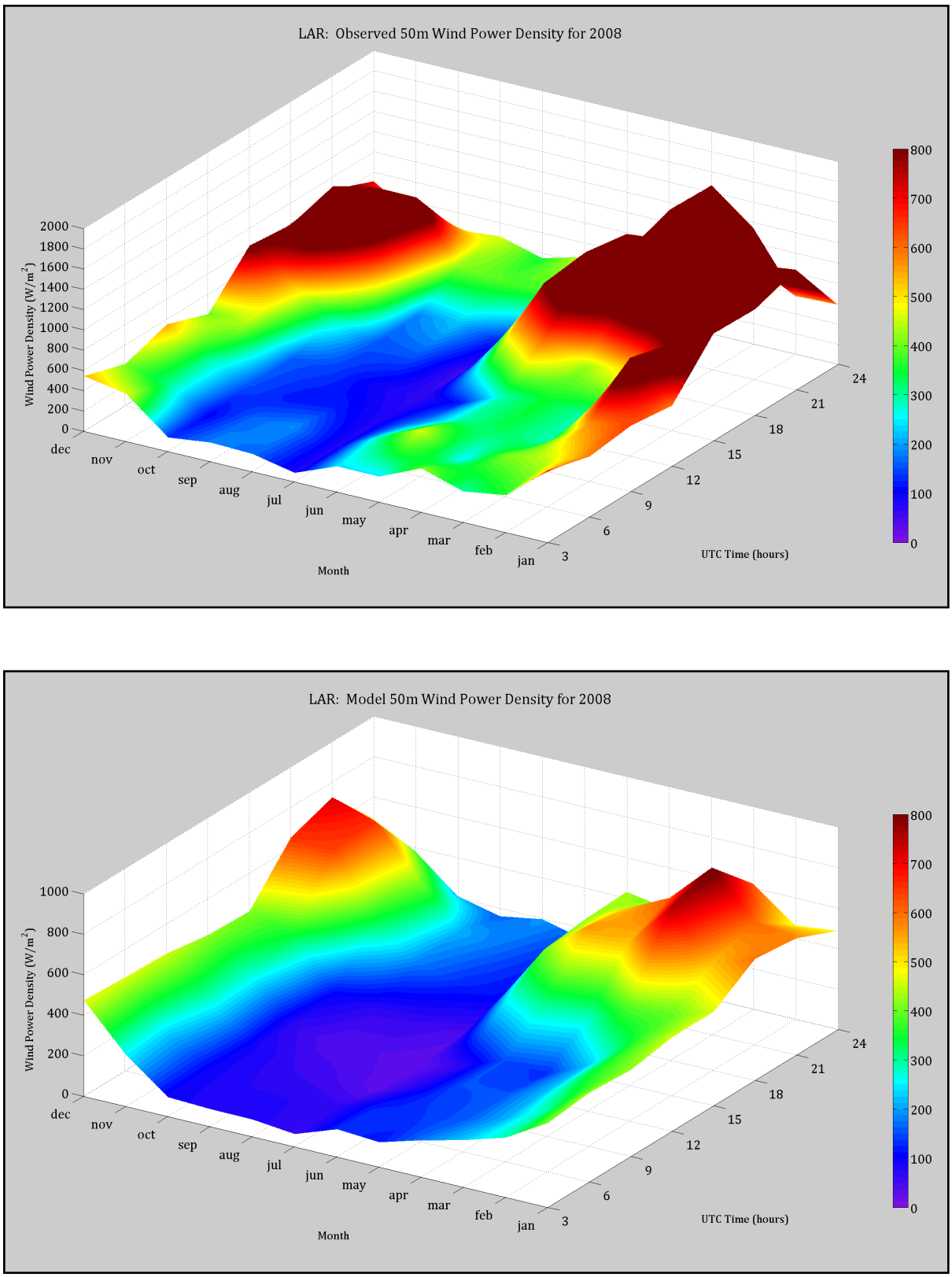

Figure 4.21: Observed and model 50-m WPD surface plots at Laramie in 2008.

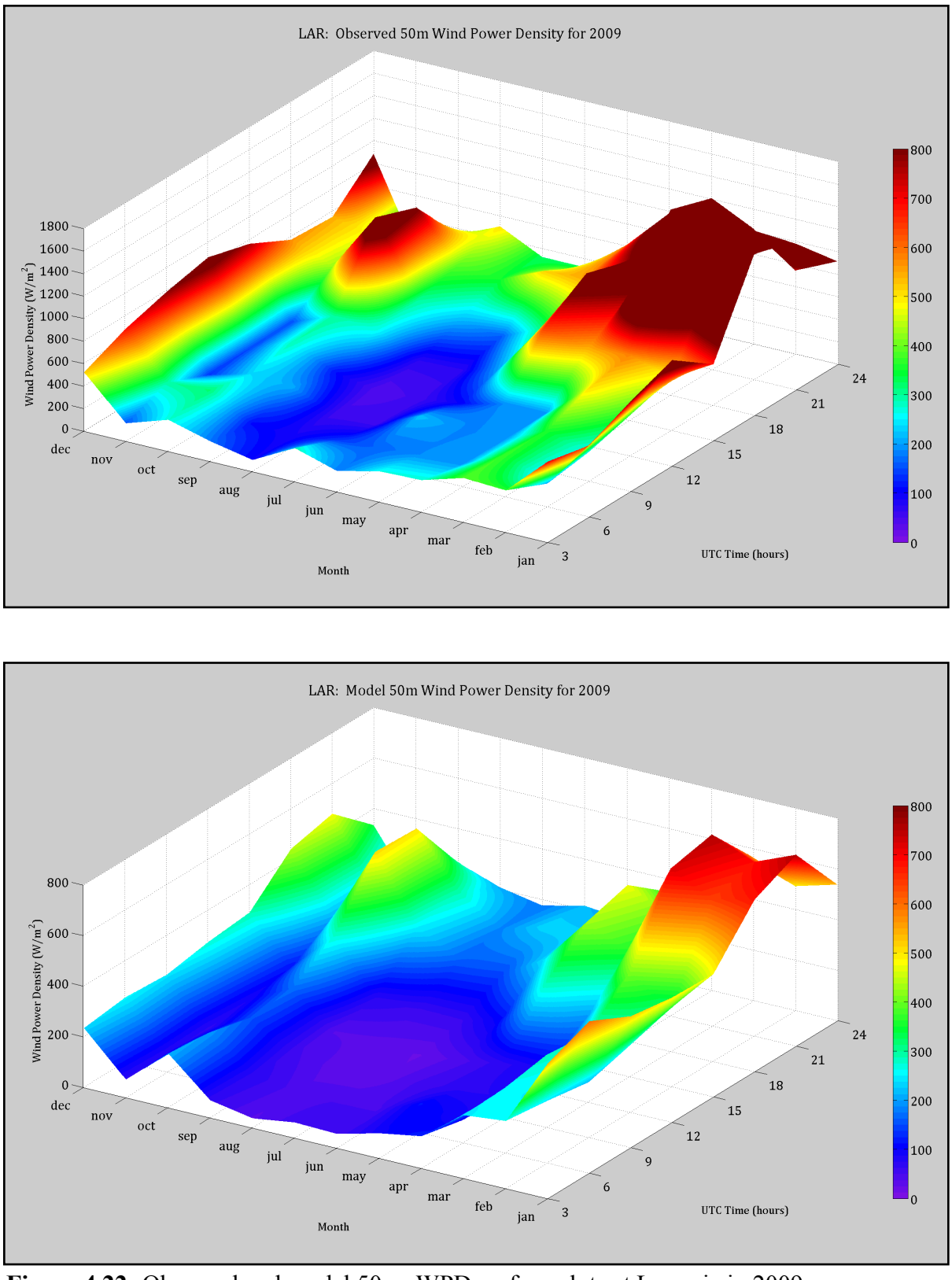

Figure 4.22: Observed and model 50-m WPD surface plots at Laramie in 2009.

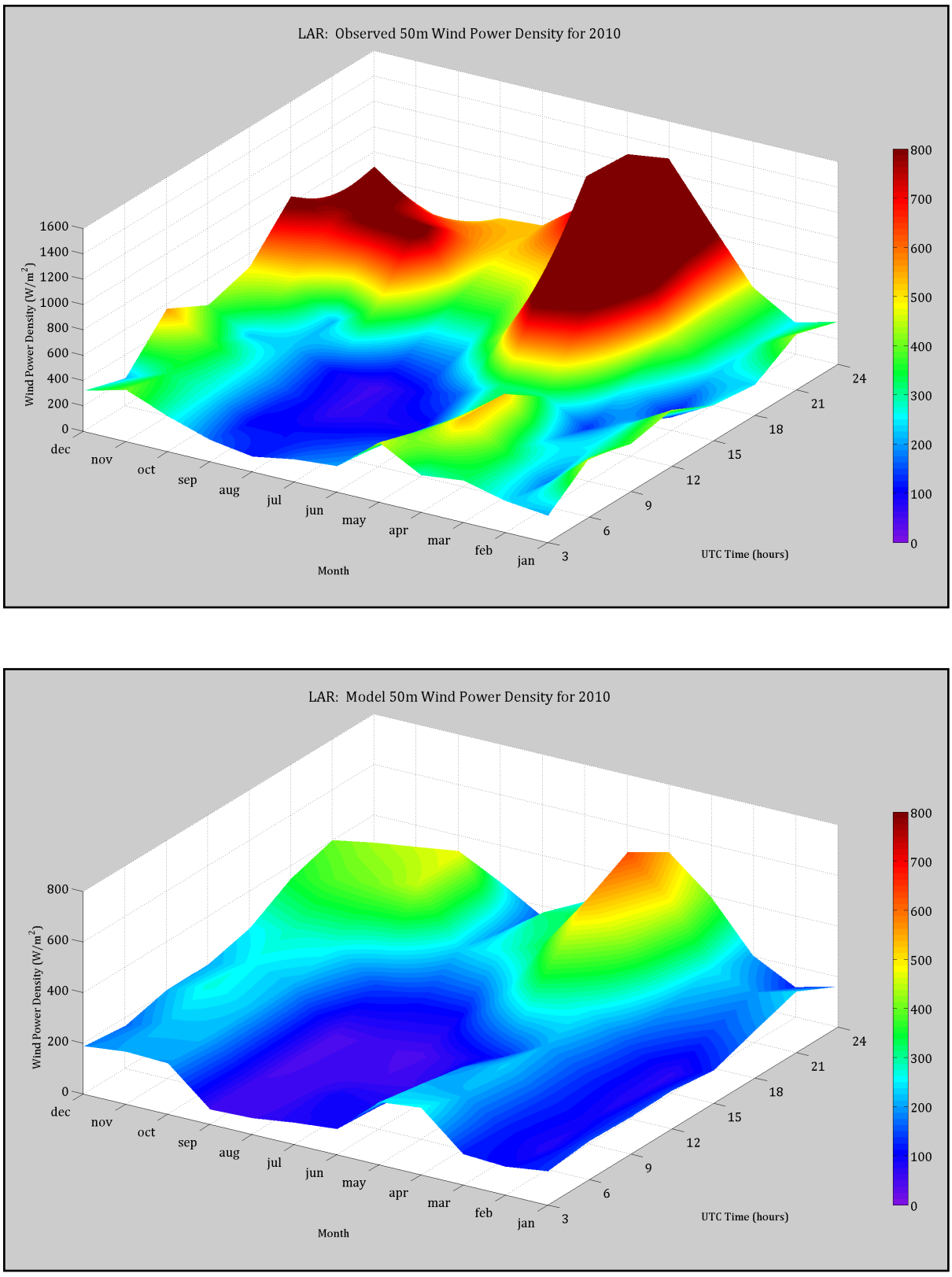

Figure 4.23: Observed and model 50-m WPD surface plots at Laramie in 2010.

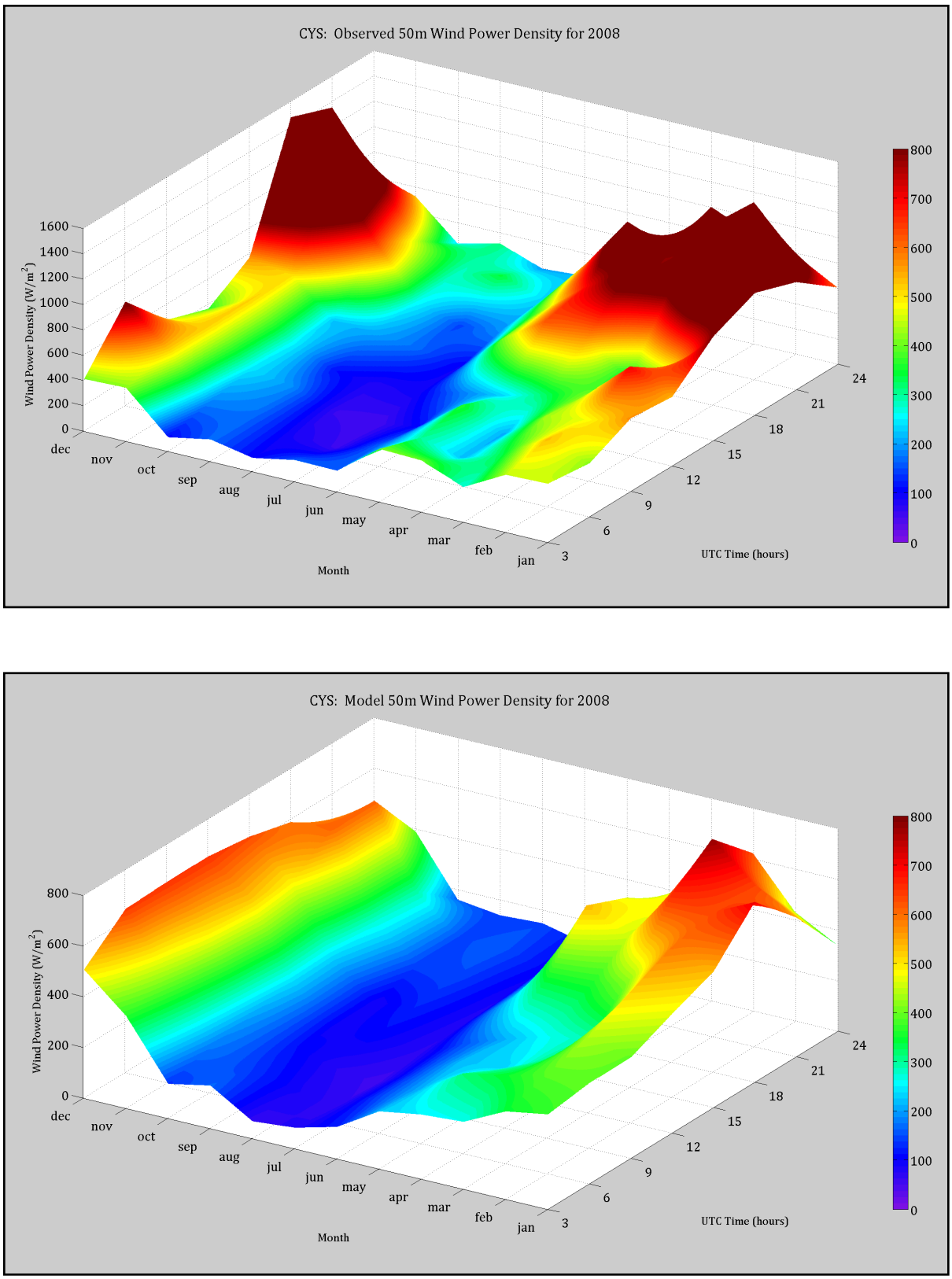

Figure 4.24: Observed and model 50-m WPD surface plots at Cheyenne in 2008.

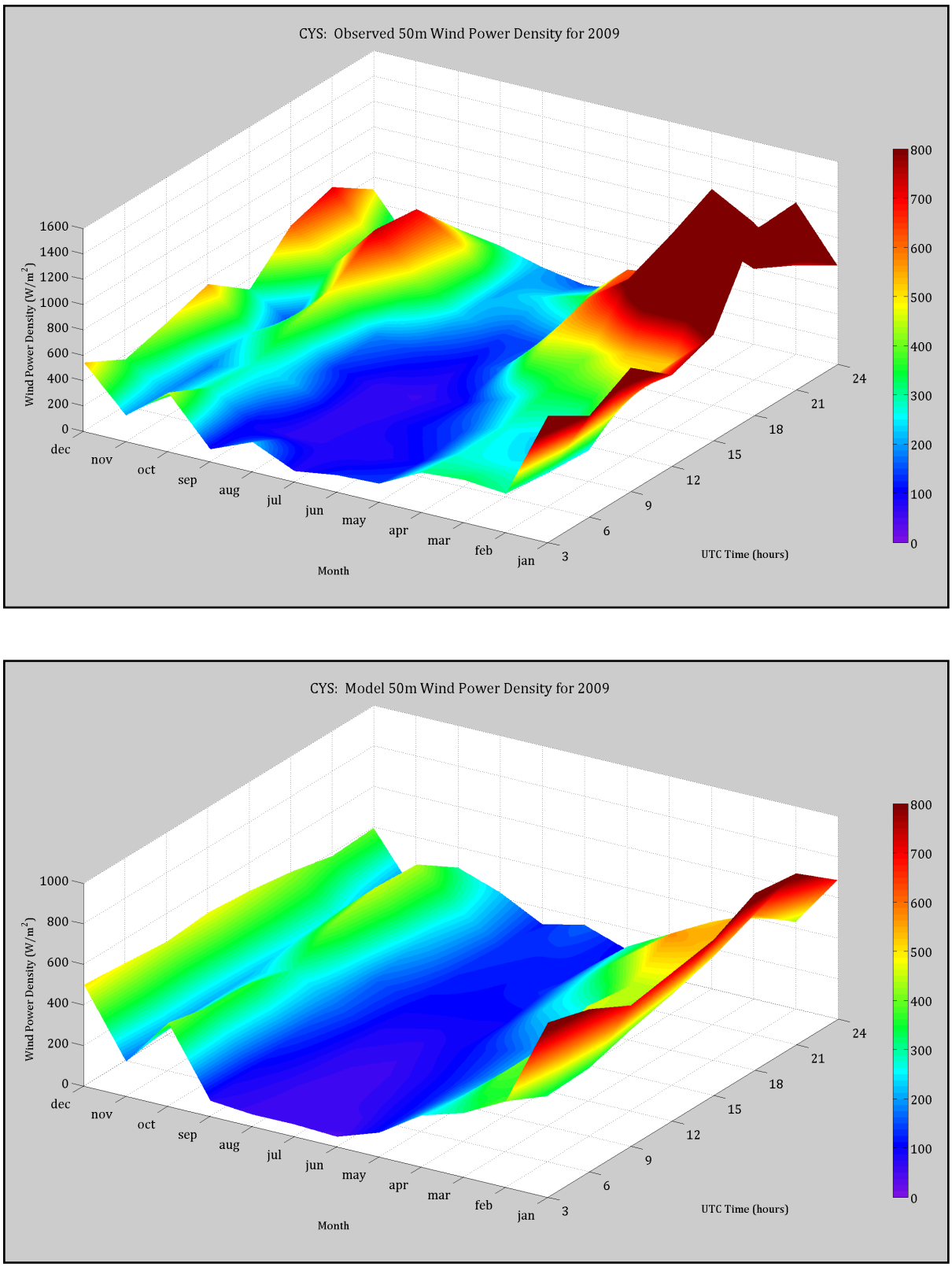

Figure 4.25: Observed and model 50-m WPD surface plots at Cheyenne for 2009.

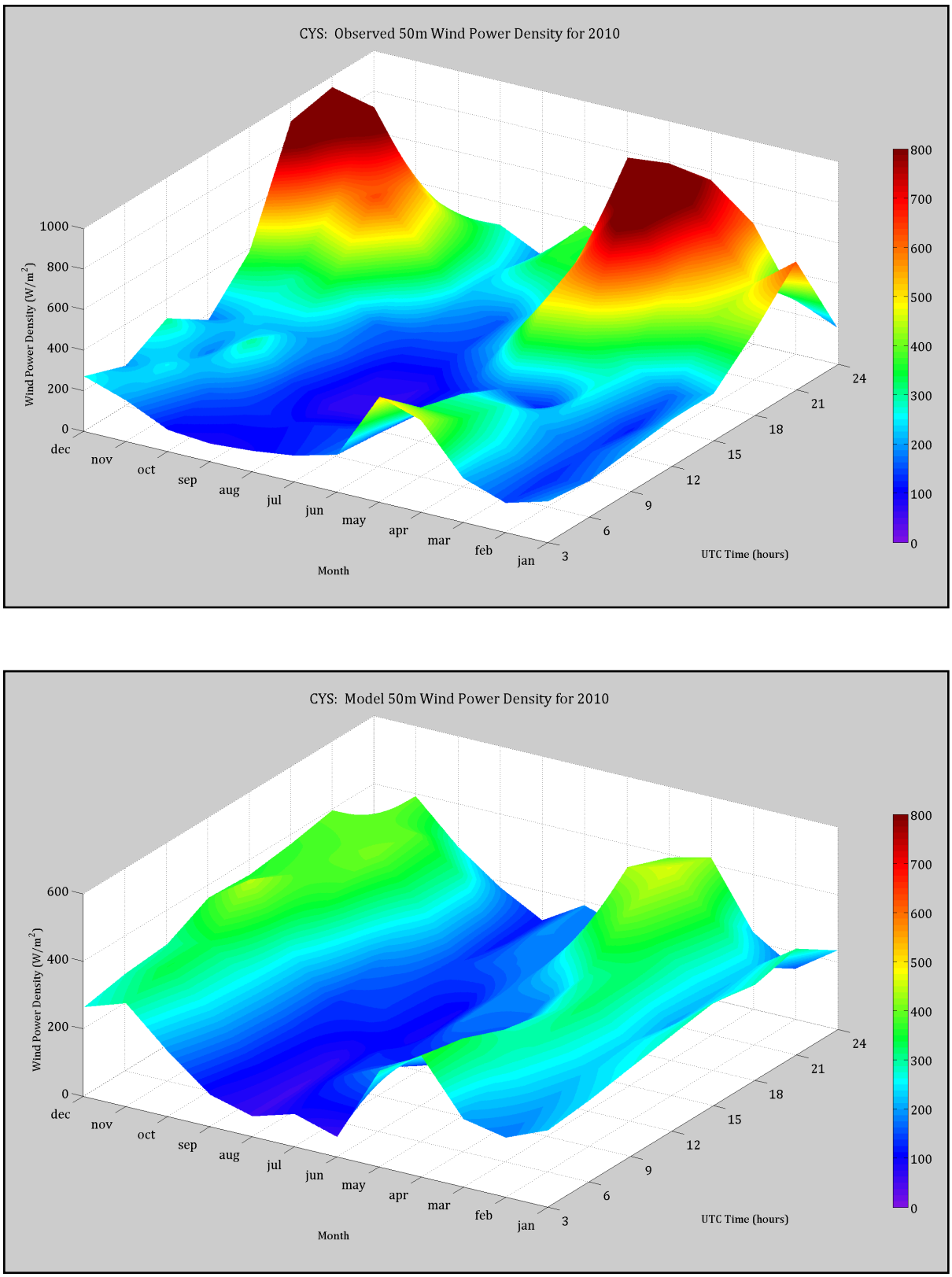

Figure 4.26: Observed and model 50-m WPD surface plots at Cheyenne for 2010.

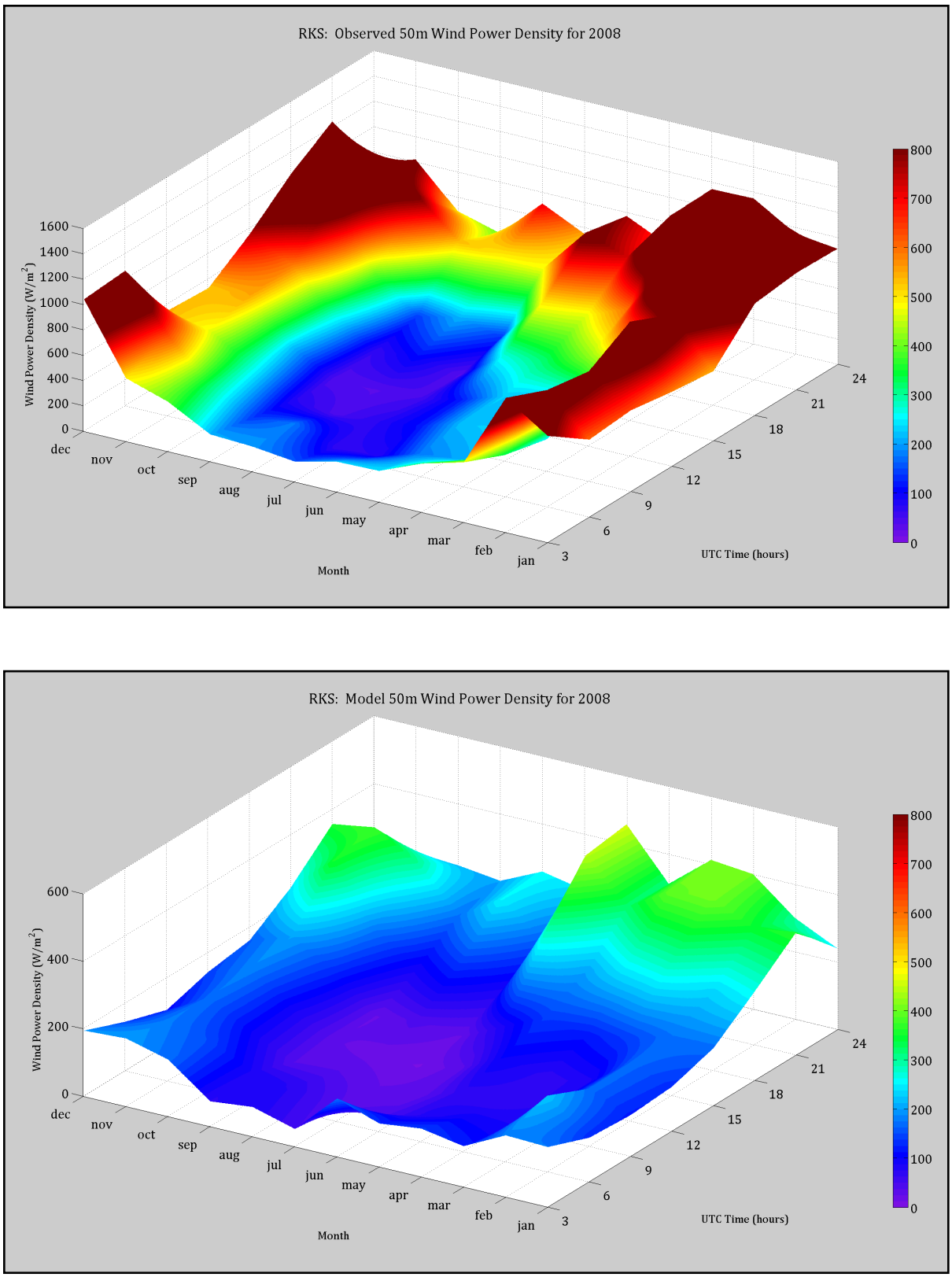

Figure 4.27: Observed and model 50-m WPD surface plots at Rock Springs for 2008.

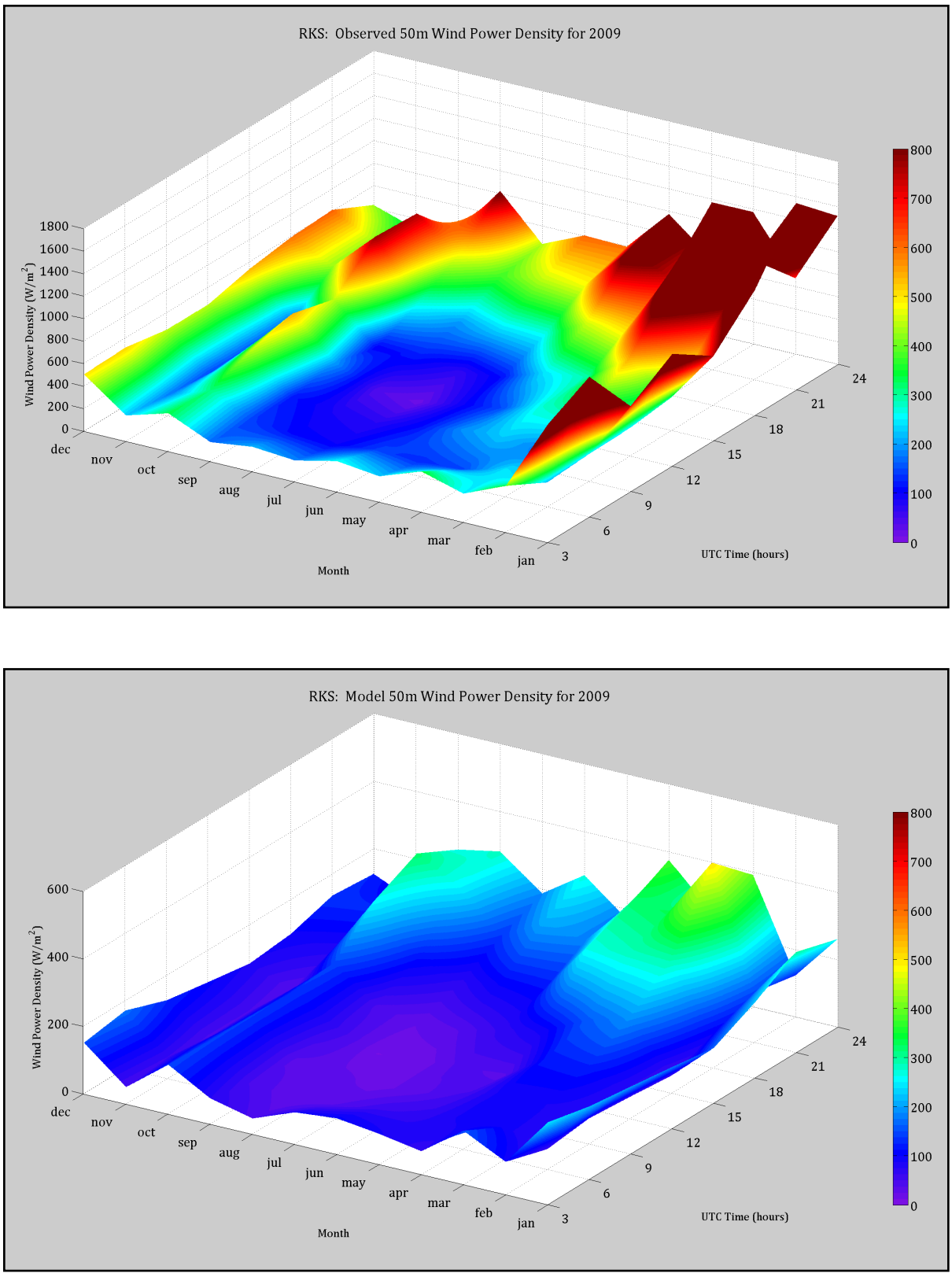

Figure 4.28: Observed and model 50-m WPD surface plots at Rock Springs for 2009.

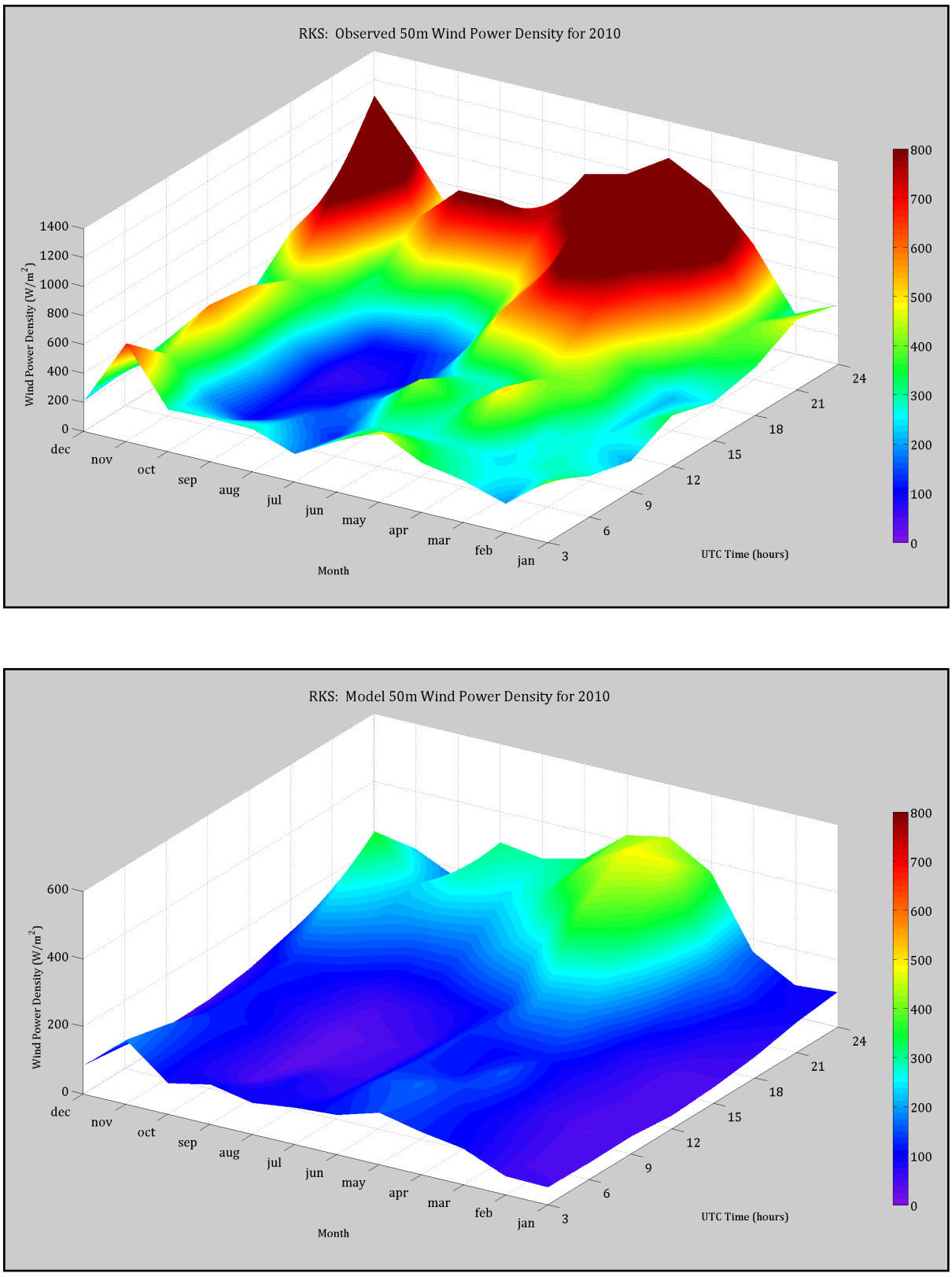

Figure 4.29: Observed and model 50-m WPD surface plots at Rock Springs for 2010.

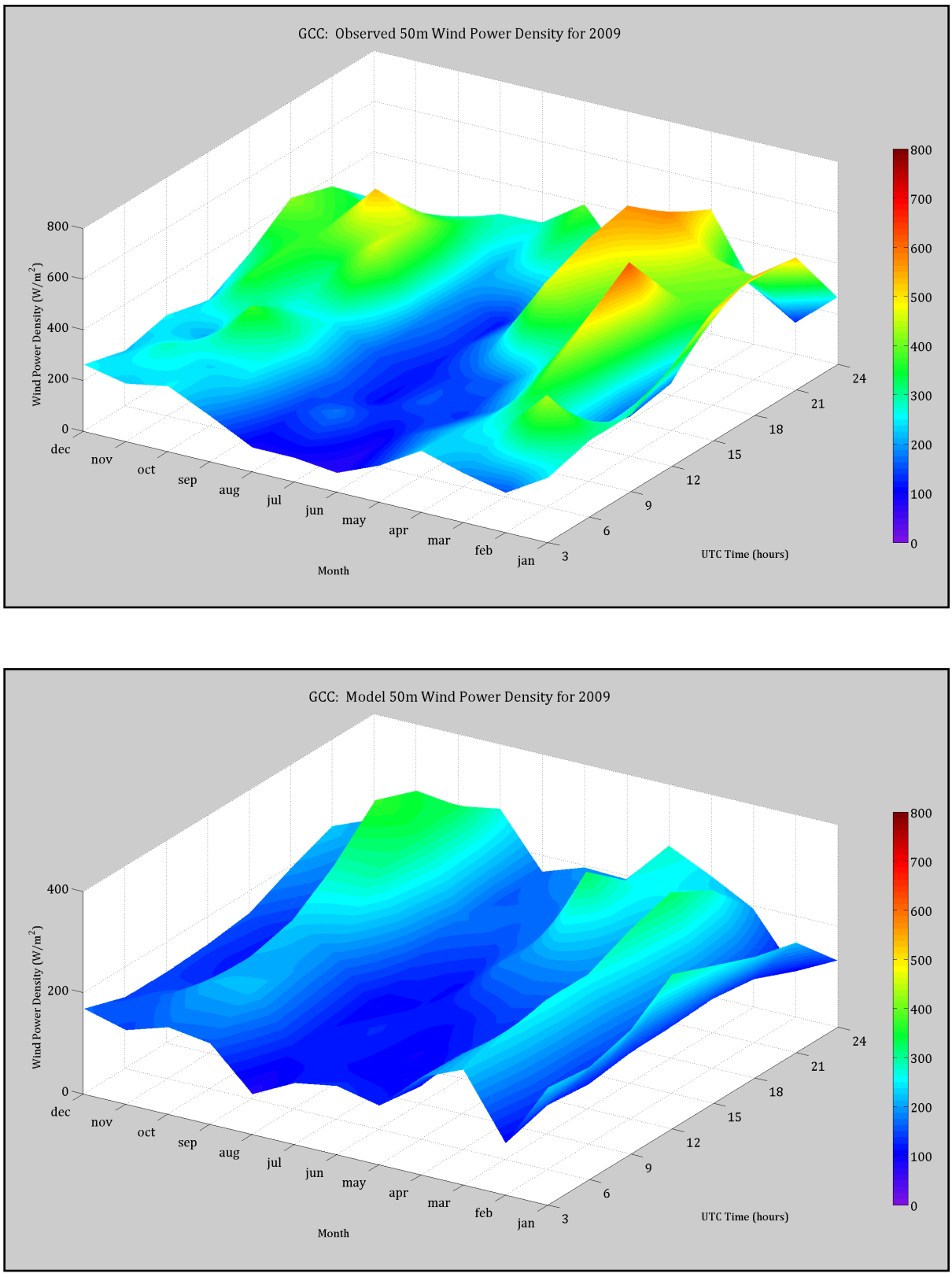

Figure 4.30: Observational and model WPD surface plots at Gillette for 2009

The good news is that the trends detailed in the model output match quite nicely with those seen in the observations: the summer sees little wind power as evidenced by the valley of blues and purples. The winter exhibits strong wind power, peaking towards the afternoon; again, corresponding to what was seen in the model output. Though the shapes of the observational and model surface plots are similar, the discouraging differences are the actual values of the wind power densities.

The maximum observed wind power in Laramie in 2009 is on the order of 1800 W m^{-2}. The same geographic location in the model peaks at 800 W m^{-2}. Though within the same wind class, this is a difference of 1000 W m^{-2}: the breadth of the entire wind class spectrum! The windier year, 2008, exhibits the same problem with the same difference between observed and model output. The atypical year of 2010 shows the greatest discrepancy between the model and real life, hovering around a difference factor of 1/2. The anomalously strong spring, coupled with the unusually weak winter stretched the model to its limits.

The model near Cheyenne did a marginally better job in predicting WPD compared to the Laramie cases. The maximum differences in WPD for Cheyenne were on the order of 500 W m^{-2}. Though still a difference of several wind classes, its improvement cannot be completely dismissed. What the model had a tough time simulating was the afternoon peak of WPD in the winter months. The gradual increase to 1600-W m^{-2} in 2008 is utterly lost in the model. This diurnal cycle is totally absent in the model. During this time, the model predicts a constant 700 W m^{-2}. The same thing happens in 2010, though the afternoon peak is a bit lower than in 2008.

The model simulations of Rock Springs, like Laramie, are under-predicted. Differences of 1000 W m^{-2} are common throughout all three years. The model never predicts any WPD over 600 W m^{-2} when the observational WPD routinely exceeds 1000 W m^{-2}. The model also overlooks the small peak in 2008 at the beginning of the day. Although this peak occurs at an unusual time, the fact that this peak generated over 1000 W m^{-2} of wind resource makes it an anomaly with which the model must contend. The maximum WPD at Rock Springs occurs in the beginning months of the year, and the model captures this behavior. In both the model and observational surface plots, the maximum WPDs occur at the same time. But as has been said many times, this is simply not good enough.

Contrasting these three windy places with Gillette, several of the same problems are present: the model captures the trends, but under predicts WPD. Even in a place whose wind potential is dwarfed by the other three sites, the model still has trouble predicting the actual WPD. The observed maximum at Gillette compares with the predicted maximum from the model at the other three locations. The model is obviously capable of simulating WPDs on the order of 800 W m^{-2}, but stumbles when simulating the wind in places where it is strong. The most significant difference between the three windy sites and Gillette is terrain. Laramie, Cheyenne and Rock Springs are all located near or within the wind corridor whereas Gillette is located on flatlands, 160 km from the nearest mountain range. Because the strong winds in the southern part of the state are almost entirely topographically induced, it becomes critical for the model to correctly render the surrounding terrain. A high-resolution model with incorrect terrain is all but worthless in predicting surface winds in this region. The importance of understanding and integrating the relationship between wind and topography

cannot be stressed enough. The poor performance by both flavors of the NAM in the wind corridor serves as ideal example of the work that has to be done to improve the accuracy of wind forecasts.

Chapter 5: Analysis

5.1: Fast Fourier Transform Analysis

It is necessary to analyze the wind speeds in efforts to mathematically validate the patterns observed and discussed in Chapter 4. To recap: the winter afforded the greatest amount of wind resource. During the day, the wind resource tended to reach a maximum in the early afternoon. The theories behind this behavior were as follows:

- The jet stream wanders southward in the winter, providing the required ingredients for strong synoptic systems which translate to intense surface winds across Wyoming. In the summer, the jet stream retreats northward and with it, the strong synoptic systems (Martner 1986).
- The wind resource peaks in the afternoon, matching the time of greatest solar insolation and thus when the boundary layer is well mixed, brining turbulent kinetic energy from upper levels to the surface (Martner; Marwitz 1982).

The easiest way to verify these theories is to perform a Fast Fourier Transform (FFT). The underlying principle of FFT analysis is to find dominant frequencies or harmonics in a time series that might look something like Figure 5.1.

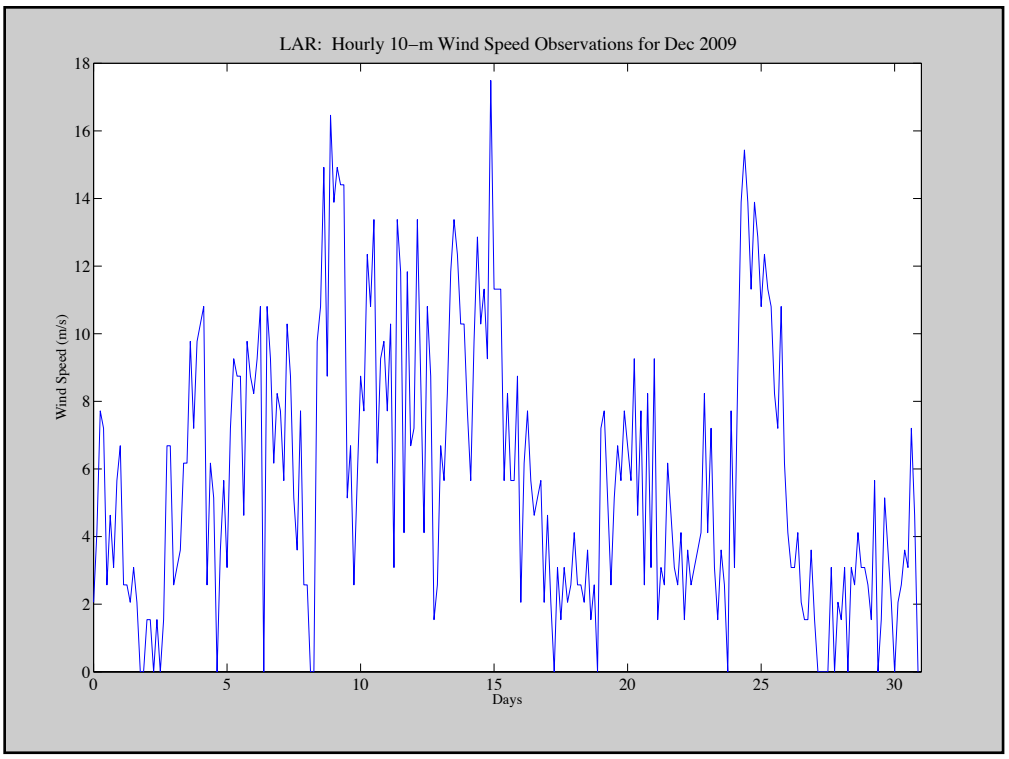

Figure 5.1: Three hourly wind speed observations for Laramie for December 2009.

To a naïve observer, it may look like there are no underlying frequencies in this data at all and that, in reality, it is actually a seismograph. But in fact, through FFT analysis, the dominant modes of data like this can be extracted and the plotted in a different domain. Typically, time series data, like Figure 5.1, are used as input to an FFT. The output is displayed in frequency space, meaning that frequency, instead of time, occupies the horizontal axis. FFT analysis of the three year period of observational 10 m data for Laramie, Cheyenne and Rock Springs can be seen in the following Figures.

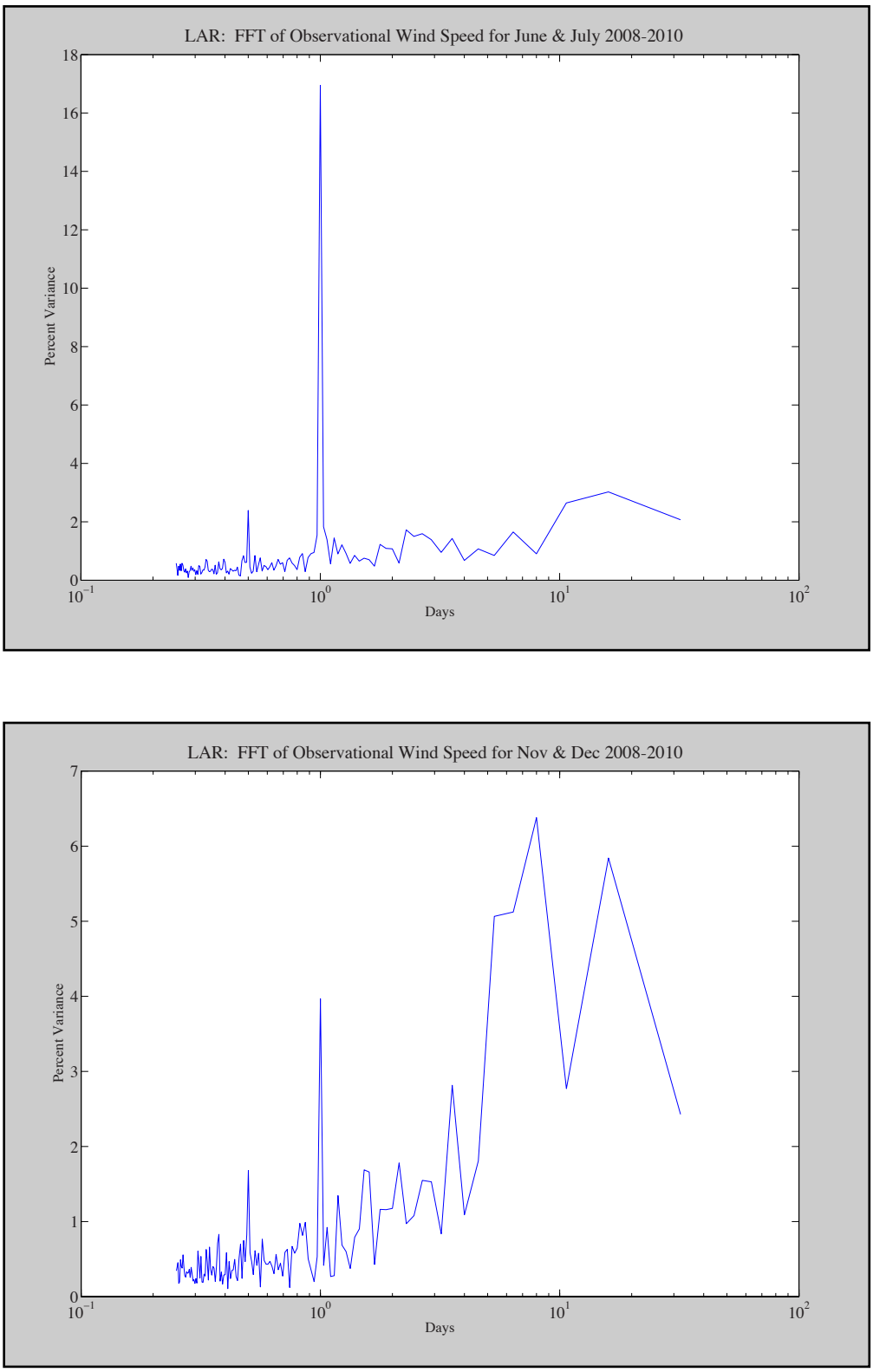

Figure 5.2: FFT of Laramie for June and July (summer) and November and December (winter) 2008-2010.

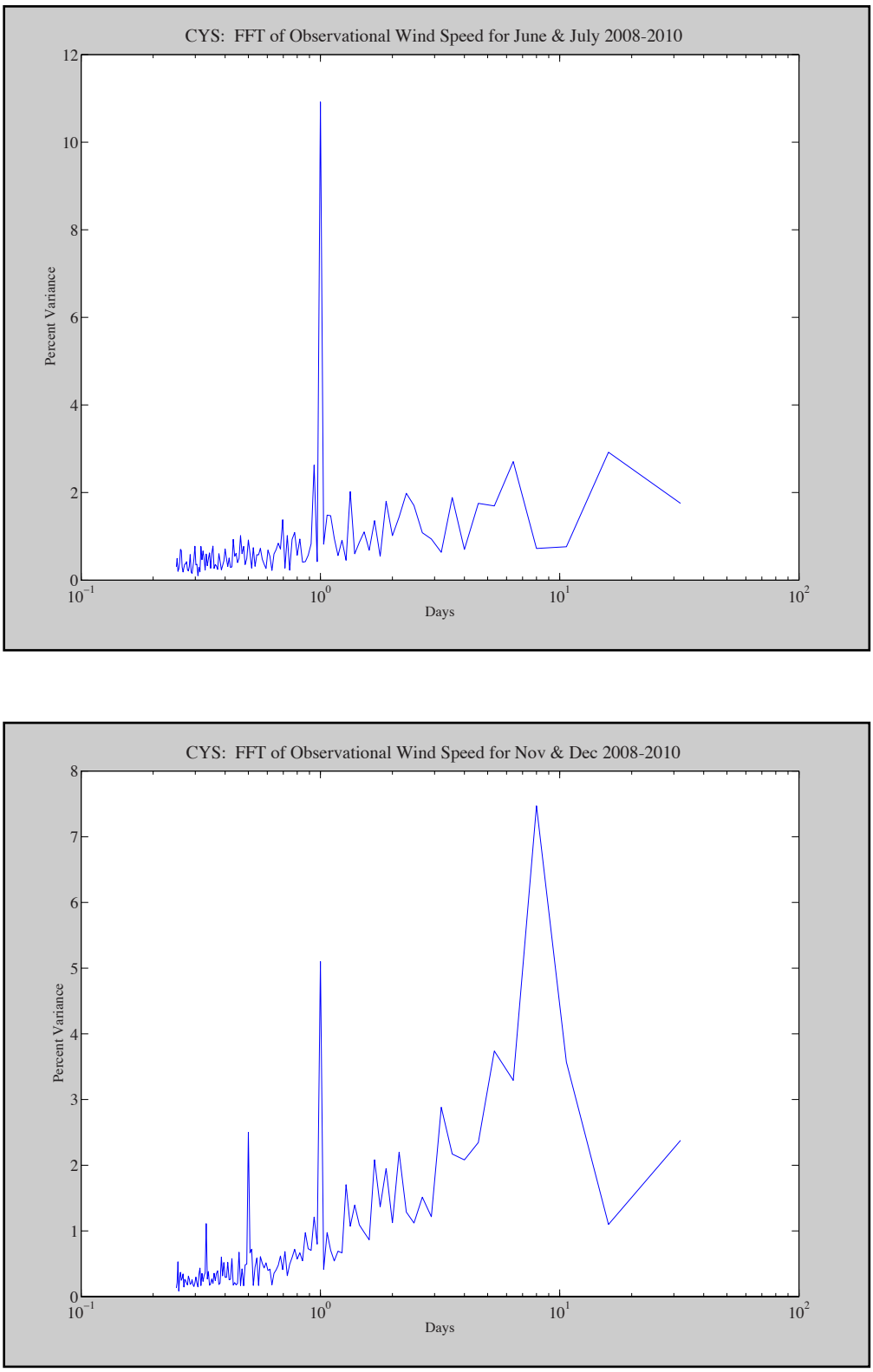

Figure 5.3: FFT of Cheyenne for June and July (summer) and November and December (winter) 2008-2010.

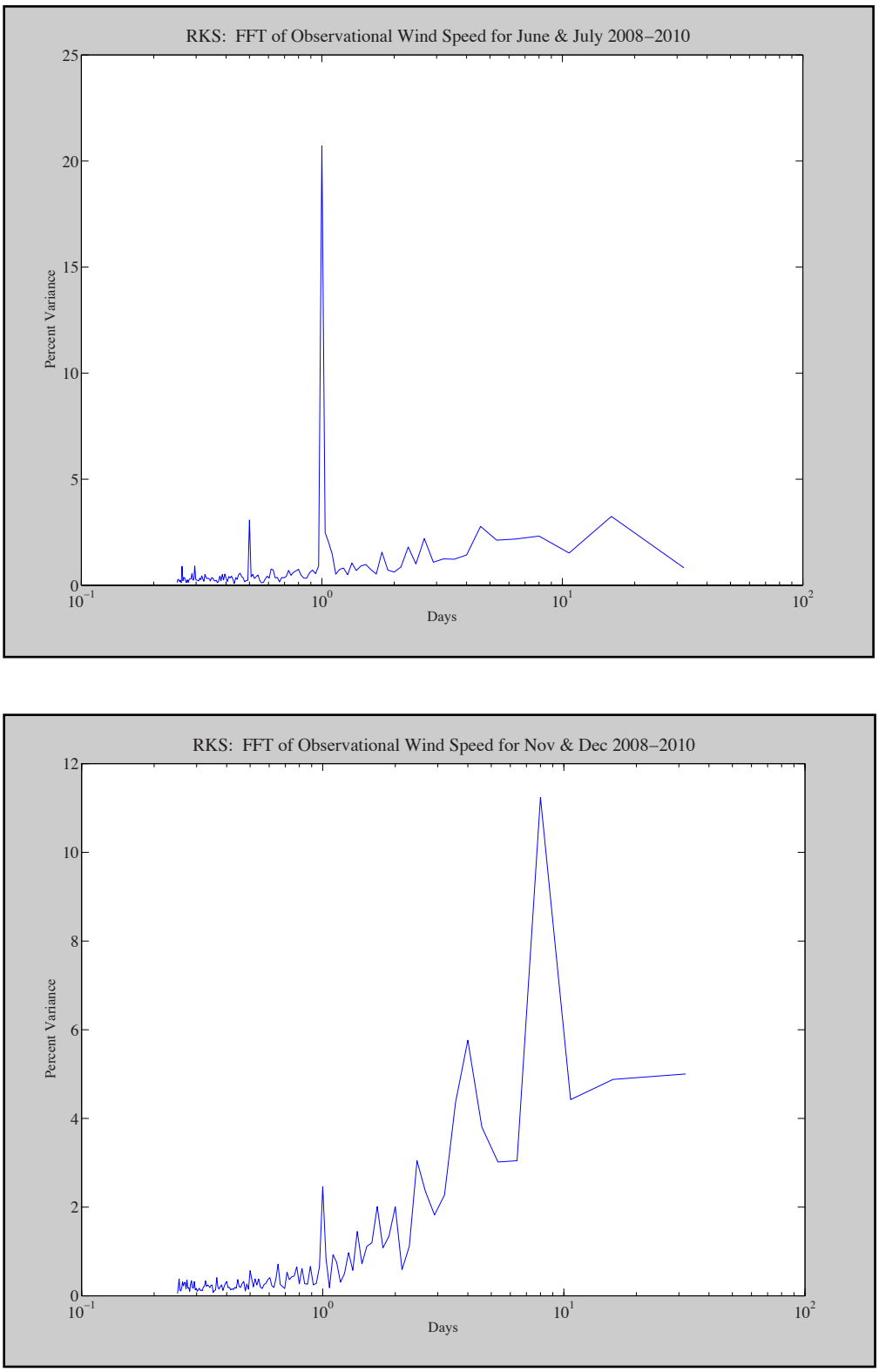

Figure 5.4: FFT of Rock Springs for June and July (summer) November and December (winter) 2008-2010.

The two contrasting time periods, summer and winter, were analyzed in efforts to corroborate the atmospheric theories behind the behavior observed in the wind resource. To verify the climatological credibility, all three years of observational data were analyzed to generate these plots. The frequency (horizontal axis) is reported as a period in units of days. The sum of the points along each curve equals the variance for that particular time period and location. The area under the curve for these Figures is meaningless.

A quick inspection reveals two striking things about these Figures. The summertime is dominated by a diurnal mode. At Laramie and Rock Springs, about 20% of the variance is associated with the diurnal mode. The only other spike in the data that represents spectrally coherent events occurs at 12 hours. Similar behavior is seen for Cheyenne. The diurnal mode captures about 11% of the variance and the 12 hour mode is undetectable. The magnitude of the noise at higher periods (lower frequencies) captures more variance, decreasing the variance associated with the diurnal mode.

The wintertime plots display an additional source of variance. The diurnal mode associated with the winter is lower: in Laramie the diurnal mode dropped to 4%, in Cheyenne the diurnal mode dropped to 5% and in Rock Springs the diurnal mode is almost nonexistent, having dropped to 2%. Intriguing are the high period synoptic modes now present in the spectra. In Laramie, the synoptic frequencies are bimodal: one spike occurs at seven days and the other spike occurs at fourteen days. In Cheyenne, the wintertime boasts only one spike at ten days, splitting the difference between the two synoptic modes in Laramie. The synoptic modes at Rock Springs dominate the wintertime frequency spectrum. One large spike at ten days accounts for over 10% of the variance and a smaller spike occurs at five days. Rock

Springs is located near the entrance of the wind corridor, making it more susceptible to the synoptic events that occur in the winter. Since Laramie is located at the exit of the wind corridor, the winds must be reasonably strong to get through the wind corridor. Cheyenne, located to the east of the Laramie Range, only experiences the synoptic events producing winds which blow through the wind corridor and then around or over the Laramie Range. These additional topographic constraints do not apply at Rock Springs and as such, the synoptic modes have a much greater impact.

These results confirm that the atmospheric reasoning behind the behavior of the wind resource is sound: the winter time is dominated by a synoptic mode. Per the discussion in Chapter 4, as the jet stream travels south in the winter, areas of low and high pressure form to the east and west of Wyoming, resulting in a strong pressure gradient across the state. The frequency of the jet stream is, on average, on the order of a week to ten days. Conversely, during the summer time when the jet stream has retreated northward, the synoptic mode is all but gone from the summertime FFT plots; and thus the wind resource is weaker during the summer months.

5.2: Probability Distribution Analysis

The persistence of the wind, up to now, has been taken on merit and a few maps with rated velocities. A PDF is a statistical tool that can help verify the persistence of the wind in the southeastern corner of Wyoming. All the 10-m wind speeds during winter of 2009 were extracted from the North American Model (NAM) 12-km output at a representative point,

denoted by the burgundy asterisk in Figure 5.4. The darkened black area corresponds to the white areas of Class 7 wind resource in the maps in Chapter 4.

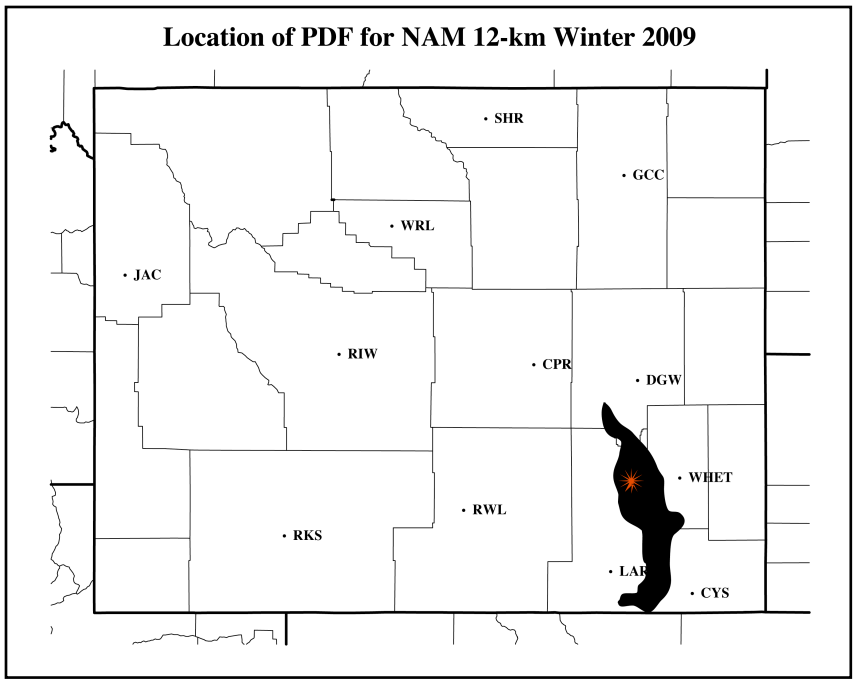

Figure 5.5: Location where NAM 12-km winter 2009 data was extracted for probability analysis. The filled in black area denotes Class 7 wind resource.

The data were binned in increments of 1.5 m s^{-1} from 0 to 21 m s^{-1}. The first bin, for example, contains all wind speeds between 0 and 1.5 m s^{-1}, the second bin contains all wind speeds from 1.5 m s^{-1} to 3 m s^{-1}, *etc*. The probabilities were all calculated by Equation 3.8. A Weibull curve, as outlined by Equation 3.9 was also calculated. The PDF can be seen in Figure 5.6. The horizontal axis labels correspond to the middle value of each bin. The first bin contains wind speeds for 0 to 1.5 m s^{-1} and the midpoint is 0.75. The shape parameter (k) and the scale parameter (c) of the Weibull curve, the standard deviation (ϕ) and the mean ($\bar{u}$) are outlined in Table 5.1. The shape and scale parameters were calculated per Equations 3.10 and 3.11.

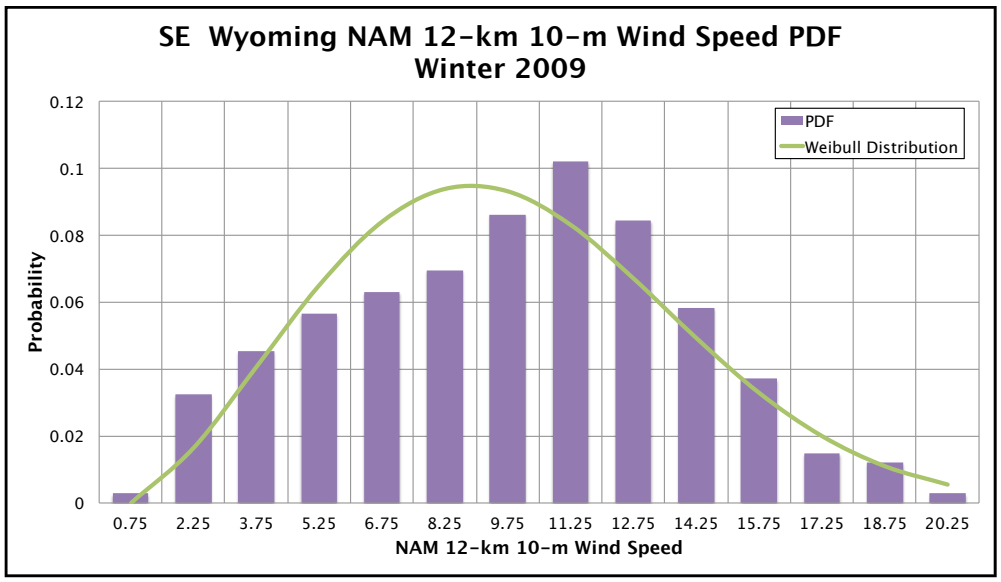

Figure 5.6: PDF of the NAM 12-km winter 2009 data in southeastern Wyoming. The green line denotes the calculated Weibull fit.

Table 5.1: Statistical and fit parameters for the Weibull curve in Figure 5.6.

Parameter	Value
k	2.38
c	10.23-m s^{-1}
ϕ	4.09-m s^{-1}
$\bar{u}$	9.07-m s^{-1}

This is exactly the type of PDF one would hope to see in a windy area. The highest probability, which can be taken as a proxy for the average, is the bin of wind speeds between 10.5 m s^{-1} and 12 m s^{-1}. For reference, the maximum average 10-m wind speed for Class 7 wind resource is 9.4 m s^{-1}. The most common wind speeds at this location are beyond the specifications for Class 7 wind proving that the winds in this area are persistently strong.

Though this PDF nicely illustrates the regularity of the winds, the PDF reflects NAM 12-km data. The location chosen is also atop the Laramie Range, an unlikely site for a wind farm. More useful would be PDFs at places where model data can be corroborated with observational data. PDFs for summer and winter 2008-2010 at three sites: Laramie, Cheyenne and Rock Springs and three year averages are shown on the following pages. Red bars represent summer and blue bars represent winter. Lighter reds and blues are for the observational data and darker reds and blues are for the NAM 12-km. Each plot also has a Weibull distribution fitted to it, plotted in green. The vertical scale for the plots of the individual years are different than those in the three year average plots. Table 5.2 summarizes the averages, standard deviations and Weibull fit parameters for 2008-2010 plus the three year averages for each site. The three hourly data were binned in 1.5 m s^{-1} increments according to the seasonal divisions outlined in Table 3.4. The horizontal labels, as in Figure 5.6, reflect the midpoint of each division.

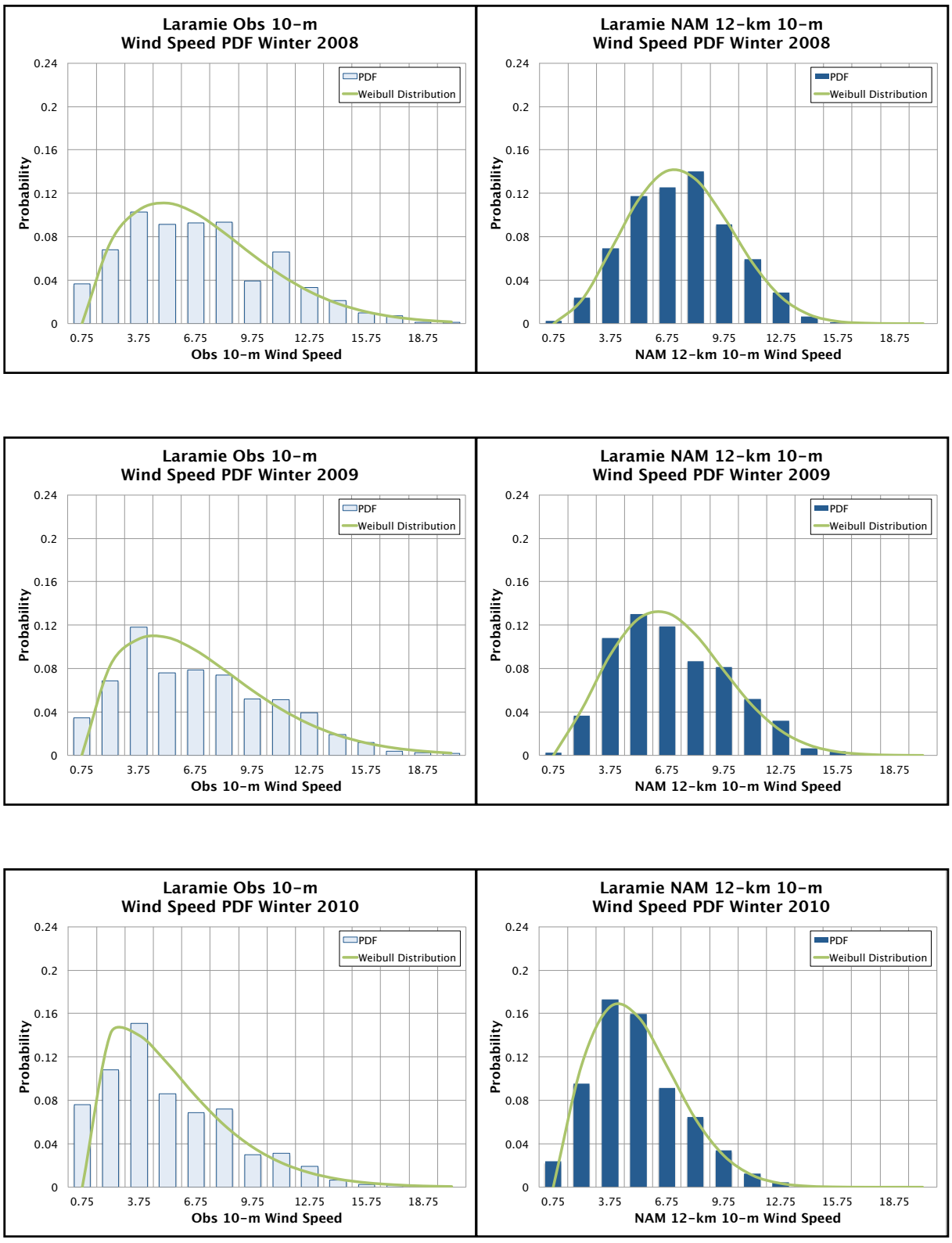

Figure 5.7: Laramie observations (Obs) and NAM 12-km PDF winter 2008-2010.

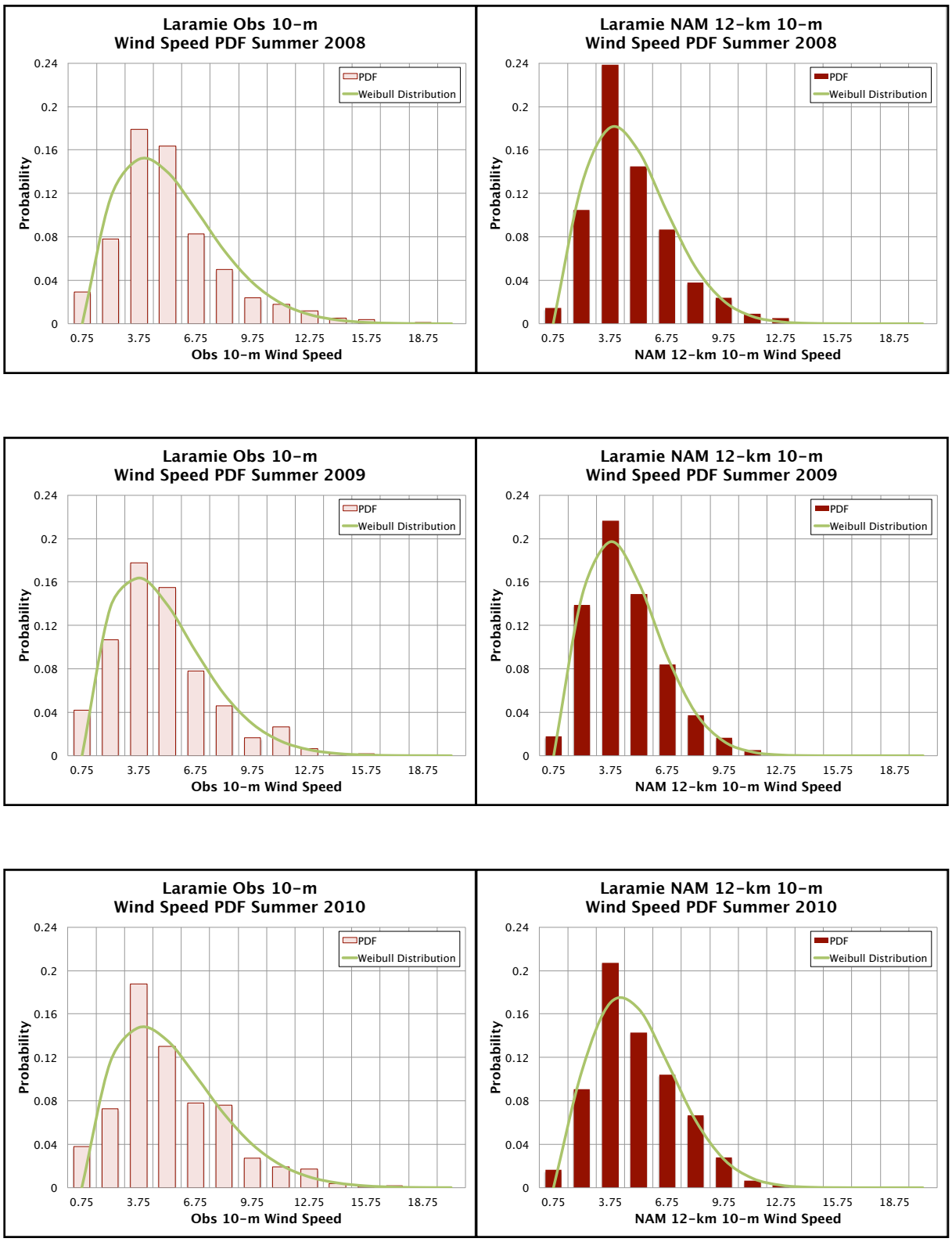

Figure 5.8: Laramie observations (obs) and NAM 12-km PDF summer 2008-2010.

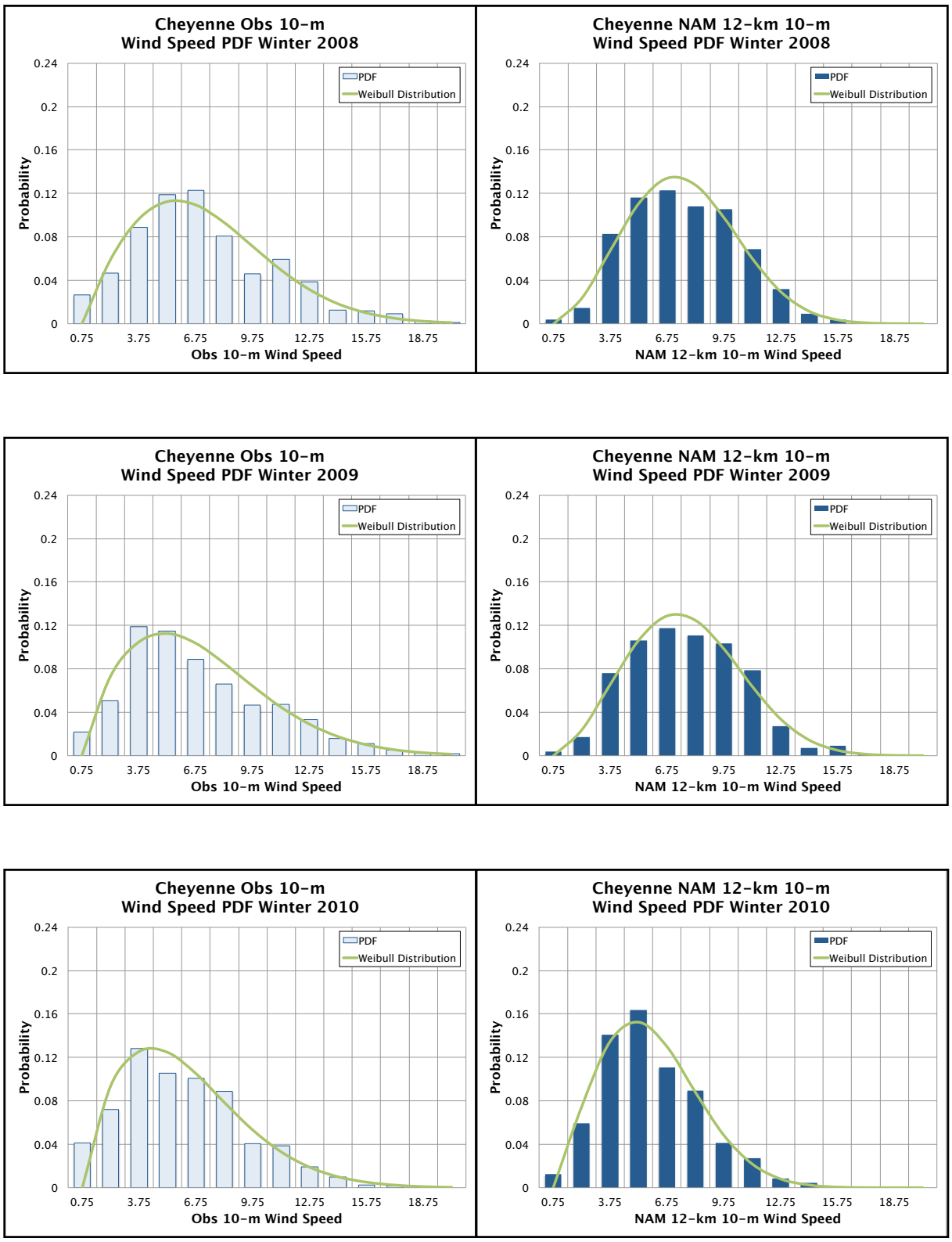

Figure 5.9: Cheyenne observations (obs) and NAM 12-km PDF winter 2008-2010.

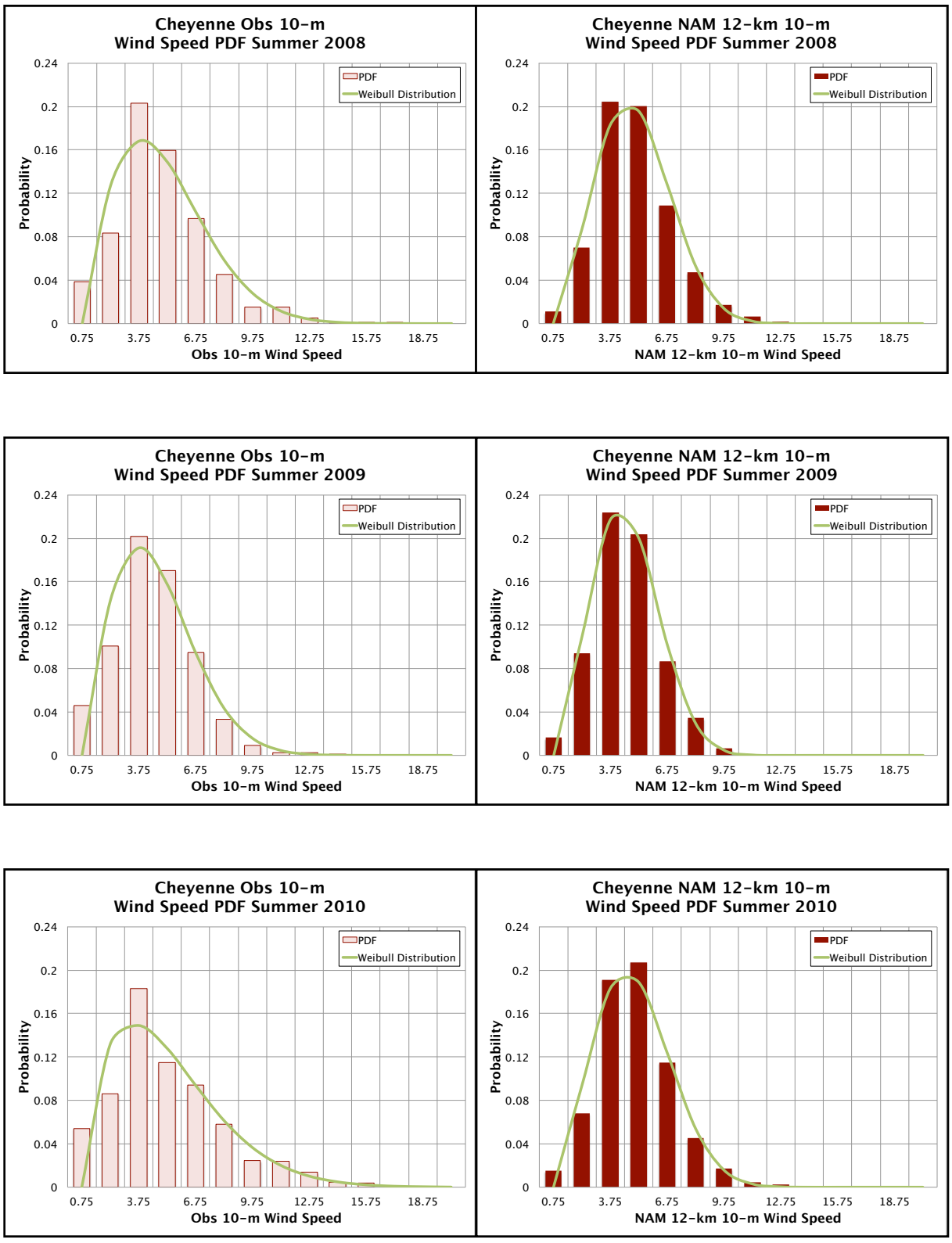

Figure 5.10: Cheyenne observations (obs) and NAM 12-km PDF summer 2008-2010.

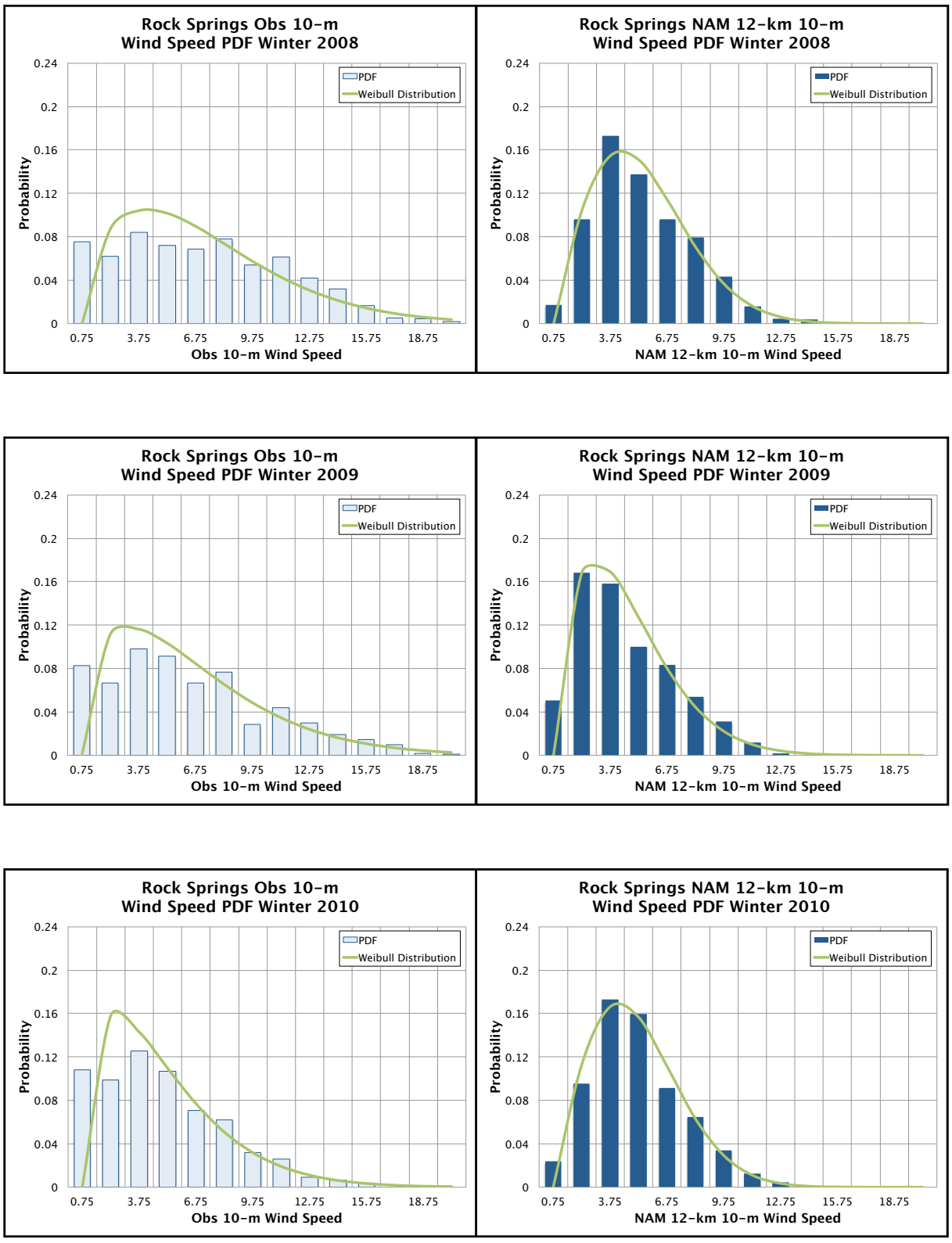

Figure 5.11: Rock Springs observations (obs) and NAM 12-km PDF winter 2008-2010.

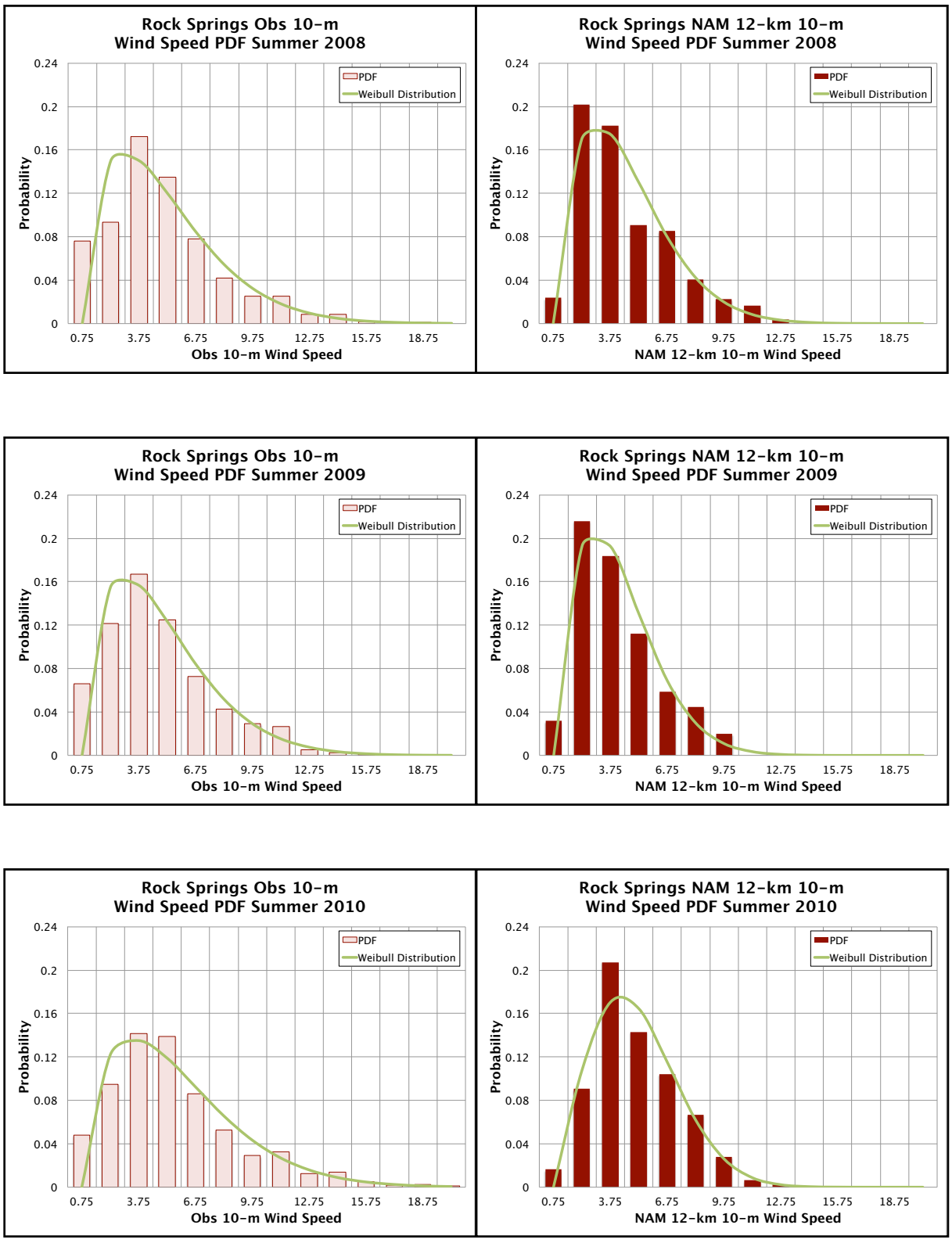

Figure 5.12: Rock Springs observations (obs) and NAM 12-km PDF summer 2008-2010.

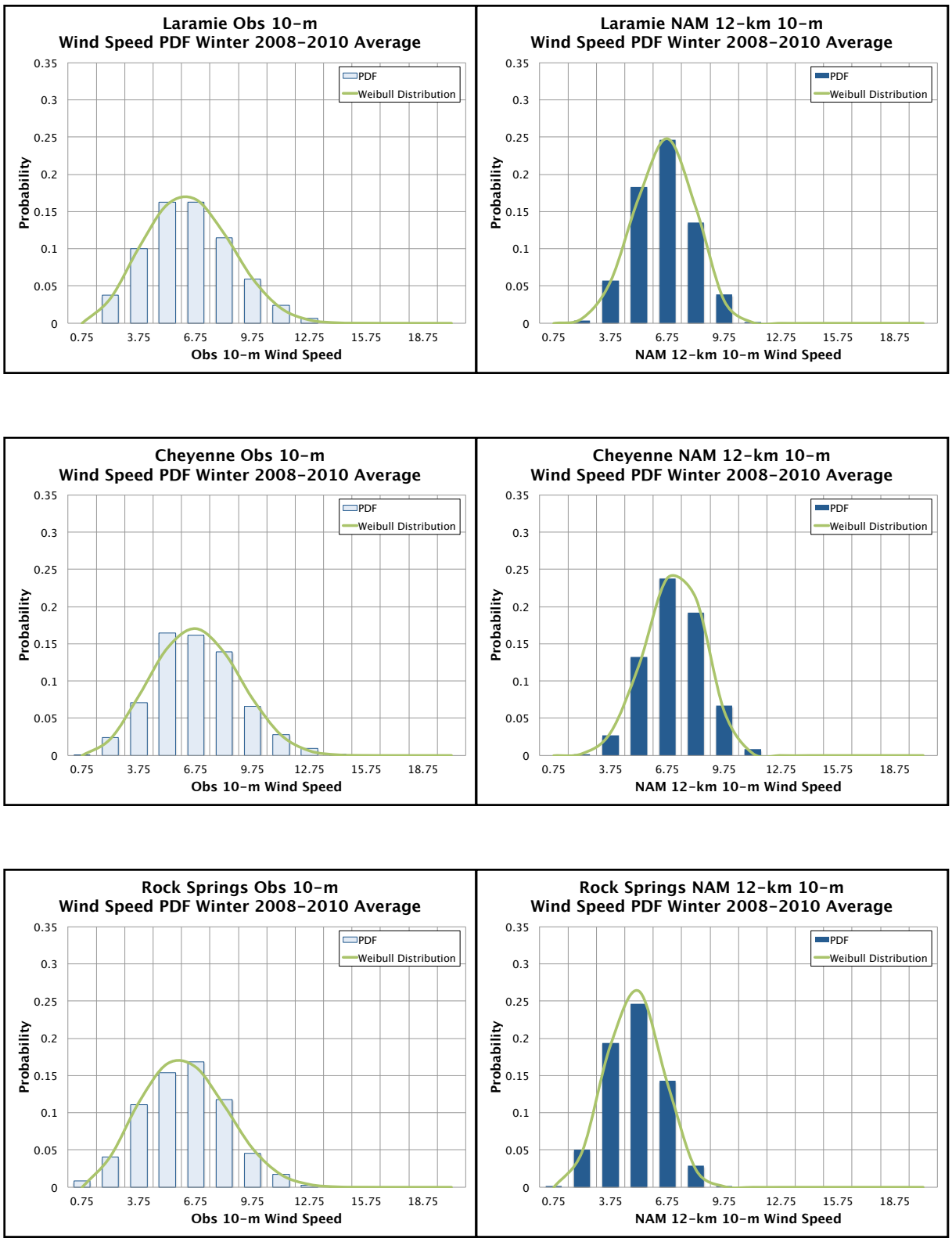

Figure 5.13: winter three year averages of observations (obs) and NAM 12-km for LAR, CYS and RKS. Note the vertical scale has increased to 0.35.

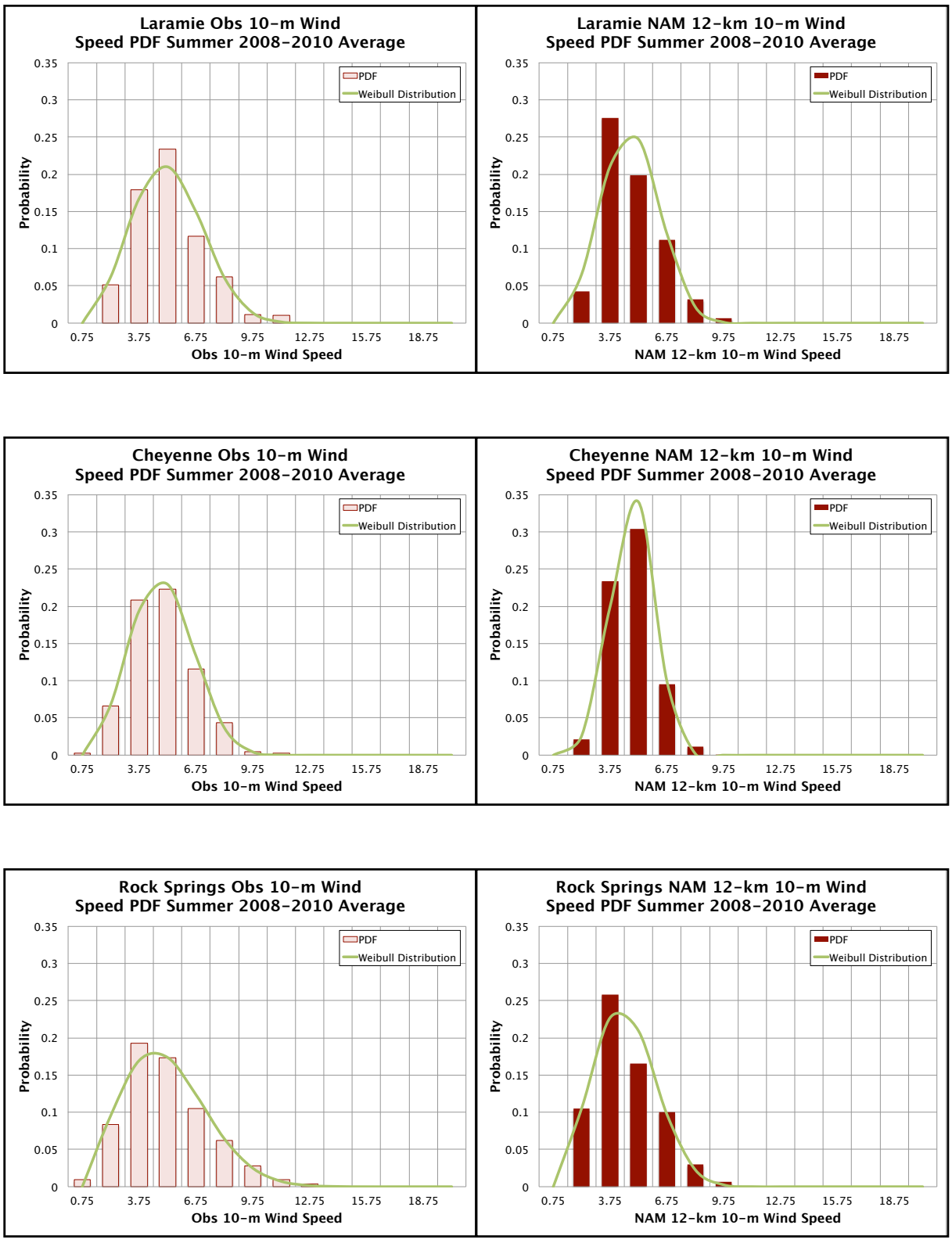

Figure 5.14: summer three year averages of observations (obs) and NAM 12-km for LAR, CYS and RKS. Note the vertical scale has increased to 0.35.

			Observation				Model			
			c	***k***	ū	ϕ	***c***	***k***	ū	ϕ
LAR	**2008**	**Winter**	7.06	1.72	6.29	3.82	7.59	2.71	6.75	2.70
		Summer	5.23	1.76	4.65	2.76	4.65	1.95	4.12	2.23
	2009	**Winter**	6.95	1.62	6.21	3.98	7.09	2.28	6.28	2.93
		Summer	4.78	1.71	4.26	2.60	4.28	1.95	3.79	2.05
	2010	**Winter**	5.04	1.41	4.58	3.34	5.00	1.95	4.43	2.39
		Summer	5.32	1.72	4.74	2.87	4.97	2.05	4.40	2.27
	3-yr Avg	**Winter**	6.38	2.75	5.68	2.24	6.40	4.18	5.82	1.56
		Summer	5.12	2.71	4.56	1.82	4.59	3.03	4.11	1.48
CYS	**2008**	**Winter**	7.33	1.90	6.50	3.60	7.72	2.61	6.86	2.84
		Summer	4.83	1.83	4.29	2.45	4.88	2.44	4.33	1.90
	2009	**Winter**	7.04	1.75	6.27	3.74	7.90	2.56	7.01	2.95
		Summer	4.39	1.93	3.89	2.12	4.38	2.45	3.88	1.70
	2010	**Winter**	6.12	1.71	5.45	3.32	5.84	2.12	5.17	2.59
		Summer	5.08	1.59	4.55	2.96	4.85	2.34	4.30	1.96
	3-yr Avg	**Winter**	6.80	2.95	6.07	2.24	6.93	4.66	6.34	1.54
		Summer	4.77	2.84	4.25	1.62	4.59	4.17	4.17	1.12
RKS	**2008**	**Winter**	7.12	1.51	6.42	4.40	5.26	1.92	4.67	2.56
		Summer	4.75	1.47	4.29	3.01	4.19	1.61	3.75	2.42
	2009	**Winter**	6.25	1.38	5.70	4.23	4.24	1.56	3.81	2.53
		Summer	4.58	1.51	4.13	2.83	3.76	1.67	3.36	2.09
	2010	**Winter**	4.63	1.34	4.25	3.24	5.00	1.95	4.43	2.39
		Summer	5.52	1.52	4.97	3.38	4.97	2.05	4.40	2.27
	3-yr Avg	**Winter**	6.15	2.64	5.46	2.24	4.78	3.28	4.29	1.44
		Summer	5.05	2.19	4.47	2.17	4.32	2.58	3.83	1.60

Table 5.2: Summary of scale (*c*) and shape (*k*) Weibull curve parameters, averages (ū) and standard deviations (ϕ) for Laramie (LAR), Cheyenne (CYS) and Rock Springs (RKS) for 2008-2010 and the three year average of observational and NAM 12-km data. All quantities are in m s^{-1} except the scale parameter.

The overall shape of the PDFs and Weibull curves speaks to the variability of the resource. The shape parameter, *k*, dictates the width of the Weibull curve: higher values of *k* correlate to narrower curves. Narrower curves imply the data is more concentrated, resulting in a smaller standard deviation. Table 5.2 verifies this general relationship: the Cheyenne summer 2009 model plot, for example, is quite narrow with a *k* value of 2.45 and a standard deviation of 1.70 m s^{-1}. Wider curves exhibit higher standard deviations suggesting more variability. During both winter and summer, but especially in the winter, the observational plots have much more spread than their modeled counterparts. These fluctuations present, at best, a challenge to simulate. The yearly model plots seem to be more symmetric about the peak of the PDF value than the observational plots and the three year average plots of both modeled and observed datasets display the greatest degree of symmetry.

Comparing the shape and magnitude of the model and observational PDFs, the summertime claims the greatest similarity. Both sets of PDFs are consistent with lower wind speeds, which, as has been demonstrated, are more prevalent in the summer. In some cases, *e.g.* Rock Springs 2010 and Laramie 2008, lower model bins peak much higher than the fitted Weibull curves and all of the observational bins. One limitation of the model is that it can never simulate a 0 m s^{-1} wind-- all model output wind speeds are always greater than zero. Because higher wind speeds result in higher wind power densities (WPDs), this shortcoming of the model is usually neglected. The model's bias towards weaker nonzero wind speeds is the culprit for these anomalously high bins. The trailing edge of both the Weibull curve and the PDF is longer for the observational plots than the model plots. Since the lower wind speeds dominate in the summertime, this discrepancy becomes less of an issue. However,

when lower wind speeds are less common, these high wind speed bins significantly impact the details of the WPD landscape.

The differences between the model and observations become much more apparent in the wintertime. In general, the maxima of the model plots are higher than the observational maxima. Higher PDF peaks imply lower standard deviation meaning that the variability of the model is not representative of the observational variability. The model plots also exhibit more symmetry, indicating an equal chance of high or low wind speeds. Conversely, the observational plots are skewed to the left, indicating a higher probability of low wind speeds, consistent with the lower model WPD observed in Chapters 4 and 5. The trailing edge of the Weibull curve for the observational plots extends farther to the right compared to the model. At 10 m, a 1.5 m s^{-1} change can be the difference of two wind classes. Even though the probability of these higher wind speeds is low on the observational plots, the fact that they are absent in the model plots compromises the model's ability to accurately predict WPD. Rock Springs 2008 serves as an excellent example of this. The NAM 12-km curve posits winds 3 to 4.5 m s^{-1} occur with the highest probability. The observational plot reports roughly equal probabilities of wind from 0 to 10.5 m s^{-1}. These discrepancies underline the biases toward weaker, more organized wind speeds in the model.

The three year average PDFs, more climatologically stable and arguably more representative of the winds at these locations, further illustrate the shortcomings in the model. In every summer and winter plot, the model peak is higher and narrower than the observational plot. Table 5.2 also confirms that the three year standard deviations of the model at all three locations for both seasons is lower than the observational standard

deviations. These three year single values of average wind speed and standard deviation, however, must be interpreted within the appropriate context. Only looking at the average three year wind speeds in Table 5.2 for each season masks many of the characteristics of the resource. In the winter, the average three year model wind speed for Laramie and Cheyenne is larger than the three year average of the observed wind speeds. Armed with only this information, one would conclude that the model over-predicts the wind and thus the WPD. The comparisons in Chapter 4 show that is not the case. The standard deviations, which can be taken as an indicator of the variability of the resource, reveal the observational data has much more variability, or spread, than their modeled counterparts. Knowing that the model under-predicts strong winds and over-predicts weaker winds helps explain the narrowness of the model plots. The agreement between the PDFs and the fitted Weibull curves in these plots further justifies modeling the resource with the Weibull function.

This behavioral difference between the model and observation may be partly responsible for the model's poor performance. Unfortunately, the solution is not as simple as "making the model more random," as simulating randomness is limited with current NWP models. These plots do however emphasize the need for more realistic simulations. Since the model is able to capture the longer term trends in the resource (diurnal and seasonal), simulating short-term ramp events are probably the model's largest handicap.

5.3: Validity of the 1/7 Power Law

Not much has been said about the validity of the 1/7 Power Law, the method used by the wind industry and in all the maps in Chapter 3 to calculate the wind at 50 m. The

Cooperative Surface-Atmosphere Exchange study field campaign of October 1999 (CASES-99) was a month long investigation of the nocturnal boundary layer. Data was recorded on a tower in 10-m increments from 10 m to 50 m at a sample rate of 5 minutes (Banta et al. 2002). Figure 5.14 shows the results for the first five days. The left vertical axis references the recorded 50-m wind speed and the extrapolated 50-m wind speed via the 1/7 Power Law (Equation 3.1). The right vertical axis references the contour number, *n*, in the 1/7 Power Law. The green and black lines correspond to sunset and sunrise, respectively. The pink line represents the value of 1/7 and the olive yellow line is the calculated contour number based on the wind at 50 m and the wind at 10 m.

Several trends become apparent just within the first few days. The second and third days are windiest, illustrating the diurnal variability of the resource. The winds tend to increase between sunset and sunrise: after day three is a prime example of this. Most relevant, however, are the discrepancies between the actual 50-m wind and the extrapolated 50-m wind via the 1/7 Power Law. During the day, the two lines shadow each other quite well, *e.g.* days two and four. When the two lines are in agreement, the contour line (olive yellow) is nearly atop the 1/7 line (pink). During the night, though, the two lines diverge substantially. The extrapolated winds are always lower than the actual winds and the corresponding contour number is greater than 1/7. Physically this makes sense. The 1/7 Power Law is designed to calculate upper level winds based on lower level winds. During the day, when the boundary layer is turbulent and well mixed, there is a stronger link between the 10-m wind and the 50-m wind. Thus the 1/7 Power Law accurately predicts winds at 50 m based on winds at 10 m. At nighttime, the boundary layer becomes stratified and much less

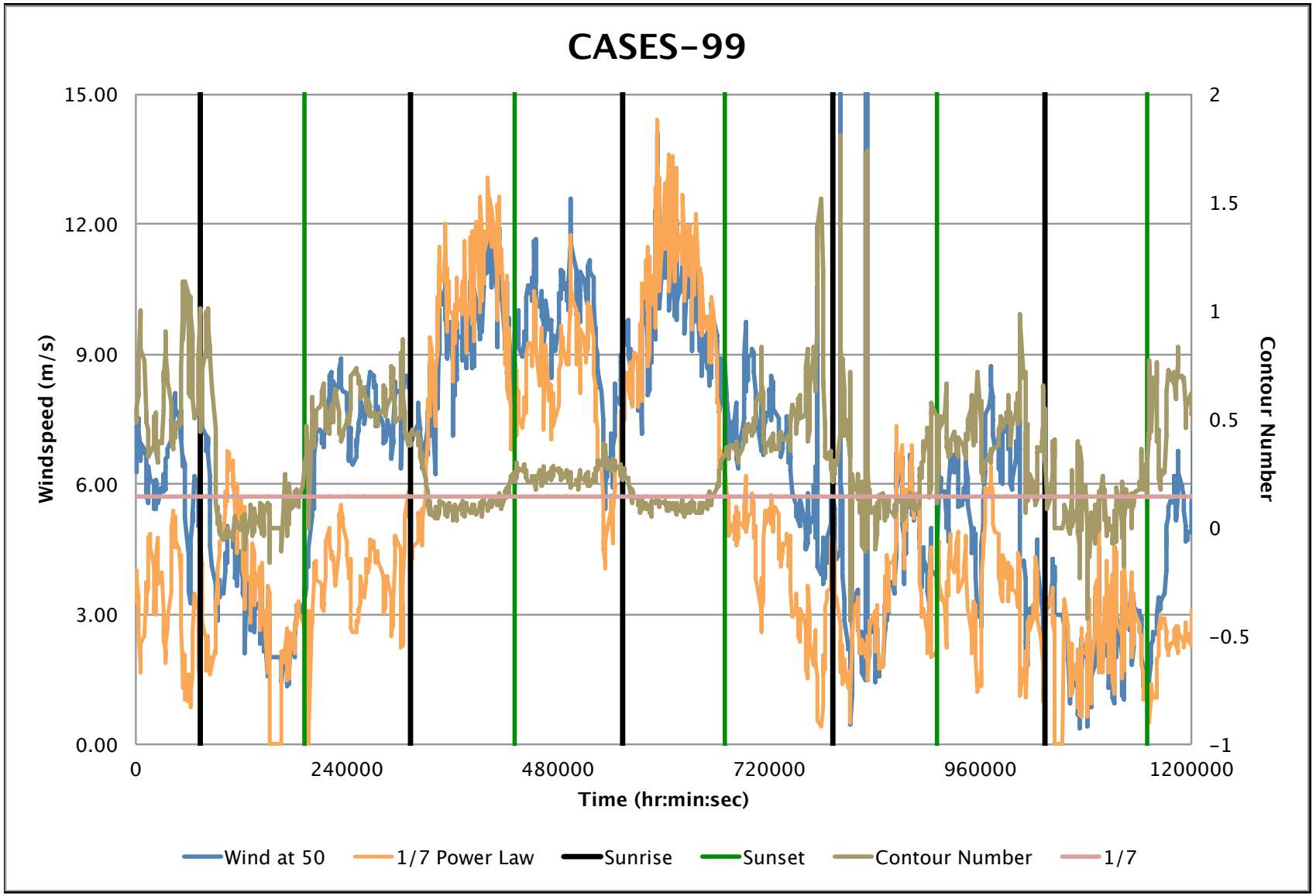

Figure 5.15: CASES-99 data: 50-m wind speed, extrapolated 50-m wind speed and contour number.

vertical mixing occurs, breaking this link. Trying to discern wind aloft based on the winds at the surface when the two are acting independently of each other is a recipe for error. Absent this link, the 1/7 power law poorly predicts wind aloft as evidenced by Figure 5.14. Between sunrise and sunset, the lines corresponding to 50-m winds and extrapolated 50-m winds are never aligned on any of the five days graphed. Better methods for extrapolating to 50 m at night must be explored if nocturnal winds at hub height are to be accurately simulated.

5.4: Weather Research and Forecasting Model Simulations

The FFT analysis answered the questions associated with the modes of variability of the resource. The PDF proved the consistency of the winds in the wintertime is not due to a few strong synoptic systems but rather southeastern Wyoming is persistently windy. The CASES-99 study illustrated the coupled nature between the 1/7 Power Law and the state of the boundary layer: the 1/7 Power Law breaks down when the boundary layer becomes stratified. But the problem of poor model prediction still remains. In efforts to alleviate this issue, additional statistical analysis was conducted on both the observational and simulated data. The question was asked if it would be possible to statistically correct the model data once it was made available. In this sense, the model data served as the independent variable. Model data corresponding to all eighteen Automated Surface Observing System (ASOS) stations was divided in 2 m s^{-1} increments from 6 to 16 m s^{-1}. Because the model data was serving as the independent variable, that was the data that determined the bins. For example, for the first bin of 6 to 8 m s^{-1} every instance when the model data was between those wind speeds, that data point and the corresponding observational data point would be placed inside

that bin. Again, because the model data was acting as the independent variable, the value of the corresponding observational did not matter. What mattered was that the times matched between the model and observation to maintain consistency. After all the model data had been divided into the corresponding bins, the bins were averaged and then plotted. Figure 5.16 illustrates the result.

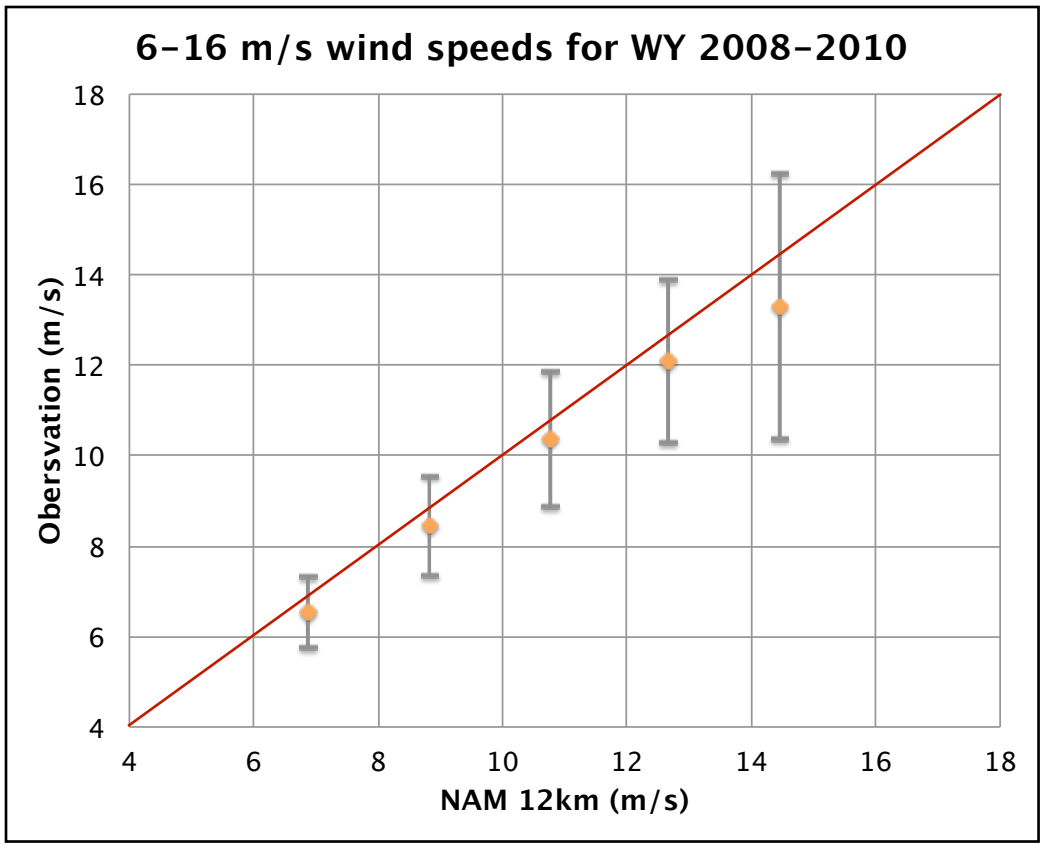

Figure 5.16: Average wind speeds of NAM 12-km and observations corresponding to the observation locations. Data was separated in bins of 2 m s^{-1}. The vertical lines denote the locations of ± 1 standard deviation.

The horizontal and vertical scales are identical, so the one-to-one line corresponds to the red line drawn down the diagonal center. The grey bars denote the values of ± 1 standard deviation. Overall these trends make sense. The data are consistently below the one-to-one

line, as expected. The model tends to under-predict the wind. If the standard deviation bars were not drawn on the graph, the initial reaction would be that the data would fit nicely on a simple linear regression. The parameters associated with the fit line could then be applied *post-mortem*; that is, apply the statistical parameters after the model has finished running to "fix" it. Unfortunately, the values of the standard deviation, especially at higher wind speeds, invalidate that approach. For example. the standard deviation of the fourth bin (12 to 14 m s^{-1}) overlaps the last data point. This speaks to the tremendous spread in the data. To emphasize this, Figure 5.17 is a basic scatterplot of the same data, not averaged or binned.

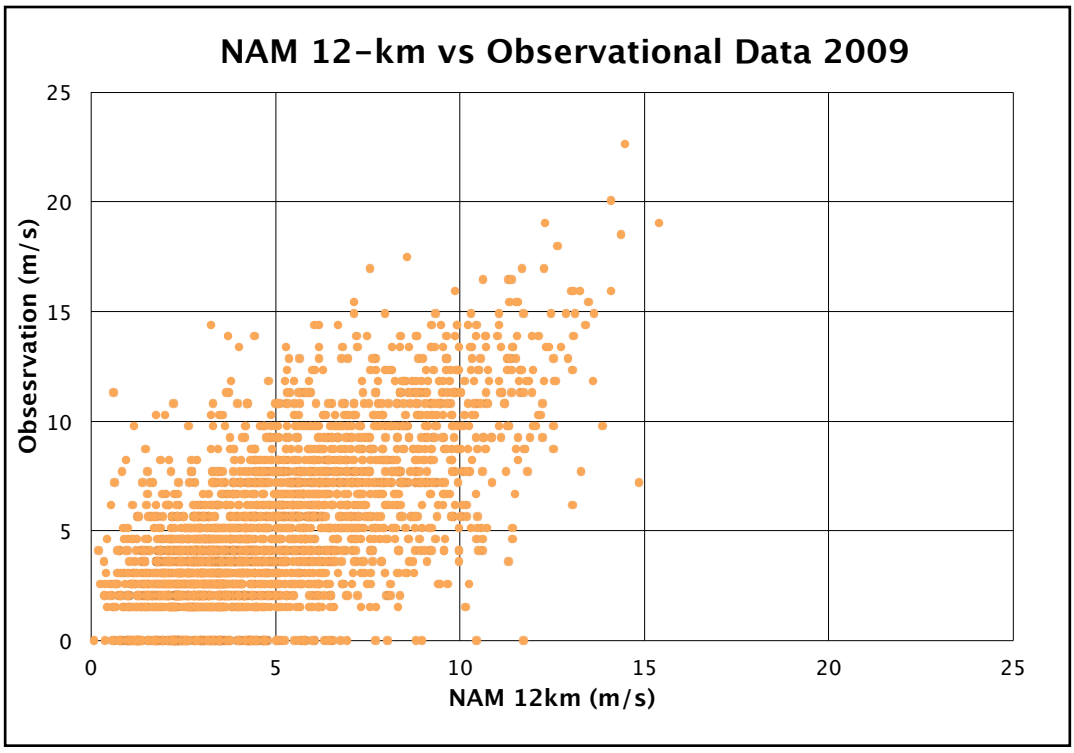

Figure 5.17: Scatter plot of model and observational data for 2009.

The amount of spread in the data is too wide to apply a simple linear regression. The model output is too complex to apply a "statistical band-aid" in efforts of improving the model's performance. Since adjusting the model output after the simulation is over does not seem to

be a viable option, perhaps changing the physical parameterizations in the model would improve the model's performance. Though it is not possible to tweak the NAM for experimentation, it is possible to tweak the parameters of its half brother: the Advanced Research Weather Research Forecasting (WRF-ARW, henceforth WRF) model.

Six different WRF runs were simulated with varying planetary boundary layer, surface layer and land surface parameterizations to investigate the potential of improving model performance. A particularly windy day was chosen for this case study (27 January 2008) to stretch the parameterization schemes to their limit. Tables 5.3 and 5.4 outline the various parameterizations used in the different WRF runs.

Table 5.3: Parameterization schemes used in each of the six different WRF runs.

Runs	Planetary Boundary Layer	Surface Layer	Land Surface
1	4	4	2
2	5	5	2
3	2	2	2
4	7	7	2
5	4	4	3
6	4	4	7

Table 5.4: Explanation of the various parameterizations used in the WRF runs.

Planetary Boundary Layer	Surface Layer	Land Surface
4: Quasi-Normal Scale Elimination PBL: A TKE prediction option that uses a new theory for stably stratified regions.	**4**: QNSE PBL surface layer option	**2:** Noah Land Surface Model: Unified NCEP/ NCAR/AFWA scheme with soil temperature and moisture in four layers, fractional snow cover and frozen soil physics.
5: Mellor-Yamada Nakanishi and Niino Level 2.5 PBL. Predicts sub grid TKE terms	**5**: MYNN surface layer scheme	**3**: RUC operational scheme with soil temperature and moisture in six layers, multi-layer snow and frozen soil physics
2: Eta operational scheme. 1-D prognostic turbulent kinetic energy scheme with local vertical mixing	**2**: Eta similarity: Used in Eta model and based on Monin-Obukhov with Zilitinkenich thermal roughness length and standard similarity functions from look up tables	**7**: Two layer scheme with vegetation and sub-grid tiling
7: Asymmetric Convective Model with non-local upward mixing and local downward mixing	**7**: Pleim-Xiu surface layer	

The WRF runs were simulated with a nested grid. The entire state of Wyoming was covered with a 12-km grid and the southeastern corner of Wyoming was nested with its own 4-km grid. Figure 5.18 illustrates the various domains included inside the the WRF simulations.

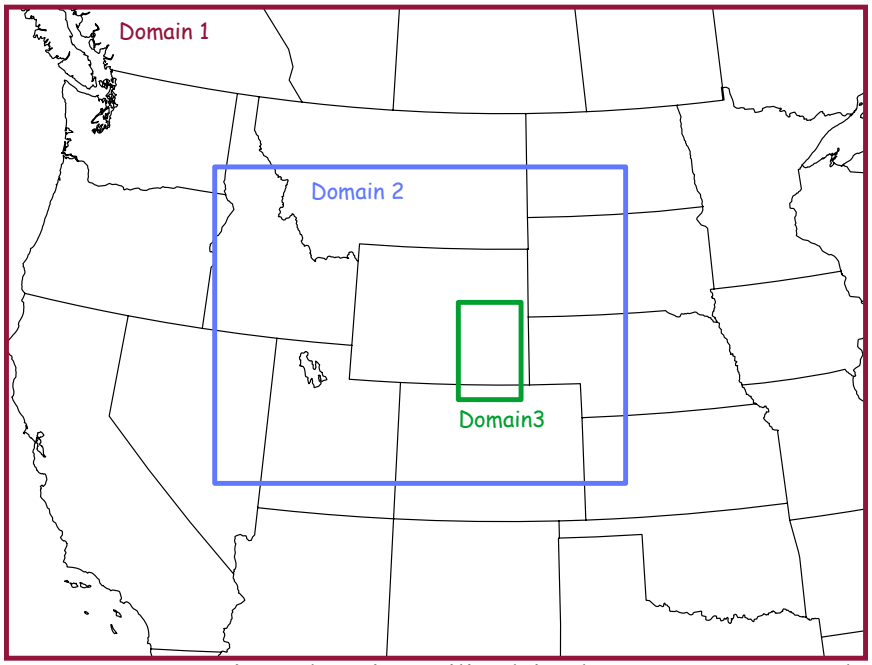

Figure 5.18: Various domains utilized in the WRF runs. Only Domain 2 and Domain 3 were of interest and their resolutions were 12-km and 4-km respectively.

In the first four WRF runs, the planetary boundary layer and surface layer parameterizations were changed. In the last two runs, the land surface parameterizations were changed. The following panel plots show an intra-comparison between the various WRF runs. The first run was chosen as a baseline and the remaining runs were subtracted from the baseline.

Each panel plot is an average of 10-m wind speeds at 4 different times: 0900, 1200, 1500, 1800 UTC. The colorbar represents the difference between the simulations: purples and blues correspond to negative values of wind speed (the current run is greater than the baseline run) and reds and blacks correspond to positive values of wind speed (the current run is weaker than the baseline run). Since the models under-predict the wind, a promising combination of parameterizations would possibly show up with purples and blues, indicating the baseline is much weaker. Unfortunately none of the plots look like that. The best is the

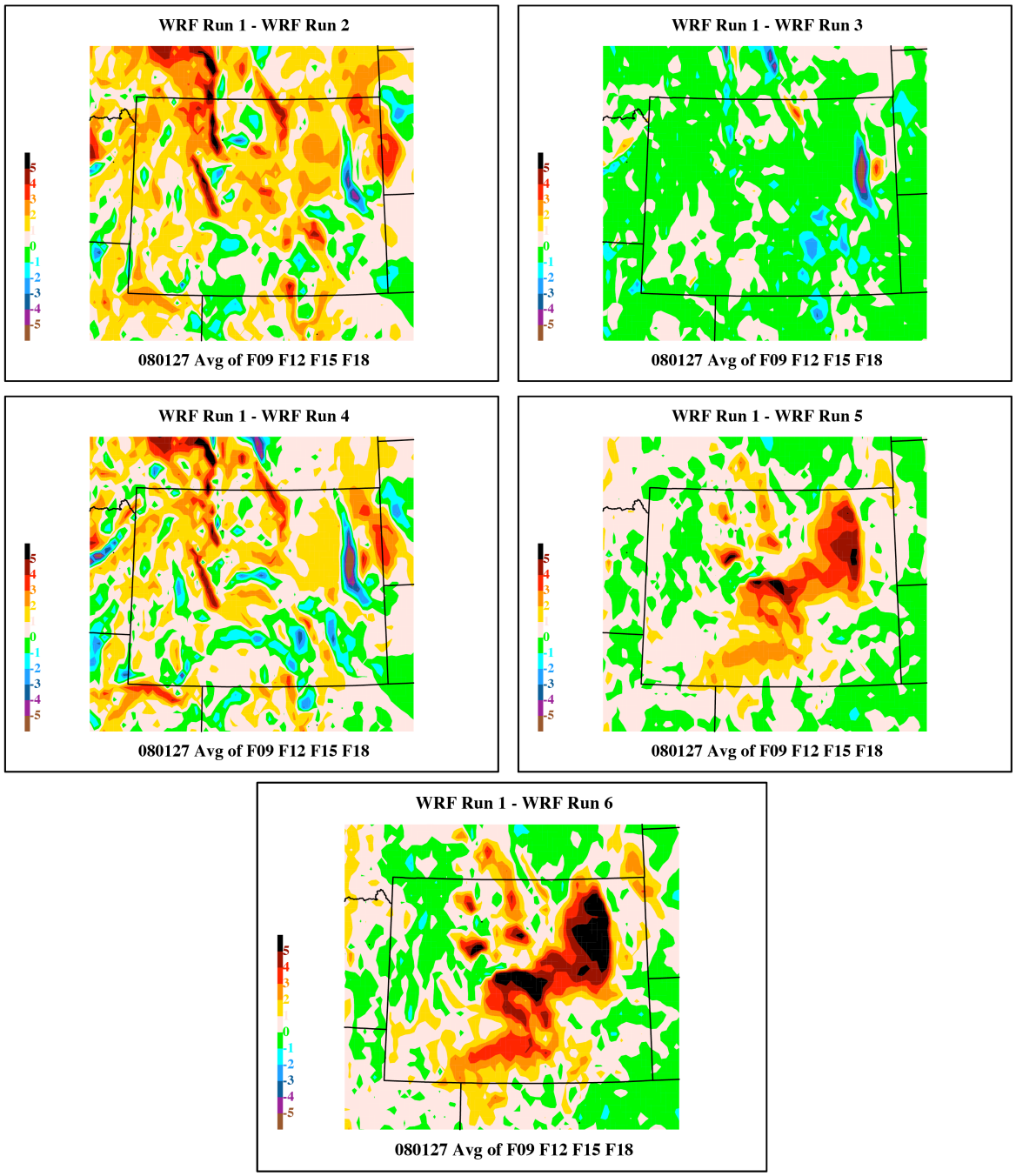

Figure 5.19: Intra-comparisons of the various 10-m wind WRF runs (using data from Domain 2). The first run was chosen as a baseline to which all others were compared.

upper right which is mostly green, indicating that the first run and the third run were quite similar. One thing that can be concluded is that changing the land surface parameterizations from their default value makes things much worse. The last two runs, five and six, were the two WRF simulations that altered that parameterization and those two simulations were the weakest of the lot.

Figures 5.20, 5.21 and 5.22 are line plots comparing the WRF simulations to the NAM (both the 12-km and 4-km flavors) and the observations. Since the last to WRF runs (those in which the land surface parameterizations were altered) were not included in this comparison because of their poor performance. Closer inspection of these figures reveals a few curious attributes. In Laramie, all of the models do a poor job of simulating the wind, especially the ramp event at the end of the day. Another bizarre characteristic in Laramie is that at almost all times, the higher resolution version of both models simulates lower winds better than its lower resolution counterpart. The blue line, corresponding to the NAM 4-km, is almost always below the green line, corresponding to the NAM 12-km. The same pattern appears in the WRF runs: the orange line, corresponding to Domain 3, (the higher resolution domain) is almost always below the maroon line, corresponding to Domain 2 (the lower resolution domain).

The Cheyenne plots, although weaker, exhibit some of the same behavior as in Laramie. The ramp event towards the end of the day is more subdued but the models still miss it. In Rock Springs, this pattern is not observed. Quite the opposite: all the models do a reasonably good job in simulating the wind. (Note that the WRF Domain 3 line is absent because Rock Springs was west of the WRF Domain 3). All the models simulate the ramp up

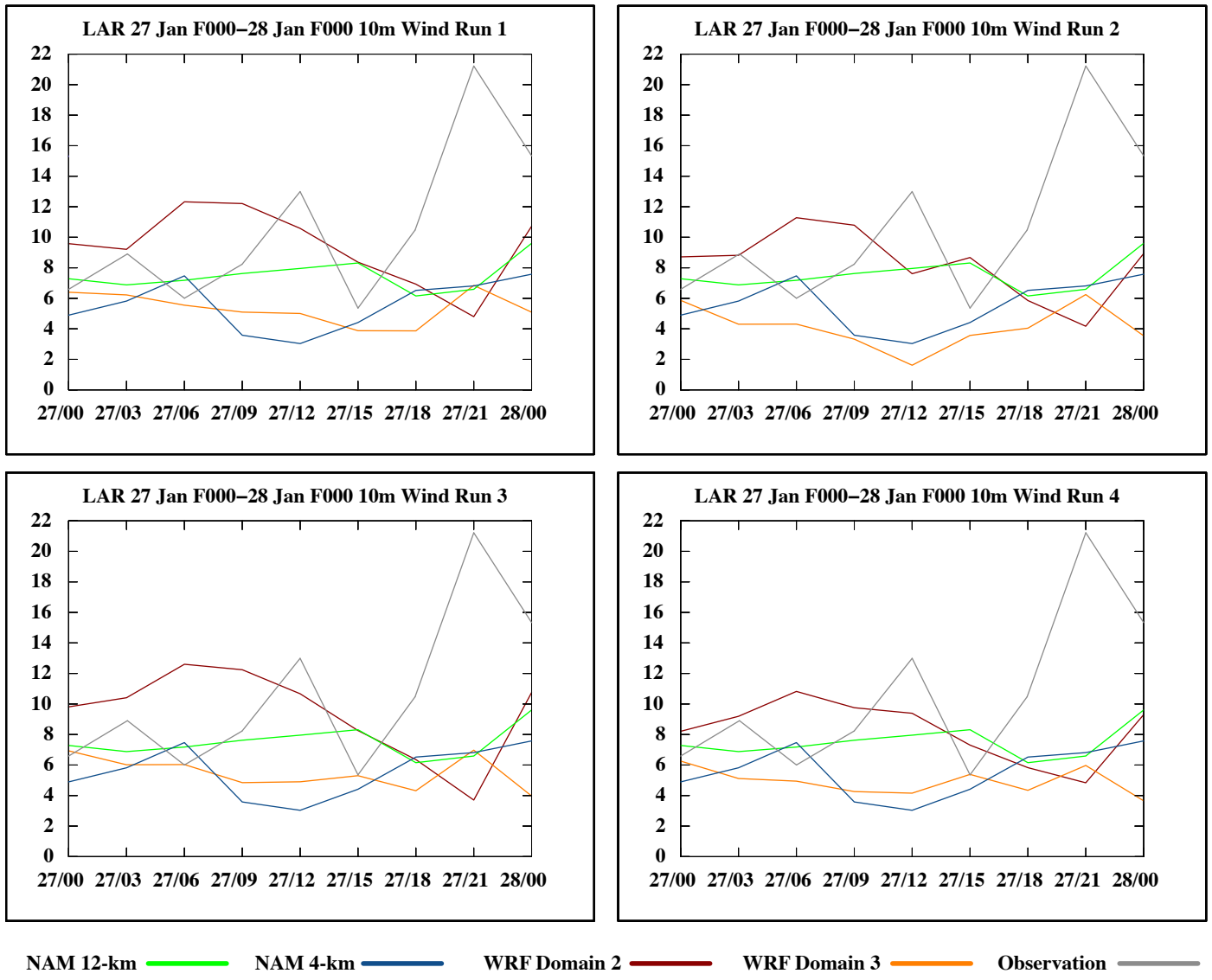

Figure 5.20: WRF, NAM and Observational time series for 27 January 2008 at Laramie.

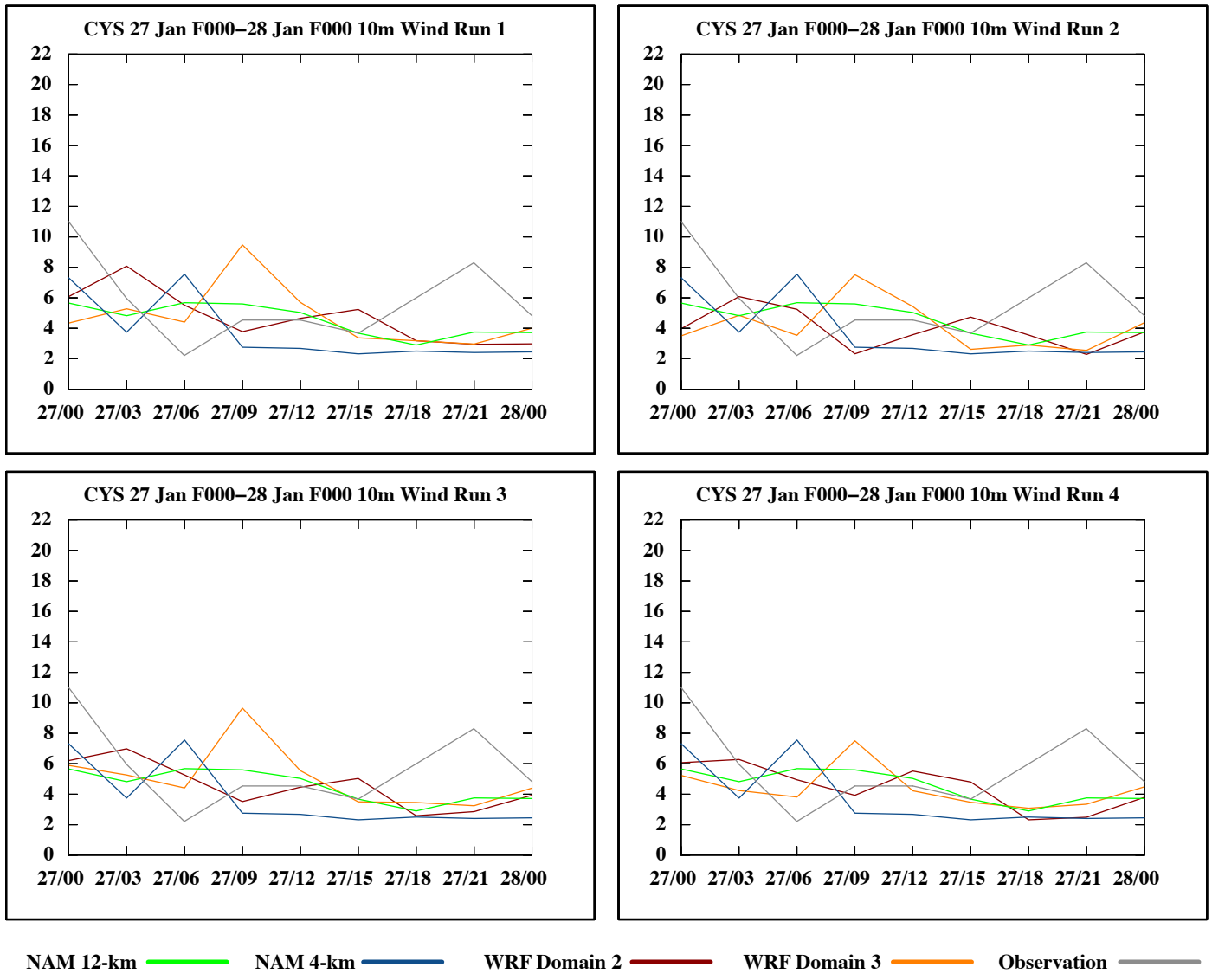

Figure 5.21: WRF, NAM and Observational time series for 27 January 2008 at Cheyenne.

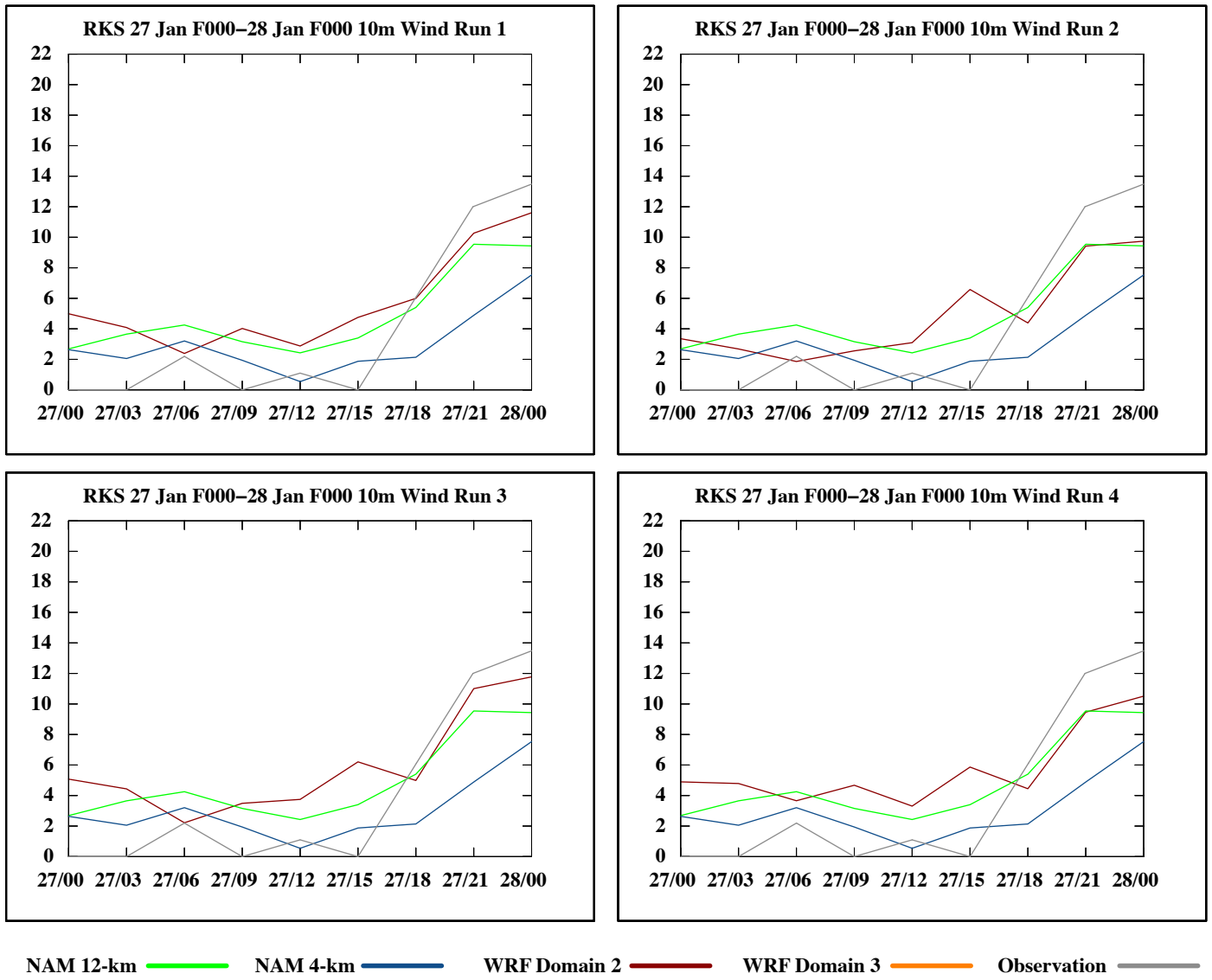

Figure 5.22: WRF, NAM and Observational time series for 27 January 2008 at Rock Springs.

of the wind towards the end of the day. The NAM 4-km is a bit weaker than the other models, but the trends are present nonetheless.

The WRF simulations, unfortunately, did not improve prediction of the wind. There was no "miracle parameterization" that resulted in a perfect forecast. Rather, all the WRF runs simulated the wind with equal skill. The only definitive conclusion is that changing the land surface parameterizations negatively affected performance. Tweaking the suite of included planetary and surface layer parameterizations resulted in only marginal improvements.

From Chapter 4, it is clear that the models successfully capture the longer term trends of the resource (diurnal and seasonal), yet consistently under-predict the WPD. These ramp events, like the one on 27 January 2008, may be the culprit for the model's poor performance. Quick accelerations in wind speed wreak havoc on wind farm operators. Improving the accuracy of predicting ramp events could have untold consequences on the ability of wind farm operators and weather forecasters to perform their jobs. Refined ramp event prediction could also remedy some of the weaknesses from which the models suffer. Granted, this was only a 24 hour simulation and many more model runs should be conducted to verify the relative performance between these three locations. Nonetheless, these preliminary results suggest the impact of terrain on model accuracy.

5.5: Topography Analysis

Since topography characterizes the wind corridor, the representation of the terrain within the model may be cause for its poor performance. Surface plots of the terrain in

southeastern corner of Wyoming can be used to compare the rendering of the topography within the various models. If, for example, the terrain in the higher resolution models differs significantly from their coarser resolution counterparts, that may be the cause for the weaker output from the higher resolution models. Figure 5.20 illustrates the location of the topographic surface plots.

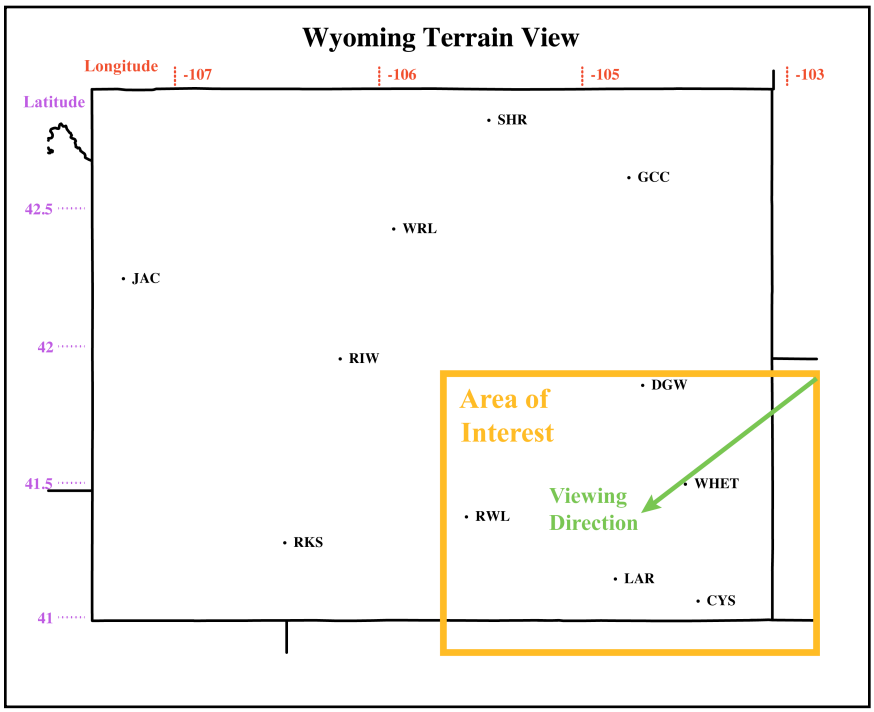

Figure 5.23: Location of surface plots and view direction. Latitude and Longitude are also outlined.

Each surface plot is oriented such that the view is directed towards the southwest, as per the green arrow in Figure 5.23. The topographic data was extracted in the same geographic area for both the NAM and WRF. As expected, the finer resolution models afford more data.

Figures 5.24-5.27 illustrate the topography in this region from the NAM 12-km, NAM 4-km and Domains 2 and 3 from the WRF simulations. The latitude and longitude are plotted on the horizontal and the elevation is plotted on the vertical, ranging from 1000 m to 3500 m

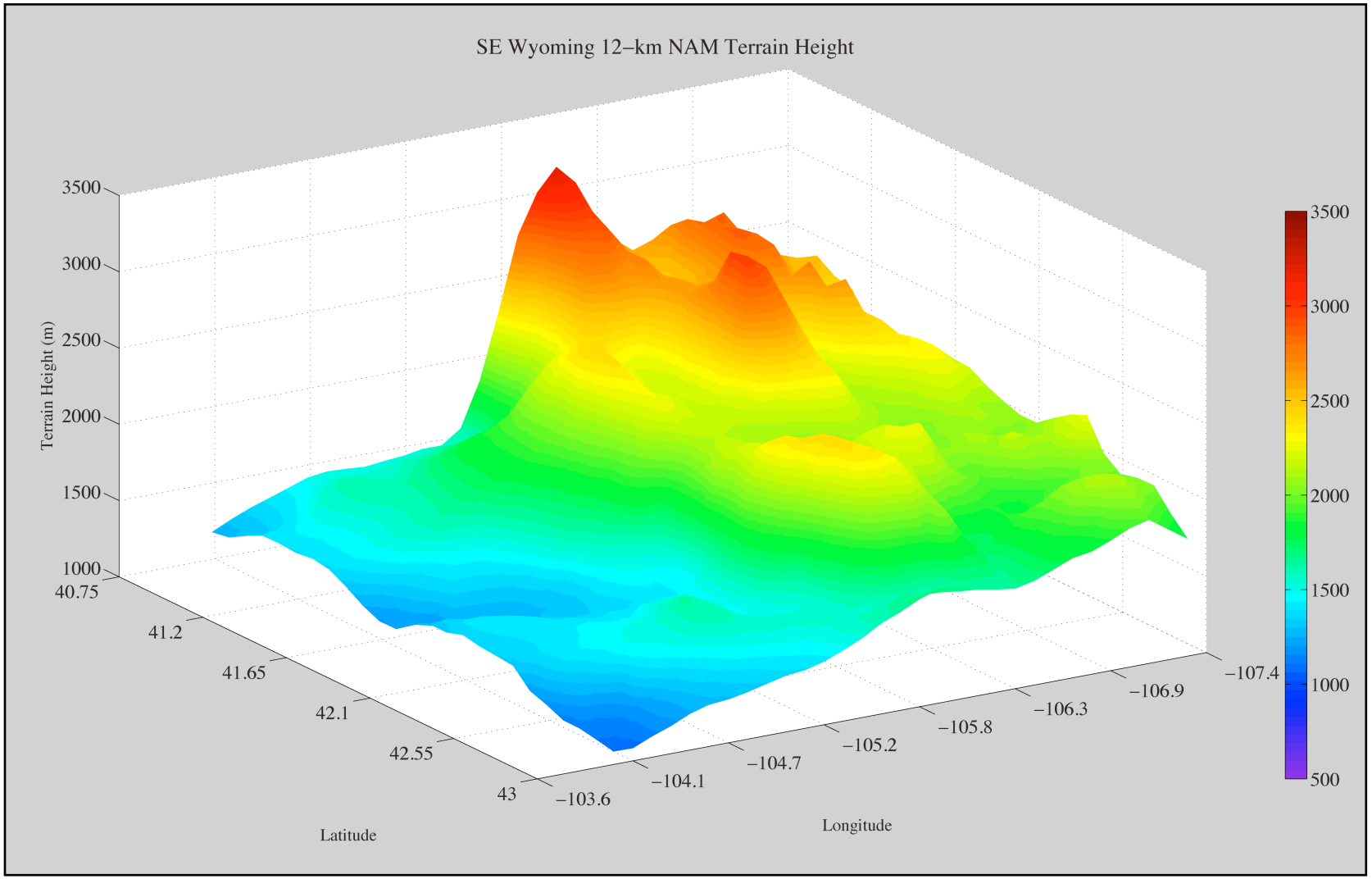

Figure 5.24: NAM 12-km topography of southeastern Wyoming looking towards the southwest.

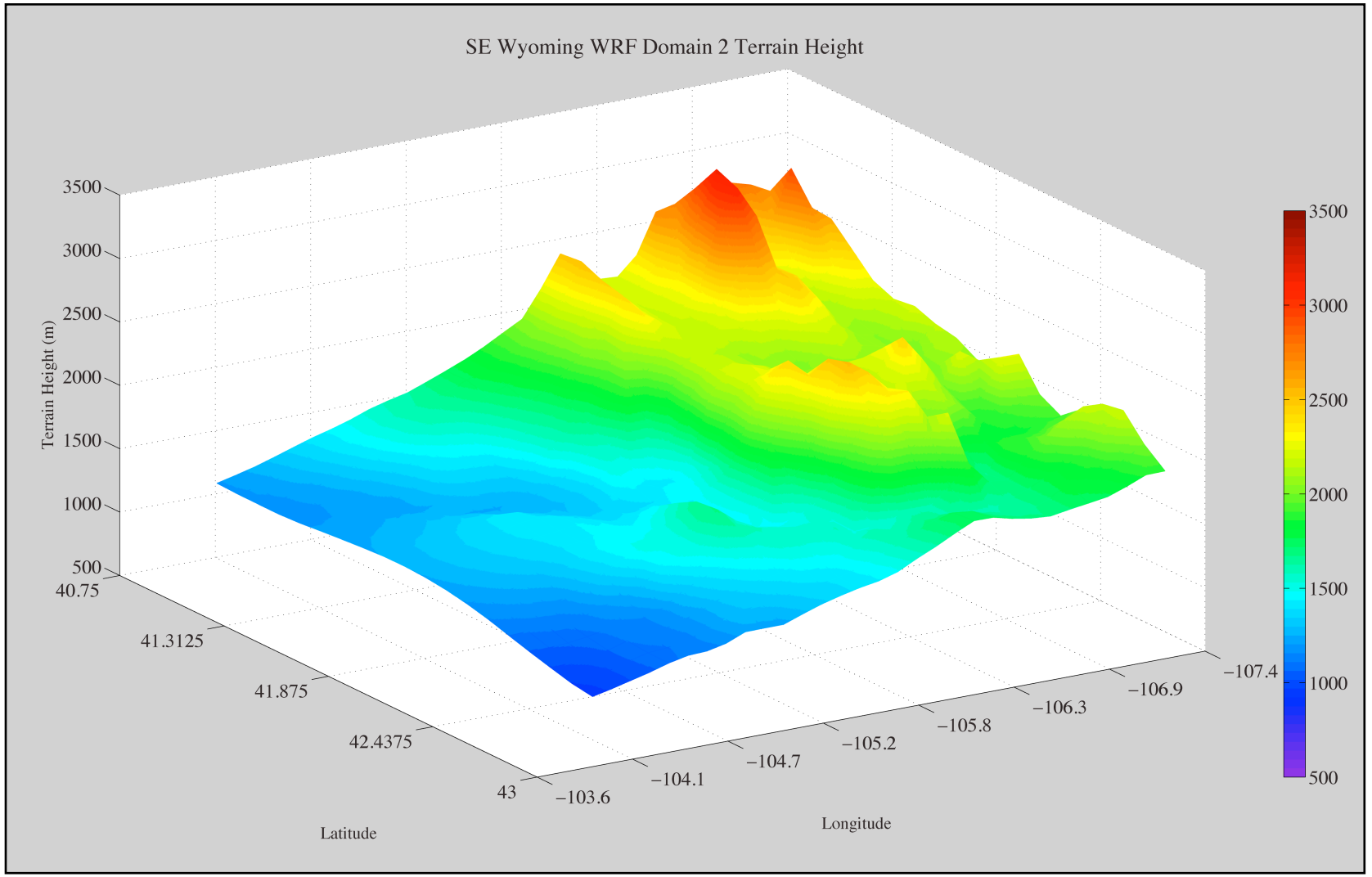

Figure 5.25: WRF Domain 2 topography of southeastern Wyoming looking towards the southwest.

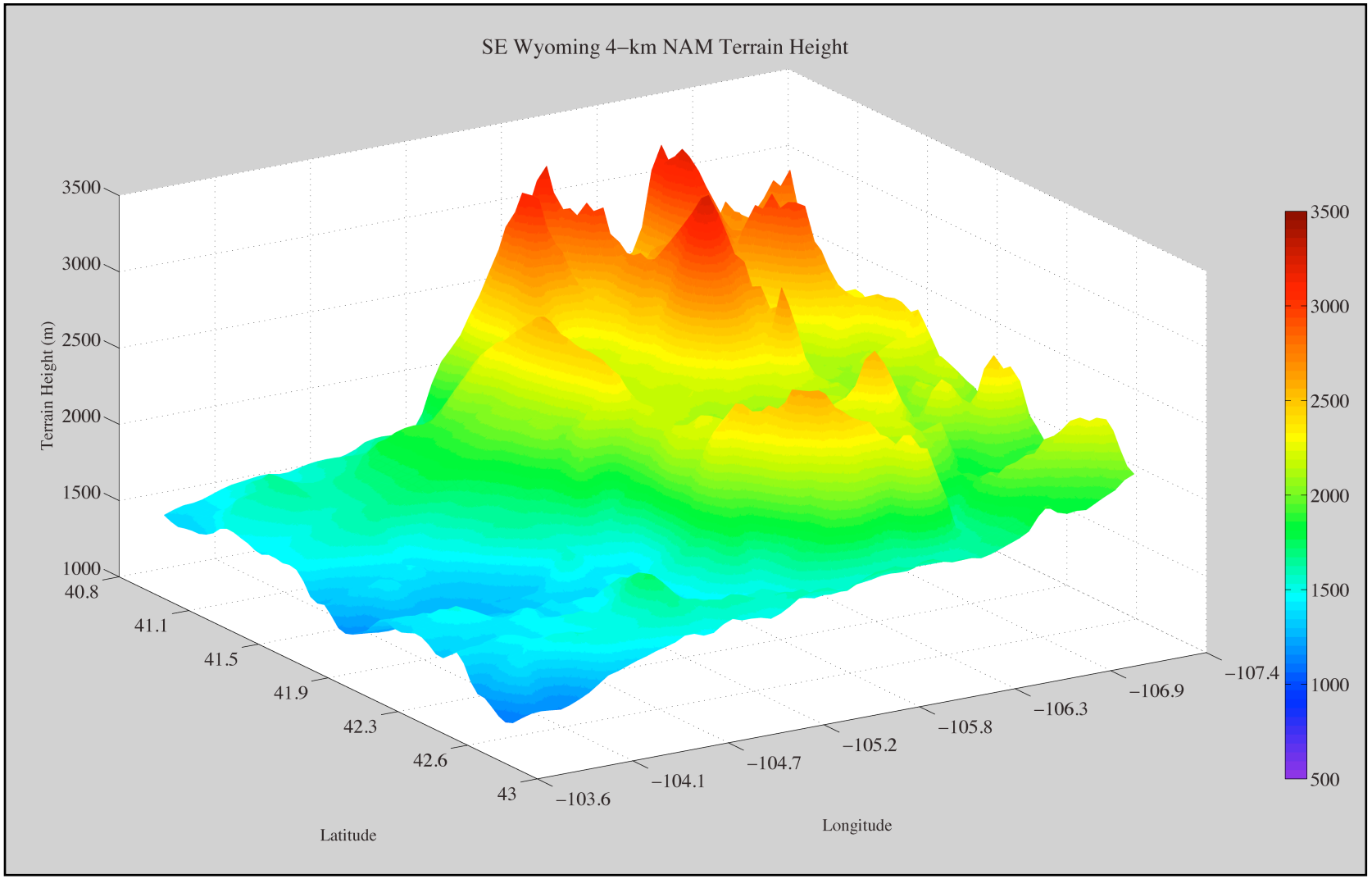

Figure 5.26: NAM 4-km topography of southeastern Wyoming looking towards the southwest.

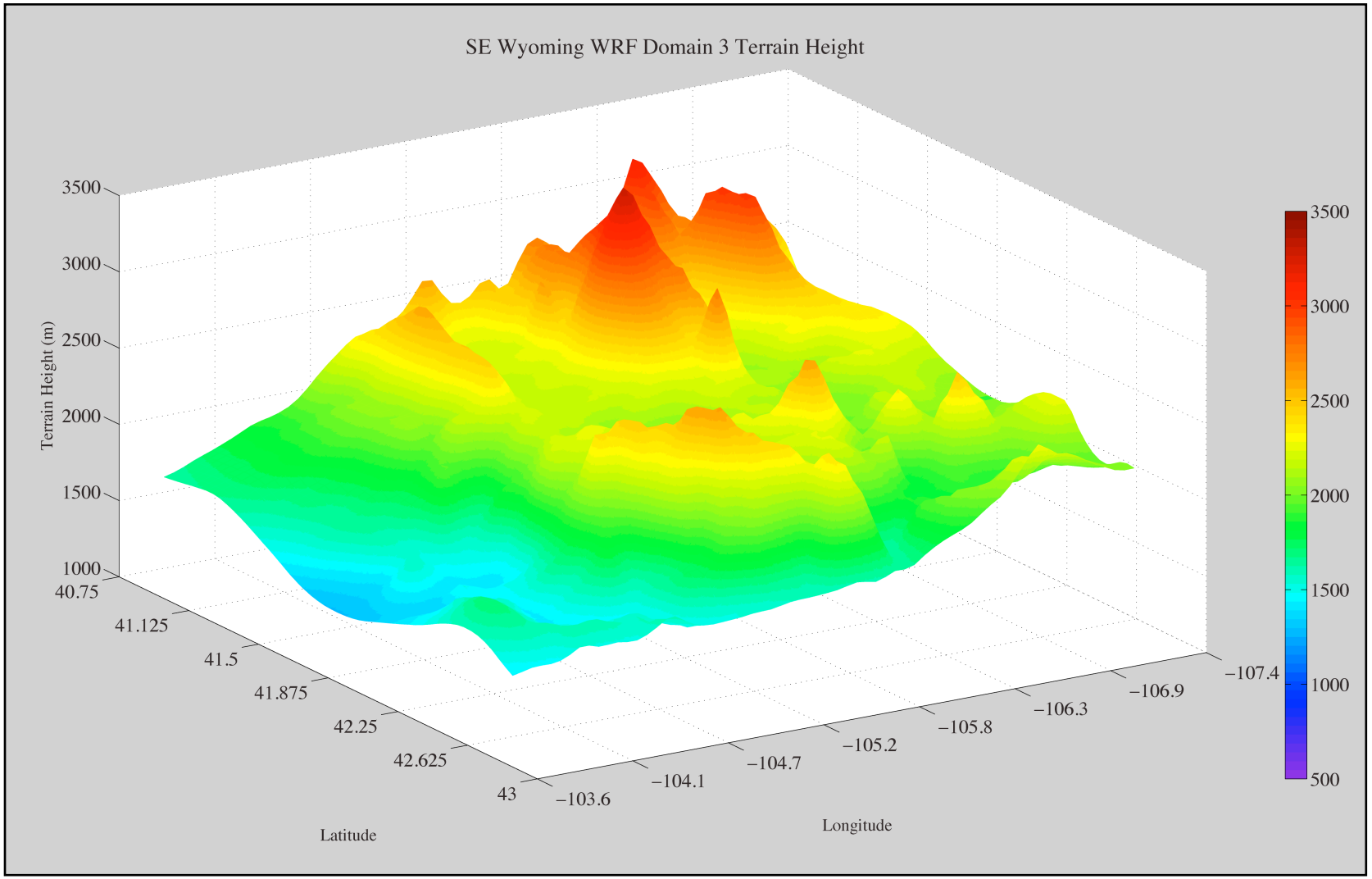

Figure 5.27: WRF Domain 3 topography of southeastern Wyoming looking towards the southwest.

above sea level. Purples and dark blues correspond to lower elevations and oranges and dark reds correspond to higher elevations. The distinctive geographic features in the region are apparent in both resolutions of both models: the Medicine Bow and Sierra Madre mountain ranges which dominate the landscape and the smaller Laramie Range to the east as well as the gradual downsloping of the terrain towards the Great Plains. However, upon further inspection, discrepancies in the models appear. Regarding the coarser resolution terrain, NAM 12-km and WRF Domain 2, these two surface plots appear to be a bit out of phase. This is worrisome to say the least, given that the same geographic region is plotted. Though a difference of a few kilometers may be inconsequential when forecasting large synoptic systems, a phasing error of a few kilometers is on the scale of a wind farm. Incorrect location of the terrain within NWP models can be just as devastating as incorrectly rendering the geographic features, especially on the scales relevant to the wind energy industry. Figures 5.24 and 5.25 clearly illustrate this problem. Even though the locations of the grid points between the NAM and WRF are different, the topography should be comparable when plotted over the same geographic bounds. The surface plot in Figure 5.25 appears to be shifted south about a degree of latitude and west about 1.5 degrees of longitude.

This phasing issue is also present in the finer resolution version of both the NAM and WRF as evidenced by Figures 5.26 and 5.27. The WRF Domain 3 topographic plot appears to have shifted southwest, like the coarser resolution Domain 2 plot. The fact that the elevation at a certain latitude and longitude differs between the two models hampers a forecaster's ability to accurately predict the surface winds. Though it is reasonable to expect some degree of topographic variability between the two models, a misplacement error of a

few kilometers in an area as topographically distinct as southeastern Wyoming drastically reduces the model's value to a wind forecaster.

The topographic differences in the NAM and WRF may account for the discrepancies in their performance when examining Figures 5.20-5.22. The anomalously weaker wind speeds from the WRF simulations at Laramie (Figure 5.20) may be due to these topographic phasing errors. Incorrect location of the terrain may have caused the error in predicting the ramp event towards the end of the day. The maroon line, corresponding to WRF Domain 2 reaches a local minimum when the observations peak at a maximum; *i.e.* the lines are going in opposite directions. The green line, corresponding to the NAM 12-km, does not exhibit this behavior. Figure 5.21, at Cheyenne, illustrates the topographic errors even more clearly. Concerning the higher resolution output, the NAM 4-km (blue line) peaks at 0600 UTC and the WRF Domain 3 (orange line) peaks three hours later. Both lines appear to follow nearly the same trajectory (especially during Run 2) but they reach a maximum at different times. Since Cheyenne is located on the downslope of the Laramie Range, topographic phasing errors can have a major impact on the prediction of surface winds.

Compared to its performance near the surface, WRF simulates upper level winds quite well. Studies in the Arctic have found that simulations of not just wind, but of temperature improve at pressure levels well above those at the surface (Wilson et al. 2011). Comparisons by Parish (informal conversation) of soundings at Riverton, Wyoming with WRF output also confirm improved model performance at upper levels.

Thus, in a relative sense, WRF seems to predict upper level winds better than lower level winds. In the free troposphere, unhampered by topography, the model is able to capture

and simulate the larger scale forcings responsible for the motion at those levels. Nearer the surface, though, is where the model has trouble. The boundary layer parameterizations as well as the interactions of the pressure gradient forces with the terrain are the areas in need of improvement.

Chapter 6: Conclusion

6.1: Summary

Wyoming is one of the windiest places in the world. Owing to its geography, the southeastern corner of the state forms a topographic funnel through which a majority of the low level air masses must flow. Aptly called the "wind corridor" this area is near the lowest point in the Continental Divide. The synoptic features of the region drive these westerly winds, especially in the wintertime. Pools of cold air gather to the west of Wyoming generating an area of high pressure. Low pressure systems often develop east of the Rocky Mountains and result in strong pressure gradient forces across the state, including the accelerated flow through the wind corridor.

The wind resource in Wyoming follows two main cycles: the resource peaks in the wintertime and subsides in the summertime, following the cycle of synoptic systems in the region. The jet stream fuels synoptic systems in the wintertime resulting in high winds through the wind corridor. By the summer, the jet stream has retreated north, leaving the area less prone to synoptic events. On shorter timescales, the wind resource follows a diurnal cycle, peaking in the afternoon. As with the seasonal mode, atmospheric conditions are responsible for the diurnal cycle. Solar insolation reaches a maximum in the afternoon, resulting in a well mixed and turbulent boundary layer. Turbulent kinetic energy from upper levels is transported to the surface.

Extrapolating the wind from 10 m to 50 m via the 1/7 Power Law (Equation 3.1) has serious limitations. During the day, when solar radiation heats the boundary layer (BL) causing turbulent mixing, the 1/7 Power Law works very well. At nighttime, though, the

equation breaks down: the BL becomes stably stratified because of the lack of solar insolation. Under stable conditions, the BL is no longer well mixed and the feedback mechanisms inherent to the 1/7 Power Law vanish. Winds at upper levels are unrelated to winds at the surface, calculating the winds at 50 m based on the winds at 10 m is a challenge at best. While this is less of an issue in Wyoming where the maximum winds occur in the afternoon, in places trying to harness the low level jet, for example, this is a critical issue since the low level jet peaks during the night. Further research is needed to determine the best way to extrapolate to upper levels under stable conditions.

The wind resource complements both intrastate and interstate power sources. In Wyoming, the wind resource peaks in the wintertime when the availability of hydropower is at a minimum. Six months later, the snow melt has increased the capacity of hydropower when wind power is at a minimum. The two power sources balance each other: when one is high, the other is low. Another source of wind power which has garnered much attention in the last decade is the low level jet (LLJ). This meteorological phenomenon impacts the Midwest in the summertime and affords a fantastic potential for wind energy. Like Wyoming hydropower, the LLJ peaks in the summertime and abates in the wintertime. Perhaps the most influential mode of variability is the diurnal cycle. The Wyoming wind resource peaks in the afternoons during times of high electricity demand. Conversely, the LLJ peaks in the middle of the night, when demand for electricity has diminished. In situations of high wind integration, the complementary nature of these power sources would help greatly with balancing efforts.

Numerical weather prediction (NWP) model performance in mountainous regions, like the wind corridor, leaves much to be desired. The models always under-predicted the wind. If NWP models are to be used to predict winds in mountainous areas, the rendering of the terrain within the model must be correct. Topography and wind are highly coupled in this region: inaccurate terrain results in inaccurate wind forecasts. The location of the terrain, too, is just as important as the actual features rendered. The topographic phasing errors present between the NAM and WRF can result in erroneous wind forecasts in places where terrain drives the development of strong surface winds, like in southeastern Wyoming.

These errors get amplified when calculating wind power density (WPD), a quantity proportional to the cube of the wind speed. Output from the 12-km and 4-km variants of the North American Model (NAM) for 2008-2010, when compared with observations, sometimes exhibited differences in WPD of 1000 W m^{-2}. Though the model captured the trends of the wind, the actual values of WPD were always below the observed values. Probability distribution functions (PDFs) of the observational and model datasets at Laramie, Cheyenne and Rock Springs revealed the decreased variability of the resource within the model. In addition to under-predicting high wind speeds, the model over-predicts low wind speeds, as it is incapable of simulating a 0 m s^{-1} wind velocity. And, all these simulations occur within a narrower range of wind speeds than the observations. The prevalence of low wind speeds and absence of high wind speeds, all within a confined range, is partially responsible for the weaker simulated WPDs. The discrepancy between forecasted and observed WPD was largest in mountainous areas, like the Laramie valley, and slightly improved near flatter regions, like Rock Springs.

In efforts to improve model performance, several simulations were run using the NAM's cousin: the Weather Research and Forecasting (WRF) model. Varying BL and surface layer schemes as well as land surface parameterizations, the WRF simulations saw no marked improvement over the NAM output. The performance of the high-resolution versions of both of these models degraded when compared to their coarser resolution counterparts. This illustrates the concept of misplacement errors. When transferring to a higher resolution domain from a coarser domain, the errors tend to amplify because of the increased density of grid points. High-resolution models may not always be better. Neither may conventional NWP models. These models were designed to predict the weather, not the wind. People care whether it will rain tomorrow, not how fast the wind will be blowing from the southwest. NWP model output is the state of the *atmosphere* at a given time, not the state of the wind. Though enhancing the topography within NWP models may improve surface wind forecasts, this does nothing to change the underlying motives of these models: predicting the weather. Alternative energy sources deserve alternative weather models. Models developed solely for accurately predicting the wind would not only benefit the energy market, but also surface/ air transportation sectors, fire safety and air quality industries, other weather organizations and even homeland security.

6.2: Public Opinion of Wind Energy

Given that wind energy is a regional power source, not everyone is directly affected by it. People living in close proximity to a wind farm in Wyoming or central Illinois may have different opinions of wind energy compared to a person living in Georgia. And some of these

opinions are less than glowing. In 2009, three wind turbines were installed off the small island community of Vinalhaven, Maine near Penobscot Bay in efforts to lower the price of electricity. Within a few days after the turbines became operational, a small group of residents began lobbying for their removal, claiming the noise generated by the turbines was loud and disturbing. This antiwind group's mantra is that "they were not accurately informed about the noise ahead of time." Said one resident, "I feel duped." Other allegations include adverse physiological affects such as increased heartbeat and nausea and reduced property values. Though the American Wind Energy Association (AWEA) published a paper in December of 2009 concluding that "there is no evidence that the audible or sub-audible sounds emitted by wind turbines have any direct adverse physiological effects." A separate study from the Department of Energy found that "property values were unaffected by nearby wind turbines." It should also be noted that ambient noise from wind turbines is much more conspicuous in small, quiet rural areas compared to suburbia. Nonetheless, wind energy cannot afford a public backlash and so the industry should take to installing the turbines at a reasonable distance from residences (Zeller 2010).

Another obstacle wind energy faces is the waning cost of natural gas. The controversial method of extracting this resource, hydraulic fracturing or "fracking," has led to discoveries of mammoth reserves within the United States. In fact, the US has passed Russia as the world's largest natural gas supplier. The cost of natural gas is around $2 and "[b]ecause 24% of electricity comes from power plants that run on natural gas, that has helped keep costs down to just 10 cents per kilowatt-hour." However, the price of natural gas, like all fossil fuels, is volatile and there is no guarantee that its price will remain low (Eilperin 2012). The

price of wind, on the other hand, is as constant as the sun. When a wind farm is built, the price of electricity it supplies is known from day one.

Arguably, the production tax credits wind energy enjoys are responsible for the current state of the industry. These tax credits are set to expire at the end of 2012 and proponents of wind energy are asserting that "they cannot be truly competitive and keep creating jobs without a few more years of government support." This credit has been in place since 1992 and provides a 2.2 cents per kW-hr credit on all electricity generated from a wind farm within the first ten years of its life. Proponents maintain that these tax credits only go to companies that are operational, reducing the possibility of a taxpayer subsidy of a failing company. And according to AWEA, "wind projects account for more than a third of all the new electric generation installed in recent years, while over the last six years, domestic wind turbine production has grown twelvefold, to more than 400 facilities in 43 states" (Cardwell 2012). With higher fossil fuel prices on the horizon, wind will become even more economically competitive. This energy competition is not only within the US. China is quickly becoming an attractive market for renewable energy and within the last five years has risen to number one in wind energy generation. "In Europe, many national governments have guaranteed prices for energy from sun or wind. As a result, renewable advocates say, many countries are on track to meet the European Union's goal of 20% of energy from renewable sources by 2020" (Wald 2010). The US has already deemed generating 20% of domestic electricity from wind is possible. America cannot idly sit on the sidelines and watch other countries get there first.

6.3: Future Work

Fundamental gaps in the knowledge of the BL are also preventing breakthroughs in improving wind forecasts. These gaps stem from an incomplete understanding of the Earth's energy budget between the Sun, atmosphere and Earth's surface. This ignorance limits the ability to predict winds, especially in nonsteady, spatially heterogeneous environments. Inadequate parameterizations of the BL may be mitigated by additional measurements (Shaw et al. 2009). Unfortunately, this is no simple task. Recall Table 3.1 that described the wind classes and the wind speeds corresponding to those classes: all the wind speeds assumed a precision of a tenth of a meter per second. In reality, it is not possible to measure the wind that precisely. One can imagine a situation where a wind developer will only build a wind farm in a Class 5 region or above. Imprecise wind measurements could lead to an erroneous Class 5 designation.

Improvements related to wind forecast technology are constantly being made. Data assimilation into high-resolution rapid update cycles, model integration with complementary scales, quantification of forecast uncertainty and analysis of consequences of ramp events are just some of the areas of active research and development. These improvements, according to Marquis et al. (2011) could potentially:

- reduce CO2 emissions
- mitigate the costs associated with implementing large scale wind projects
- reduce the amount of reserve power needed
- reduce generation costs
- maximize wind power output

How these benefits will impact the quality of wind forecasts, however, is difficult to outline. Strictly defining and quantifying a forecast's quality quickly becomes an exercise in futility. Simply put, different groups will use wind forecasts differently. Certain aspects in a wind forecast may have varying or even conflicting value to various people. One goal of improving wind forecasts is to jettison the age-old concept that a "good" forecast is one that has the smallest error. The complex economics associated with wind energy demand that this elementary viewpoint be reexamined.

Though the added benefit of generating a sizable percentage of domestic electricity from wind would surely outweigh the minor ecological consequences that may result, it is still necessary that those consequences be researched extensively before bold energy projects are undertaken. The microclimate effects a wind turbine can have on the soil moisture, for example, are not well understood. The number of frost free days due to a wind farm may impact the environment in ways not anticipated (Marquis et al. 2011).

These are all grandiose plans, but care must be taken to ensure that wind developers do not "put the blades before the tower." There are lessons to be learned from the previous WRAs, outlined in Chapter 2. The Arizona WRA showed how a state with a limited amount of wind resource can rally behind a revamped Renewable Portfolio Standard (RPS) to take advantage of what little resource resides within its borders. The Appalachian Mountain WRA illustrates the necessity for economic incentive for large scale wind projects. Proposing to install wind turbines in places with cheap electricity will not gain traction. The 1/7 Power Law analysis also demonstrated the relationship between terrain and contour number: more mountainous locations tended to display higher contour numbers. The South African WRA

demonstrated that no one NWP model solution is optimal for every location. Two different locations off the coast of South Africa were analyzed, resulting in two different solutions. The WRA of Denmark typifies the feasibility of large scale wind implementation. Already the country generates over 20% of its electricity from wind. Granted, the country is connected to German grid as a stopgap and relies on significant amounts of hydropower for balancing purposes. Nonetheless, the turbines are spinning.

The potential for wind continues to grow, especially in areas with so much wind resource, like Wyoming. Wind energy creates jobs, spurs innovation and conserves water. The rise and success of wind energy during the last decade is due to unwavering three-pronged efforts from academia, industry and government. Given the state of the technology, major strides taken today can help propel the country to energy independence by midcentury. The wind is just waiting to be harnessed by the willing, able and savvy. We've already slept through the alarm once. We can't afford to do it again.

Appendix A:

GEMPAK averaging programs

dcgrib2: This is one of several grid manipulation programs within GEMPAK designed to decode GRIB files into a GEMPAK friendly format (.gem). To automate the process, UNIX shell scripts were written to convert the entire three year NAM 12-km and 4-km model data sets.

gddiag: This is a GEMPAK program that adds scalar/ vector diagnostic grids to the queued GEMPAK file. This program was used to add the newly computed wind and power variables to each .gem file.

gdave.pl: This is a pearl script which averages variables in GEMPAK files. It takes as its input -*n* GEMPAK files and averages -*v* variables at -*l* levels at -*t* times and outputs the result to a new GEMPAK file. For example,

gdave.pl -l 800,850 -t 03,06 -v pow5017 jan09hour.gem 200901*.gem

averages the 50-m wind power density at 800mb and 850mb at 0300 and 0600 UTC in all the GEMPAK files that start with 200901 and outputs the result to jan09hour.gem.

gdlsnd: This program extracts variables at prescribed grid points (*e.g.* cities or latitude/ longitude coordinates) for a given GEMPAK file and saves the output to a text file.

Mimicking other GEMPAK gridded data programs, **gdlsnd** requires the user to identify a source grid file, specify the desired variables to output at their respective times and define a target output file.

Appendix B:

UNIX Scripts for Averaging GEMPAK Files

The following are representative scripts for the year 2009. Similar scripts were invoked for calculating the three year averages.

addpow17loopall: This script added the power variables calculated from the 1/7 Power Law. A similar script was invoked to add the power variables calculated from the rated velocities.

```
#!/bin/sh
year=2009
yr=09
for mo in 01 02 03 04 05 06 07 08 09 10 11; do
if [ "$mo" == "01" ]; then
      month=jan
fi
if [ "$mo" == "02" ]; then
     month=feb
fi
if [ "$mo" == "03" ]; then
     month=mar
fi
if [ "$mo" == "04" ]; then
     month=apr
fi
if [ "$mo" == "05" ]; then
     month=may
fi
if [ "$mo" == "06" ]; then
     month=jun
fi
if [ "$mo" == "07" ]; then
     month=jul
fi
if [ "$mo" == "08" ]; then
     month=aug
fi
if [ "$mo" == "09" ]; then
     month=sep
fi
if [ "$mo" == "10" ]; then
     month=oct
fi
if [ "$mo" == "11" ]; then
     month=nov
```

```
fi
if [ "$mo" == "12" ]; then
     month=dec
fi

for day in 01 02 03 04 05 06 07 08 09 10 11 12 13 14 15 16 17 18 19 20 21 22 23 24 25 26 27 28
29 30 31; do

for hrs in 03 06 09 12 15 18 21 24; do

gemname=${month}/${year}${mo}${day}00f0${hrs}.gem
date=${yr}${mo}${day}/0000F0${hrs}

gddiag << EOF
 gdf        = $gemname
 gdoutf    = $gemname
 glev      = 0
 gvc       = NONE
 gdat      = $date
 gfu       = quo(pres,mul(2.87,tmpk@2%HGHT))
 grdnam    = DEN^${date}@0%NONE
 cpyfil    =
 anlyss    =
 \$respond = no
 run
EOF

gddiag << EOF
 gdf        = $gemname
 gdoutf    = $gemname
 glev      = 0
 gvc       = NONE
 gdat      = $date
 gfu       = mul(quo(den,2),exp(mag(wnd@10%hght),3))
 grdnam    = POW^${date}@10%HGHT
 cpyfil    =
 anlyss    =
 \$respond = no
 run
EOF

gddiag << EOF
 gdf        = $gemname
 gdoutf    = $gemname
 glev      = 0
 gvc       = NONE
 gdat      = $date
 gfu       = mul(10.6,exp(POW@10%hght,.748))
 grdnam    = POW50^${date}@10%HGHT
 cpyfil    =
 anlyss    =
 \$respond = no
 run
EOF
```

```
gddiag << EOF
 gdf       = $gemname
 gdoutf    = $gemname
 glev      = 0
 gvc       = NONE
 gdat      = $date
 gfu       = mag(wnd@10%hght)
 grdnam    = wnd10^${date}@10%HGHT
 cpyfil    =
 anlyss    =
 \$respond = no
 run
EOF

gddiag << EOF
 gdf       = $gemname
 gdoutf    = $gemname
 glev      = 0
 gvc       = NONE
 gdat      = $date
 gfu       = mul(mag(wnd@10%hght),1.2585)
 grdnam    = wnd50^${date}@10%HGHT
 cpyfil    =
 anlyss    =
 \$respond = no
 run
EOF

gddiag << EOF
 gdf       = $gemname
 gdoutf    = $gemname
 glev      = 0
 gvc       = NONE
 gdat      = $date
 gfu       = mul(quo(den,2),exp(wnd50@10%hght,3))
 grdnam    = POW5017^${date}@10%HGHT
 cpyfil    =
 anlyss    =
 \$respond = no
 run
EOF

gddiag << EOF
 gdf       = $gemname
 gdoutf    = $gemname
 glev      = 0
 gvc       = NONE
 gdat      = $date
 gfu       = mul(smin(12.0,mag(wnd@10%hght)),1.2585)
 grdnam    = wndr50^${date}@10%HGHT
 cpyfil    =
 anlyss    =
 \$respond = no
 run
EOF
```

```
gddiag << EOF
  gdf         = $gemname
  gdoutf    = $gemname
  glev      = 0
  gvc       = NONE
  gdat      = $date
  gfu       = mul(quo(den,2),exp(wndr50@10%hght,3))
  grdnam    = POWR5017^${date}@10%HGHT
  cpyfil    =
  anlyss    =
  \$respond = no
  run
EOF

gddiag << EOF
    \$respond = yes
 exit
EOF
done
done
done
gpend
```

avetimevall: This script averaged the power variables at every hour for every month and output a single GEMPAK file in the form of ${month}${year}hour.gem. A similar script was invoked to calculate the monthly averages (*i.e.* no hourly divisions).

```
#!/bin/sh
yr=09
year=20${yr}

for mo in 01 02 03 04 05 06 07 08 09 10 11 12; do
if [ "$mo" == "01" ]; then
      month=jan
fi
if [ "$mo" == "02" ]; then
     month=feb
fi
if [ "$mo" == "03" ]; then
     month=mar
fi
if [ "$mo" == "04" ]; then
     month=apr
fi
if [ "$mo" == "05" ]; then
     month=may
fi
if [ "$mo" == "06" ]; then
     month=jun
fi
if [ "$mo" == "07" ]; then
     month=jul
fi
if [ "$mo" == "08" ]; then
     month=aug
fi
if [ "$mo" == "09" ]; then
     month=sep
fi
if [ "$mo" == "10" ]; then
     month=oct
fi
if [ "$mo" == "11" ]; then
     month=nov
fi
if [ "$mo" == "12" ]; then
     month=dec
fi
cd ${month}
var=TMPK,UREL,VREL,HGHT,TRKE
lev=1000,975,950,925,900,875,850
for time in 03 06 09 12 15 18 21 24; do
gdave.pl -s -l ${lev} -t f0${time} -v ${var} ${month}${year}hour.gem ${year}${mo}*.gem
done
```

```
var=UREL,VREL,POW,POW50,WND10,WND50,POW5017,WNDR50,POWR5017,WNDR1550,POWR155017,
WNDR2050,POWR2050,WNDR2550,POWR255017

lev=10

for time in 03 06 09 12 15 18 21 24; do

gdave.pl -s -l ${lev} -t f0${time} -v ${var} ${month}${year}hour.gem ${year}${mo}*.gem

done

cd ..

done
```

softlink_seasons_hour: This script calculated the seasonal hourly averages, outputting four files in the form ${year}_${season}_hour.gem

```
#!/bin/sh

yr=2009
path=/disk1/parish/wind/nam12km/
for hr in 03 06 09 12 15 18 21 24 ; do
gdave.pl -s -t f0${hr} ${yr}_winter_hour.gem win_*hr.gem
done

for hr in 03 06 09 12 15 18 21 24 ; do
gdave.pl -s -t f0${hr} ${yr}_spring_hour.gem spr_*hr.gem
done

for hr in 03 06 09 12 15 18 21 24 ; do
gdave.pl -s -t f0${hr} ${yr}_summer_hour.gem sum_*hr.gem
done

for hr in 03 06 09 12 15 18 21 24 ; do
gdave.pl -s -t f0${hr} ${yr}_autumn_hour.gem aut_*hr.gem
done
```

References

(2005). "GEMPAK Online Tutorial How Does GEMPAK Work?". Retrieved 7 March 2012, from http://www.unidata.ucar.edu/software/gempak/tutorial/01_introduction.html#1.2.

(2008). 20% Wind Energy By 2030: Increasing wind energy's contribution to U.S. electricity supply. D. o. Energy**:** 226.

(2009). "Impact of Model Structure and Dynamics." Retrieved 7 March 2012, from http://www.meted.ucar.edu/nwp/model_structure/index.htm.

(2010). Annual Energy Review. U. E. I. Administration.

(2011). Weather Research and Forecasting ARW User's Guide. N. C. f. A. Research. Boulder, CO**:** 354.

Acker, T. L., S. K. Williams, et al. (2007). "Wind resource assessment in the state of Arizona: Inventory, capacity factor, and cost." Renewable Energy **32**(9): 1453-1466.

Banta, R. M., R. K. Newsom, et al. (2002). "Nocturnal Low-Level Jet Characteristics Over Kansas During Cases-99." Boundary-Layer Meteorology **105**(2): 221-252.

Bessa, R. J., V. Miranda, et al. (2011). "'Good' or 'bad' wind power forecasts: a relative concept." Wind Energy **14**(5): 625-636.

Boyle, G. (2007). Renewable Electricity and the Grid. London, Earthscan.

Brockhouse, B. (2008). "Lassoing Wyoming's Wind." Rural Cooperatives **75**(4): 8-9,42.

Cardwell, D. (2012). Waning Support For Wind And Solar. The New York Times. New York City, The New York Times Company.

Christopher A, F. (2009). "History of surface weather observations in the United States." Earth-Science Reviews **93**(3,Äì4): 77-84.

Cutler, N. J., H. R. Outhred, et al. (2009). "Characterizing future large, rapid changes in aggregated wind power using Numerical Weather Prediction spatial fields." Wind Energy **12**(6): 542-555.

Cutler, N. J., H. R. Outhred, et al. (2011). "Predicting and presenting plausible future scenarios of wind power production from numerical weather prediction systems: a qualitative ex ante evaluation for decision making." Wind Energy: n/a-n/a.

Diab, R. D. and M. Garstang (1984). "Assessment of Wind Power Potential for Two Contrasting Coastlines of South Africa Using a Numerical Model." Journal of Climate and Applied Meteorology **23**(12): 1645-1659.

Eilperin, J. (2012). The Clean Tech Meltdown. Wired. San Fransico, CA, Condé Nast. **Feb 2012:** 130.

Ernst, B., B. Oakleaf, et al. (2007). "Predicting the Wind." Power and Energy Magazine, IEEE **5**(6): 78-89.

Everitt, B. S. and A. Skrondal (2010). The Cambridge Dictionary of Statistics. Cambridge, Cambridge University Press.

Foley, A. M., P. G. Leahy, et al. (2012). "Current methods and advances in forecasting of wind power generation." Renewable Energy **37**(1): 1-8.

GE (2010). Western and Solar Integration Study. U. D. o. E. N. R. E. Laboratory. Golden, CO**:** 40.

Kavasseri, R. G. and K. Seetharaman (2009). "Day-ahead wind speed forecasting using f-ARIMA models." Renewable Energy **34**(5): 1388-1393.

Krauss, C. (2011). Can We Do Without The Mideast? The New York Times. New York City, The New York Times Company. **CLXI**.

Landberg, L., L. Myllerup, et al. (2003). "Wind Resource Estimation—An Overview." Wind Energy **6**(3): 261-271.

Madrigal, A. (2011). Powering The Dream: The History and Promise of Green Technology. Philadelphia, PA, Da Capo Press.

Manwell, J. F., McGowan, J.G., Rogers, A.L. (2009). Wind Energy Explained: Theory, Design and Application. West Sussex, UK, John Wiley & Sons, Ltd.

Marquis, M., J. Wilczak, et al. (2011). "Forecasting the Wind to Reach Significant Penetration Levels of Wind Energy." Bulletin of the American Meteorological Society **92**(9): 1159-1171.

Martner, B. E. (1986). Wyoming Climate Atlas. Lincoln, University of Nebraska Press.

Martner, B. E. and J. D. Marwitz (1982). "Wind Characteristics in Southern Wyoming." Journal of Applied Meteorology **21**(12): 1815-1827.

Martner, B. E. and J. D. Marwitz (1982). "Wind Characteristics in Southern Wyoming." Journal of Applied Meteorology **21**(12): 1815-1827.

Marwitz, J. D. and P. J. Dawson (1984). "Low-Level Airflow in Southern Wyoming during Wintertime." Monthly Weather Review **112**(6): 1246-1262.

Michalakes, J., J. Dudhia, et al. (2004). "The weather Research and Forecast Model: Software Architecture and Performance." Retrieved 7 March 2012, from http://www.wrf-model.org/wrfadmin/docs/ecmwf_2004.pdf.

Möhrlen, C. (2004). Uncertainty in Wind Energy Forecasting. Civil & Environmental Engineering. Dublin, National University of Ireland. **Doctor of Philosophy:** 185.

Müller, M. D. (2011). "Effects of Model Resolution and Statistical Postprocessing on Shelter Temperature and Wind Forecasts." Journal of Applied Meteorology and Climatology **50**(8): 1627-1636.

Raichle, B. W. and W. R. Carson (2009). "Wind resource assessment of the Southern Appalachian Ridges in the Southeastern United States." Renewable and Sustainable Energy Reviews **13**(5): 1104-1110.

Rife, D. L. and C. A. Davis (2005). "Verification of Temporal Variations in Mesoscale Numerical Wind Forecasts." Monthly Weather Review **133**(11): 3368-3381.

Sedefian, L. (1980). "On the Vertical Extrapolation of Mean Wind Power Density." Journal of Applied Meteorology **19**(4): 488-493.

Shaw, W. J., J. K. Lundquist, et al. (2009). "Research Needs For Wind Resource Characterization." Bulletin of the American Meteorological Society **90**(4): 535-538.

Shin, H. and S.-Y. Hong (2011). "Intercomparison of Planetary Boundary-Layer Parametrizations in the WRF Model for a Single Day from CASES-99." Boundary-Layer Meteorology **139**(2): 261-281.

Wald, M. and M. Zeller (2010). Green Power's High Cost Makes Projects a Tougher Sell. The New York Times. New York CIty, The New York TImes Company.

Webb, W. P. (1931). The Great Plains: A Study in Institutions and Environment. Waltham, MA, Blaisdell Publishing Company.

Wilson, A. B., D. H. Bromwich, et al. (2011). "Evaluation of Polar WRF forecasts on the Arctic System Reanalysis domain: Surface and upper air analysis." J. Geophys. Res. **116**(D11): D11112.

Zeller, T. (2010). For Those Living Nearby, That Miserable Hum of Clean Energy. The New York Times. New York City, The New York Times Company. **160**.